Trapped fermions with short-range and dipolar interactions in 2D optical lattices

Anne-Louise Gadsbølle

PhD Dissertation

July 2012

The Lundbeck Foundation Theoretical Center
for Quantum System Research
Department of Physics and Astronomy
Science and Technology
Aarhus University
Denmark

We must be clear that when it comes to atoms, language can be used only as in poetry. The poet, too, is not nearly so concerned with describing facts as with creating images and establishing mental connections.

Niels Bohr

Til min familie.

Preface and acknowledgments

The work of this thesis has been done from 2008−2012 in the group of Klaus Mølmer in the Lundbeck Foundation Theoretical Center for Quantum Research. I would like to thank Klaus and the foundation for giving me the opportunity to do this PhD.
The first two years of my PhD concerned theoretical investigations of fermions with attractive on-site interactions. I would like to thank Nicolai Nygaard for giving me a very careful introduction to the complex field of cold atoms and sharing his knowledge and enthusiasm for physics. On that note, I would also like to acknowledge Uffe V. Poulsen whom together with Nicolai Nygaard, evoked my interest in cold atoms through their inspiring lectures in the course Quantum Gases.
Next, I would like to thank Karyn Le Hur who was my supervisor during my stay at Yale as a visiting assistant in research. Here, I examined models for high-temperature superconductivity and Karyn deserves the greatest thanks for making my stay very pleasant and for sharing her insight in physics. This stay resulted in a publication in collaboration with Francis Song who made figure 5.10. Collaboration with Francis was inspiring and rewarding due to his wide knowledge and intuition for theoretical physics. I am very grateful for the hospitality shown by my friends Marie Arnesson and Mike Galler during my stay in New Haven. Also to Mike's family for

opening their home to me.
For help with the intricacies of MATLAB and LaTeX I would like to thank Rasmus Handberg, Thomas Tram Bülow, Ole Søe Sørensen, and Søren Gammelmark. Furthermore I would like to thank Søren Gammelmark for making figure 6.1 and Ole Søe Sørensen for making figure 4.1 and figure 5.2. It has been a pleasure to be a part of the Lundbeck group and I would like to thank everyone in the group for physics discussions as well as the coffee break talks.
Also, I would like to thank Nikolaj Zinner, Jens Kusk Block, Jakob Sherson and Manuel Valiente Cifuentes for always being willing to help with questions regarding my work. A special thanks goes to Manuel Valiente Cifuentes and Jake Gulliksen for proof-reading my thesis.
I would especially like to thank Georg Morten Bruun who has been my supervisor during the last years of my PhD - a collaboration which without a doubt has made me a better physicist. It has been a pleasure to work in his group.
Finally, I would like to thank my family and friends for always being very supportive.

List of publications

- Anne-Louise Gadsbølle and G. M. Bruun, *Dipolar fermions in a two-dimensional lattice at non-zero temperature*, e-print arXiv:1206.4974. Submitted to Phys. Rev. A.
- Anne-Louise Gadsbølle, H. Francis Song, and Karyn Le Hur, *d-wave Superfluid with Gapless Edges in a Cold Atom Trap*, Phys. Rev. A **85**, 051603(R) (2012).
- Anne-Louise Gadsbølle and G. M. Bruun, *Harmonically trapped dipolar fermions in a two-dimensional square lattice*, Phys. Rev. A **85**, 021604(R) (2012).
- Anne-Louise Gadsbølle, *Exploring superfluidity and vortices in a Fermi gas in a 2D optical lattice with harmonic confinement*, Progress report (2010).

English summary

Ultracold atoms in optical lattices are ideal quantum simulators of complex many-body Hamiltonians that arise in condensed matter systems. Manipulation of these model systems allows us to explore a variety of physical phenomena taking place in solid state systems. Here, we present mean-field calculations of trapped fermions in optical lattices with on-site interactions. If we restrict ourselves to the strongly repulsive regime, we can simulate the physics of high-temperature superconductors. We also consider dipolar fermions. The anisotropic nature of the dipolar interaction results in order parameters of different symmetry. Depending on the orientation of the dipoles we find either checkerboard or striped patterns. However, when the dipoles are tilted sufficiently, the dipoles exhibit p-wave pairing. The melting of the p-wave pairing order parameter is examined using Berezinskii-Kosterlitz-Thouless theory.

Danish summary (dansk resumé)

Kolde atomer i optiske gitre er ideelle til at simulere fysikken i faste stoffer. Fordelen ved disse modelsystemer er, at man kan styre parametre såsom gitterafstanden, gitterdybden og antallet af partikler på en kontrolleret måde. Dette betyder, at man kan udforske en bred vifte af fysiske fænomener i faste stoffer. I denne afhandling benytter vi middelfeltsteori til blandt andet at beskrive mange-legemesystemet bestående af fermioner i optiske gitre med punktvekselvirkninger. Vi ser på en del af fysikken i højtemperatursuperledere ved at lade fermionerne være meget stærkt frastødende. Hvis fermionerne vekselvirker gennem dipolvekselvirkningen, kan et antal af faser fremkomme. Vi undersøger, hvordan den anisotrope natur af vekselvirkningen giver anledning til konkurrerende tæthedsfaser og en p-bølge-fase. Smeltningen af den sidstnævnte fase beskriver vi med Berezinskii-Kosterlitz-Thouless-teori.

Contents

Chapter

1 Introduction and thesis outline

1.1 Introduction

The experimental realization of a Bose-Einstein condensate (BEC) in 1995 [1, 2] led to an explosive growth of the field of ultracold bosons. The majority of the explored physics was captured by mean-field theory, effectively a single particle theory, described by the Gross-Pitaevskii equation. The path toward stronger interacting and correlated systems was opened by the use of Feshbach resonances [3–6] allowing for a control of the interaction strength and sign. The regime of strong interactions was also reached by the introduction of optical lattices [7, 8] which can freeze out tunneling of particles between wells and reduce the number of dimensions to induce stronger fluctuations.

The experimental achievement of a Fermi degenerate ^{40}K gas was obtained in 1999 at JILA by B. DeMarco and D. Jin [9]. Following this major advance a group in Florence were successful in achieving a quantum degenerate ^{40}K gas [10]. Another five groups also reached the quantum degenerate regime using ^{6}Li [11–15].

A groundbreaking result using optical lattices was obtained in 2002, when a phase-transition from a Mott-insulating state to a superfluid state was observed in a BEC after being loaded into a three-dimensional (3D)

optical lattice [7]. Not only 3D systems, but also 2D and 1D systems have attracted attention during the years. In 2D systems with continuous symmetry no true BEC can be formed. However, a quasi-BEC with quasi-long range order can exist and the system can indeed be superfluid. A phase-transition from a normal state to a state with such quasi-long range order was indeed observed in 2006 [16].

Many indications for fermionic superfluidity were presented during the years but in 2005 unambiguous evidence for a Fermi superfluid was found at MIT with the demonstration of vortex lattices in a strongly interacting Fermi gas set into rotation [17]. A direct observation of superfluidity of fermions in an optical lattice was reported in 2006 by the group of Ketterle at MIT from the observation of interference peaks [18].

The desire to understand the complex physics taking place in high-temperature superconductors gives rise to a lot of experimental as well as theoretical work. Experimental work has been performed in the BEC-BCS (Bardeen-Cooper-Schrieffer) crossover where spin fluctuations have been studied [19]. These are predicted to be of great importance to d-wave superfluidity in the repulsive Hubbard model [20–23].

So far a lot of work has been done for fermions with on-site interactions. However, the interest in trapping and cooling atoms and molecules with a permanent electric or magnetic dipole moment is increasing. So far Bose-Einstein condensates of magnetically dipolar ^{52}Cr atoms [24, 25] and of ^{164}Dy atoms [26] have been realized as well as electrically dipolar fermionic gases of ^{40}K^{87}Rb [27, 28] and ^{23}Na^{6}Li [29] and even more species have recently been presented [30].

1.2 Thesis outline

In this thesis we explore fermions in 2D square optical lattices. Section 2.1 is devoted to a general introduction to fermions and their statistics. Section 2.2 gives a tutorial introduction to optical lattices [31] and how to make the optical lattice quasi-2D.

Chapter 3 gives a short introduction to the Berezinskii-Kosterlitz-Thouless (BKT) transition since we will use the framework of BKT theory [32–34] in Chapter 7.

Chapter 4 concerns a trapped two-component fermionic gas in a 2D optical lattice with attractive on-site interactions. We analyze this system in a mean-field picture by deriving the self-consistent Bogoliubov-de Gennes (BdG) equations [35] and solving them numerically using a Broyden's method. In Section 4.5 we extend the analysis of the trapped system to include rotation. This is done by introducing the Peierls factors on the tunneling amplitudes [36] which gives rise to a vortex with a corresponding 2π phase-winding in the central part of the pairing order parameter. Section 4.6 is devoted to a study of the superfluidity in a two-component 2D lattice system. We derive an analytical expression for the superfluid density in real space as well as in momentum space and solve both cases numerically - the trapped system being solved in a local density approximation (LDA) [37]. The behavior is explored as a function of temperature.

In Chapter 5 we make a toy-model for a high-temperature superconductor. This means that we change the sign and strength of the interaction so that the system becomes extremely repulsive. An appropriate model for this system is the t-J model [22] in which we project onto the singly occupied space [23, 38, 39]. We solve the Bogoliubov-de Gennes equations self-consistently taking the projection into account using the Gutzwiller renormalization factors [38] and assuming d-wave pairing in the system. We first consider an untrapped system for which we find the phase-diagram. In the following section we add a harmonic trapping potential which allows us to map a great part of the phase-diagram in one system.

Next, we consider dipolar fermions which have an anisotropic interaction giving rise to completely new physics. In Chapter 6 we consider a single-component dipolar fermionic gas at zero temperature. We again use a mean-field picture and explore different regimes of the system giving rise to a variety of phases such as a striped and a checkerboard density order parameter and a p-wave superfluid for the trapped system as well as the untrapped system. In Chapter 7 we extend our analysis to include the effects of non-zero temperature. We use the framework of BKT theory and calculate the critical temperature from the superfluid density.

Finally, we make concluding remarks in Chapter 8 and give a short outlook.

Chapter

2 Fermions in optical lattices

2.1 Fermions and spin statistics

One of the major concepts in quantum mechanics which is absent in classical mechanics is that of indistinguishability. In quantum mechanics indistinguishability implies that the fermionic or bosonic wave-function can only differ by a sign when the coordinates of two identical particles are interchanged. The fermionic wave-function is anti-symmetric under particle exchange:

$$\Psi(..., \boldsymbol{x}_i, ..., \boldsymbol{x}_j, ...) = -\Psi(..., \boldsymbol{x}_j, ..., \boldsymbol{x}_i, ...), \tag{2.1}$$

where $\boldsymbol{x}_i = (\boldsymbol{r}_i, \sigma_i)$ denote the position $\boldsymbol{r}_i$ and the spin σ_i of the i'th fermion. Due to the anti-symmetry of the wave-function, fermions obey Pauli's exclusion principle, stating that no two identical fermions can occupy the same quantum mechanical state. On the contrary, bosons can occupy the same quantum mechanical state.

In thermal equilibrium, the occupation probability of fermions is described by the Fermi-Dirac distribution $f(E) = 1/(e^{\beta(E-\mu)} + 1)$, with $\beta = 1/k_{\mathrm{B}}T$ where T is the temperature and k_{B} the Boltzmann constant,

and the chemical potential $\mu = (\partial E/\partial N)_{VS}$ depends on the total energy E and the number of particles N.

One can characterize atoms of mass m_a at temperature T by the de Broglie wavelength $\lambda_\mathrm{dB} = h/\sqrt{2\pi m_\mathrm{a} k_\mathrm{B} T}$, which increases as temperature decreases. When the de Broglie wavelength becomes comparable to the interatomic distance the particles start to overlap. At this point the quantum mechanical nature of the particles becomes important. When bosons reach this temperature they start occupying the same single-particle state of lowest energy, hereby forming a Bose Einstein condensate.

In this thesis we deal with single and two-component fermionic gases. To describe the physics of an ensemble of interacting fermions, we make use of second quantization, where the symmetry of the wave-function is incorporated through the anti-commutation relations of the fermionic annihilation and creation operators, i.e.,

$$\left\{\hat{\psi}_\sigma(\boldsymbol{r}), \hat{\psi}^\dagger_{\sigma'}(\boldsymbol{r}')\right\} = \hat{\psi}_\sigma(\boldsymbol{r})\hat{\psi}^\dagger_{\sigma'}(\boldsymbol{r}') + \hat{\psi}^\dagger_{\sigma'}(\boldsymbol{r}')\hat{\psi}_\sigma(\boldsymbol{r}) = \delta_{\sigma\sigma'}\delta(\boldsymbol{r}-\boldsymbol{r}'), \quad (2.2)$$

$$\left\{\hat{\psi}^\dagger_\sigma(\boldsymbol{r}), \hat{\psi}^\dagger_{\sigma'}(\boldsymbol{r}')\right\} = \left\{\hat{\psi}_\sigma(\boldsymbol{r}), \hat{\psi}_{\sigma'}(\boldsymbol{r}')\right\} = 0. \quad (2.3)$$

The effect of $\hat{\psi}^\dagger_\sigma(\boldsymbol{r})$ is to act on the vacuum state and create a particle at position $\boldsymbol{r}$ in spin state $|\sigma\rangle$. A system containing an arbitrary number of particles can be created by acting with appropriate creation operators on the vacuum state.

When the interactions are absent, the fermions will behave as free particles. At zero temperature and in the absence of an external confinement, the occupation probability of the fermions will be a step function where the edge of the step function is denoted the Fermi energy. When there is no external potential, the fermions are set to constitute a Fermi sea corresponding to a ground state of the form $|\mathrm{GS}\rangle = \prod_{|\boldsymbol{k}|<k_\mathrm{F}} \hat{c}^\dagger_{\boldsymbol{k}} |0\rangle$, with $\hat{c}^\dagger_{\boldsymbol{k}}$, the creation operator in momentum space and k_F the Fermi wave vector. By including an arbitrarily small attractive interaction, the Fermi sea becomes unstable leading to a new ground state with a finite gap in the single-particle excitation spectrum. This comes from the formation of Cooper pairs [40–42] usually condensing into states of zero center-of-mass momentum but for some cases even non-zero momentum. The use of

magnetic Feshbach resonances allows a firm control over the character and strength of the interparticle interaction [3–6].

2.2 Optical lattices

The use of optical lattices, created by counter-propagating laser beams, as quantum simulators of electrons in solid state crystals is of great significance. An optical lattice provides us with an enlarged version of a solid state crystal making it easier for experimentalists to examine phenomena such as high-temperature superconductivity. In optical lattice experiments the cold atoms play the role as the electrons in solid state systems and the optical lattice the role of the ion-potential as illustrated in figure 2.1 with the potential represented by the gray solid line. The use of optical lattices gives a simplified model of condensed matter systems with no or very few unknown parameters. These systems provide the experimentalists with a very clean system due to the absence of defects, and the lattice depth as well as the lattice spacing can be manipulated through the control of the lasers generating the optical lattices. Furthermore, the ability to control the alignment of the laser beams gives the possibility of different lattice structures. Special focus is on the fermionic Hubbard model with strong repulsive interactions which is believed to hold the key to understanding high-temperature superconductivity.

The optical lattice is created by three sets of counter-propagating laser beams. Often atoms are loaded in an optical lattice by preparing a fermionic gas and then ramping up the laser intensities, hereby forming the optical lattice. Once the fermions obtain equilibrium the experiments can proceed. Depending on the dimensions of the systems one wants to explore, the intensities of the laser beams can be increased along certain directions hereby practically freezing out the motions in these directions, resulting in a 1D or 2D system.

A direct consequence of the periodic potential is the single particle energy band structure. When single particles are placed in a periodic potential of periodicity a the non-interacting Hamiltonian describing the system is diagonalized by the Bloch states $\psi_{\boldsymbol{k}n}(\boldsymbol{r}) = e^{i\boldsymbol{k}\cdot\boldsymbol{r}}u_{\boldsymbol{k}n}(\boldsymbol{r})$, where $u_{\boldsymbol{k}n}(\boldsymbol{r})$ is a function with the same periodicity as the lattice, n is an integer label for the bands, and $\boldsymbol{k}$ is the quasi-momentum which lies in the first Brillouin

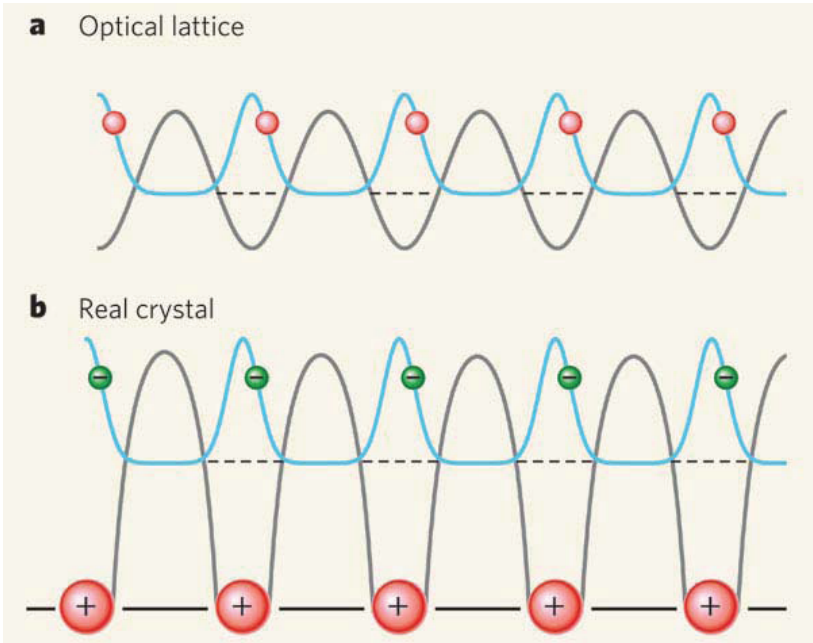

Figure 2.1 | An illustration of an optical lattice potential in (a) and the potential of a real crystal in (b) from [43].

zone $k_i \in [\, -\frac{\pi}{a}, \frac{\pi}{a} \,[$ for $i \in \{x, y, z\}$.

We here briefly describe the physics of atoms in standing wave laser fields to see how this results in a periodic potential experienced by the atoms. When an atom is placed in an external field, the field will induce a dipole moment of the atoms, which interacts with the external field leading to an AC stark shift of the atomic energy-levels. This effect is used to trap and cool cold dilute gases. When the spatial extent of the atom is small compared to the wavelength of the laser field, the interaction between the atom and the laser beam can be described in the dipole approximation

$$\hat{H} = -\boldsymbol{d} \cdot \boldsymbol{E}_{\mathrm{L}}, \tag{2.4}$$

where $\boldsymbol{d} = -e\boldsymbol{r}$ is the induced dipole moment and $\boldsymbol{E}_{\mathrm{L}}(\boldsymbol{r}, t)$ is the electric field. This second order perturbative effect will then give rise to a shift of the atomic ground state $|g\rangle$

$$V_g(\boldsymbol{r}) = -\frac{1}{2}\alpha_{\mathrm{L}} \left\langle E_{\mathrm{L}}(\boldsymbol{r},t)^2 \right\rangle_t . \tag{2.5}$$

Here t denotes a time-average and α_{L} is the real part of the polarizability of the atom. The polarizability depends on the lifetime Γ_e of the excited state $|e\rangle$, and the detuning $\Delta = \omega_{\mathrm{L}} - \omega_{eg}$ of the laser frequency ω_{L} from the atomic transition frequency ω_{eg} when the frequency of the laser is close to resonance with a single transition $|g\rangle \rightarrow |e\rangle$. The energy shift of the ground state is then

$$V_g = \frac{\hbar \Omega_{\mathrm{R}}^2 \Delta}{\Delta^2 + \Gamma_e^2/4}, \tag{2.6}$$

where $\Omega_{\mathrm{R}} = |\langle e|\boldsymbol{d}\cdot\boldsymbol{E}_L(\boldsymbol{r})|g\rangle|/\hbar$ is the Rabi-frequency. A laser which is blue-detuned with respect to the atomic transition ($\Delta > 0$) will attract atoms to the intensity minima whereas a red-detuned laser ($\Delta < 0$) will attract atoms toward larger laser intensities. A strongly focused red-detuned laser can then trap the atoms.

A standing wave created by counter-propagating laser beams along the x-direction will create a potential of the form

$$V_{\mathrm{L}}(x) = V_{x\sigma}^0 \sin^2(k_{\mathrm{L}} x), \tag{2.7}$$

where $k_{\mathrm{L}} = 2\pi/\lambda_{\mathrm{L}}$, with λ_{L} the wavelength of the laser and $a = \lambda_{\mathrm{L}}/2$ the lattice spacing. A typical value for a laser-wavelength used in experiments is $\lambda_{\mathrm{L}} = 1064\mathrm{nm}$ (for further details see [31]). Using three sets of counter-propagating laser beams in the three spatial directions the potential becomes

$$V_{\mathrm{L}}(\mathbf{r}) = \sum_i V_{i\sigma}^0 \sin^2(k_{\mathrm{L}} r_i). \tag{2.8}$$

It is possible to freeze out the motion in any given direction, e.g. the z-direction, by applying a sufficiently intense laser field along that direction. Due to the separation of the potential along the axes, it is possible to

consider the z-direction separately such that $V^0_{z\sigma} \gg V^0_{x\sigma}, V^0_{y\sigma}$. The deep lattice potential can then be approximated with a harmonic potential, $V^0_i \sin^2(\pi z/a) \approx V^0_i (\pi z/a)^2$. The eigenenergies are thus approximately $\hbar\omega_0(n+1/2)$ with $\omega_0 = \pi/a\sqrt{2V^0_{z\sigma}/m}$ and $n \in \mathbb{N}_0$. Therefore, it is possible to freeze out this third dimension, if the energies involved are small compared to the excitation energy $\hbar\omega_0$.

Chapter

3 A short introduction to the Berezinskii-Kosterlitz-Thouless transition

In the following we give a short introduction to the Berezinskii-Kosterlitz-Thouless (BKT) theory describing the superfluid phase transition taking place in the two-dimensional lattice system. The phase-transition of the superfluid order parameter in the 2D systems we are describing is in the Berezinskii-Kosterlitz-Thouless universality class since the free energy forms a sombrero. The result of this section will be used to calculate the critical temperature for the superfluid phase in Chapter 7.

3.1 The XY-model

We first consider the XY-model in a 2D system. The Hamiltonian is given by

$$\hat{H} = -J^{\mathrm{XY}} \sum_{\langle ij \rangle} \cos(\theta_i - \theta_j) = -J^{\mathrm{XY}} \sum_{\langle ij \rangle} \mathbf{s}_i \cdot \mathbf{s}_j, \tag{3.1}$$

where the sum is taken over nearest neighbors and θ_i is the phase of the spin of unit length $\mathbf{s}_i = e^{i\theta_i}$ or the phase of an order parameter as in our system. According to the Mermin-Wagner theorem [44], no long-range

order can exist in a 2D system with rotational symmetry. This means that the spin-spin correlation function must behave according to

$$\lim_{|\mathbf{r}_l-\mathbf{r}_m|\to\infty} \langle \mathbf{s}_l \cdot \mathbf{s}_m \rangle = \lim_{|\mathbf{r}_l-\mathbf{r}_m|\to\infty} \langle \cos(\theta_l - \theta_m) \rangle = 0, \tag{3.2}$$

with $\mathbf{r}_l$ denoting site l. Despite of this a transition does take place at non-zero temperature as shown by Berezinskii, Kosterlitz and Thouless [32–34]. To see this one must consider the high-temperature regime and the low-temperature regime independently to find the behavior of the correlation function.

3.2 The high-temperature limit

When the temperature is much larger than the coupling strength $T/J^{\mathrm{XY}} \gg 1$ the exponential in the correlation function of the N spins may be Taylor expanded

$$\langle \mathbf{s}_l \cdot \mathbf{s}_m \rangle = \frac{1}{Z} \operatorname{Tr} \left[e^{\beta J^{\mathrm{XY}} \sum_{\langle ij \rangle} \cos(\theta_i - \theta_j)} \cos(\theta_l - \theta_m) \right], \tag{3.3}$$

with $\operatorname{Tr} = \int_0^{2\pi} d\theta_1 ... \int_0^{2\pi} d\theta_N$ to give

$$\langle \mathbf{s}_l \cdot \mathbf{s}_m \rangle \approx e^{-|\mathbf{r}_l - \mathbf{r}_m|/\xi^{\mathrm{XY}}}, \tag{3.4}$$

with the coherence length given by $\xi^{\mathrm{XY}} = 1/\ln(2k_{\mathrm{B}}T/J^{\mathrm{XY}})$. A way to obtain this result is by finding the terms that contribute to the correlation function using that only terms connecting site l and m contribute to the numerator and only terms connecting a site to itself contribute to the denominator [45].

3.3 The low-temperature limit

When the temperature is small compared to the interaction strength we assume a small phase variation on neighboring lattice sites. From this we Taylor expand the Hamiltonian to obtain

$$\hat{H} = -J^{\mathrm{XY}} \sum_{\langle ij \rangle} \cos(\theta_i - \theta_j) \approx -J^{\mathrm{XY}} \sum_{\langle ij \rangle} \left[1 - \frac{1}{2} (\theta_i - \theta_j)^2 \right]$$
$$\approx \frac{J^{\mathrm{XY}}}{2} \int d^2 r |\nabla \theta|^2, \tag{3.5}$$

where the last equality corresponds to the continuum limit and we have not included the constant energy term. In this limit we write the correlation function as

$$\langle \mathbf{s}_l \cdot \mathbf{s}_m \rangle = \frac{1}{2} \langle e^{i(\theta_l - \theta_m)} + e^{-i(\theta_l - \theta_m)} \rangle$$
$$= e^{-\frac{1}{2}\langle (\theta_l - \theta_m)^2 \rangle}, \tag{3.6}$$

obtained from Gaussian integrals. The derivation of the correlation function in this limit is a straight-forward but lengthy calculation that requires a Fourier expansion and Gaussian integrals [45]

$$\langle \mathbf{s}_l \cdot \mathbf{s}_m \rangle \approx \left(\frac{|\mathbf{r}_l - \mathbf{r}_m|}{a} \right)^{-k_{\mathrm{B}} T / 2\pi J^{\mathrm{XY}}}, \tag{3.7}$$

with a the lattice constant. This correlation function in the low temperature regime indicates quasi-long range order decaying as a power law in contrast to the correlation function in the high-temperature regime. The different behavior of the correlation function in the two temperature regimes hints that something happens for a temperature in between. This transition is known as the Berezinskii-Kosterlitz-Thouless transition and is driven by the formation of vortex-antivortex pairs.

3.4 Vortices

Due to the periodicity of the spin $\mathbf{s}_i = e^{i\theta_i}$ it is possible to have spin configurations

$$\oint \nabla\theta \cdot d\mathbf{l} = n2\pi, \tag{3.8}$$

with $n \pm 1, \pm 2, ...$ named the winding number with $\nabla\theta = \hat{\mathbf{e}}_\phi n/r$. Inserting this into equation (3.5) we obtain for the energy of the vortex

$$E = E_\mathrm{c} + \pi n^2 J^\mathrm{XY} \log\left(\frac{R}{a}\right), \tag{3.9}$$

with R the size of the system and E_c the core-contribution to the energy. By exploiting the fact that the entropy scales with $k_\mathrm{B} \log\left(\frac{R^2}{a^2}\right)$ we see that the free energy $F = E - TS$ changes sign when

$$J^\mathrm{XY} = 2k_\mathrm{B}T/\pi, \tag{3.10}$$

which is actually the onset of the Berezinskii-Kosterlitz-Thouless transition obtained from a renormalization group analysis. This result of the critical coupling strength is used in Chapter 7 to find the critical temperature in our 2D system.

Chapter

4 Trapped fermions in a 2D square lattice with attractive on-site interactions

4.1 The Hubbard Hamiltonian of fermions with on-site interactions

In order to simplify the many-body Hamiltonian of a two-component trapped fermionic gas we neglect all collisions other than binary, since we consider a dilute gas. Also, due to the anti-symmetry of the wave-function of indistinguishable fermions only collisions with odd angular momentum will contribute for fermions in the same spin state. Such collisions will be "frozen out" for dilute gases at low temperature, and we can therefore safely neglect interactions between equal spins in the following. Hence, the Hamiltonian of a two-component gas takes the following form

$$\hat{H} = \sum_{\sigma} \int \hat{\psi}_{\sigma}^{\dagger}(\boldsymbol{r}) \left(\frac{-\hbar^2}{2m} \nabla^2 + V_{\sigma}(\boldsymbol{r}) \right) \hat{\psi}_{\sigma}(\boldsymbol{r})\, d\boldsymbol{r} + \frac{1}{2} \sum_{\sigma} \int \int \hat{\psi}_{\sigma}^{\dagger}(\boldsymbol{r})\, \hat{\psi}_{\bar{\sigma}}^{\dagger}(\boldsymbol{r'})\, U(\boldsymbol{r} - \boldsymbol{r'}) \hat{\psi}_{\bar{\sigma}}(\boldsymbol{r'})\, \hat{\psi}_{\sigma}(\boldsymbol{r})\, d\boldsymbol{r} d\boldsymbol{r'}, \tag{4.1}$$

with $\bar{\uparrow} = \downarrow$ and $\bar{\downarrow} = \uparrow$ [46]. Since the typical range of the atom-atom interaction is much shorter than the interparticle spacing it can be approximated

with a pseudo-potential of the form $U(\boldsymbol{r}-\boldsymbol{r'}) = g\delta(\boldsymbol{r}-\boldsymbol{r'})$, with $g<0$ for attraction.

When an additional external potential $V_\sigma^{\text{ext}}(x,y)$ such as a harmonic trap is added on top of the optical lattice potential $V_\sigma^{\text{L}}(x,y)$, the discrete translational invariance is broken and the Bloch states no longer diagonalize the Hamiltonian. We therefore perform a unitary transformation to the Wannier basis, whose elements are localized states on the lattice sites with only a small weight on neighboring sites, which gets smaller for a deeper lattice. The field operators may be expanded in this basis, i.e. $\hat{\psi}_\sigma(x,y) = \sum_{i,n} \hat{c}^n_{\sigma i} W^n_{\sigma i}(x,y)$, where $\hat{c}^n_{\sigma i}$ annihilates a particle of spin σ at the i'th lattice site in band n, $W^n_{\sigma i}(x,y)$ is the amplitude of the Wannier state in position space and n refers to the band index. We proceed by inserting the expansions into the Hamiltonian (4.1) and leave out the band index, since we assume that only the lowest band is occupied. This is a good approximation if the energy splitting of the bands is large compared to the other energy scales involved and if the population on each lattice site is small. The effective Hamiltonian becomes

$$\begin{aligned}\hat{H} \approx & \sum_\sigma \int \sum_{ij} \hat{c}^\dagger_{\sigma i}\hat{c}_{\sigma j} W^*_{\sigma i}(x,y)\left(\frac{-\hbar^2}{2m}\nabla^2 + V_\sigma^{\text{L}}(x,y)\right) W_{\sigma j}(x,y)d^2r \\ & + \sum_\sigma \int \sum_{ij} \hat{c}^\dagger_{\sigma i}\hat{c}_{\sigma j} W^*_{\sigma i}(x,y) V_\sigma^{\text{ext}}(x,y)\, W_{\sigma j}(x,y)d^2r \\ & + g\int \sum_{ijkl} \hat{c}^\dagger_{\uparrow i}\hat{c}^\dagger_{\downarrow j}\hat{c}_{\downarrow k}\hat{c}_{\uparrow l} W^*_{\uparrow i}(x,y)W^*_{\downarrow j}(x,y)W_{\downarrow k}(x,y)W_{\uparrow l}(x,y)d^2r. \end{aligned} \tag{4.2}$$

Since the largest contribution to the interaction will be the on-site interaction, we only include this in our Hamiltonian. The Hamiltonian can then be rewritten as

$$\begin{aligned}\hat{H} = & -\sum_{\sigma i}\left(t_{\sigma x, x+e_x}\hat{c}^\dagger_{\sigma i}\hat{c}_{\sigma i+e_x} + t_{\sigma x, x-e_x}\hat{c}^\dagger_{\sigma i}\hat{c}_{\sigma i-e_x}\right) \\ & -\sum_{\sigma i}\left(t_{\sigma y, y+e_y}\hat{c}^\dagger_{\sigma i}\hat{c}_{\sigma i+e_y} + t_{\sigma y, y-e_y}\hat{c}^\dagger_{\sigma i}\hat{c}_{\sigma i-e_y}\right) \\ & + U\sum_i \hat{c}^\dagger_{\uparrow i}\hat{c}^\dagger_{\downarrow i}\hat{c}_{\downarrow i}\hat{c}_{\uparrow i} + \sum_{\sigma i} V_{\sigma i}\hat{c}^\dagger_{\sigma i}\hat{c}_{\sigma i}. \end{aligned} \tag{4.3}$$

Here $t_{\sigma x,x+e_x} \equiv -\int W^*_{\sigma i}(x,y)\left(\frac{-\hbar^2}{2m}\nabla^2 + V^{\mathrm{L}}_{\sigma}(x,y)\right) W_{\sigma i+e_x}(x,y)\,dx\,dy$ is the hopping matrix element to the nearest neighbor in the positive x-direction, where $e_x = (1,0)a$ and a is the lattice spacing. Note that we have made the assumption that the confining potential has a small curvature compared to the lattice spacing so that the change in the hopping amplitude due to the confining potential can be neglected. If the lattice is sufficiently deep, the tunneling to the next-nearest neighbor will be small, as well as the nearest neighbor interaction, which has been neglected. The on-site interaction term is then given by $U \equiv g\int d^2r\,|W_{\uparrow i}(x,y)|^2\,|W_{\downarrow i}(x,y)|^2$. We

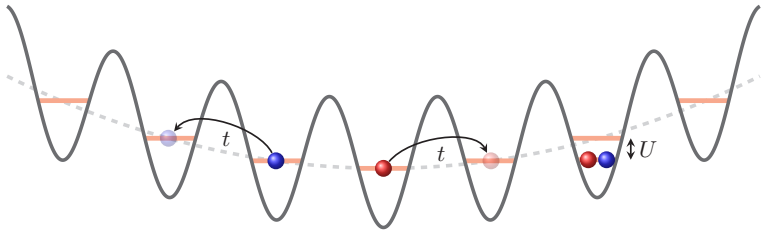

Figure 4.1 | An illustration of two spin-components (blue and red) in a 1D lattice tunneling with an amplitude t and interacting with an interaction strength U.

have left out the constant energy of the lowest vibrational state in each lattice site and only keep the external confining on-site matrix element $V_{\sigma i} = \int d^2r V^{\mathrm{ext}}_{\sigma}(x,y)\,|W_{\sigma i}(x,y)|^2$, which varies in space. However, since the variation is slow it will almost be constant over a cell situated at the i'th lattice site and can therefore be taken outside the integral, $V_{\sigma i} \equiv V^{\mathrm{ext}}_{\sigma}(x_i,y_i)\int d^2r\,|W_{\sigma i}(x,y)|^2 = V^{\mathrm{ext}}_{\sigma}(x_i,y_i)$ due to the orthonormality of the Wannier-states. A more detailed discussion can be found in [47]. A representation of the single-band nearest neighbor Hubbard Hamiltonian that we will use in our work is given in figure 4.1

4.2 Mean-field theory

To find an approximate ground state of the many-body Hamiltonian (4.3), we use mean-field theory, where every particle is moving in a mean-field generated by the other particles. To do this we define the local pairing order parameter and the particle density as

$$\Delta_i = U \langle \hat{c}_{\downarrow i} \hat{c}_{\uparrow i} \rangle \,, \tag{4.4}$$

$$\langle \hat{n}_{\sigma i} \rangle = \langle \hat{c}^\dagger_{\sigma i} \hat{c}_{\sigma i} \rangle \,. \tag{4.5}$$

Applying Wick's theorem and including only the pairing terms, we obtain the mean-field Hamiltonian

$$\begin{aligned} \hat{H}_{\mathrm{MF}} = &- \sum_{\sigma i} (t_{\sigma x, x+e_x} \hat{c}^\dagger_{\sigma i} \hat{c}_{\sigma i+e_x} + t_{\sigma x, x-e_x} \hat{c}^\dagger_{\sigma i} \hat{c}_{\sigma i-e_x}) \\ &- \sum_{\sigma i} (t_{\sigma y, y+e_y} \hat{c}^\dagger_{\sigma i} \hat{c}_{\sigma i+e_y} + t_{\sigma y, y-e_y} \hat{c}^\dagger_{\sigma i} \hat{c}_{\sigma i-e_y}) \\ &+ \sum_{\sigma i} (V_{\sigma i} - \mu_\sigma) \, \hat{c}^\dagger_{\sigma i} \hat{c}_{\sigma i} + \sum_i \left(\Delta_i \hat{c}^\dagger_{\uparrow i} \hat{c}^\dagger_{\downarrow i} + \Delta_i^* \hat{c}_{\downarrow i} \hat{c}_{\uparrow i} \right) . \end{aligned} \tag{4.6}$$

In the above expression, we have neglected the Hartree and Fock terms and the constant energy terms. We have also introduced the chemical potential, which has the effect of a Lagrange-multiplier to keep the mean number of particles in each spin state $\langle \hat{N}_\sigma \rangle = \sum_i \langle \hat{c}^\dagger_{\sigma i} \hat{c}_{\sigma i} \rangle$ fixed. This is necessary due to the fact that the mean-field Hamiltonian (4.6) no longer commutes with the number operator $\hat{N} = \sum_{\sigma i} \hat{c}^\dagger_{\sigma i} \hat{c}_{\sigma i}$, since it includes terms like $\Delta_i \hat{c}^\dagger_{\uparrow i} c^\dagger_{\downarrow i}$, which creates two particles in a spin-up and spin-down state, respectively. We are thus forced to work in the grand canonical ensemble. Upon minimization of the grand canonical potential $\Omega = \langle \hat{H} \rangle - TS - \sum_\sigma \mu_\sigma \langle \hat{N}_\sigma \rangle$, we obtain the thermodynamic ground state.

4.3 Derivation of the Bogoliubov-de Gennes equations

The Hamiltonian (4.6) is a quadratic form, and can therefore be diagonalized by a unitary Bogoliubov transformation (see [35])

$$\hat{c}_{\uparrow i} = \sum_{E_\eta > 0} \left(u^i_{\eta\uparrow} \hat{\gamma}_{\eta\uparrow} - v^{i*}_{\eta\downarrow} \hat{\gamma}^\dagger_{\eta\downarrow} \right), \quad \hat{c}_{\downarrow i} = \sum_{E_\eta > 0} \left(u^i_{\eta\downarrow} \hat{\gamma}_{\eta\downarrow} + v^{i*}_{\eta\uparrow} \hat{\gamma}^\dagger_{\eta\uparrow} \right). \tag{4.7}$$

Here, $\hat{\gamma}^\dagger_{\eta\sigma}$ creates a quasi-particle with quantum numbers (η,σ) and is a linear combination of particles and holes. The ground state of the superfluid corresponds to the quasi-particle vacuum, defined as $\hat{\gamma}_{\eta\sigma}|\Psi\rangle = 0$. These new quasi-particle operators must still be fermionic operators and should therefore obey the fermionic anti-commutation relations

$$\hat{\gamma}^\dagger_{\eta\sigma}\hat{\gamma}_{\alpha\sigma'} + \hat{\gamma}_{\alpha\sigma'}\hat{\gamma}^\dagger_{\eta\sigma} = \delta_{\alpha\eta}\delta_{\sigma\sigma'}, \tag{4.8}$$

$$\hat{\gamma}_{\eta\sigma}\hat{\gamma}_{\alpha\sigma'} + \hat{\gamma}_{\alpha\sigma'}\hat{\gamma}_{\eta\sigma} = 0. \tag{4.9}$$

The occupation probability of the non-interacting quasi-particles will, in thermal equilibrium, be described by the Fermi-Dirac distribution:

$$\left\langle \hat{\gamma}^\dagger_{\eta\sigma}\hat{\gamma}_{\alpha\sigma'} \right\rangle = \delta_{\eta\alpha}\delta_{\sigma\sigma'} f_{\eta\sigma} = \tfrac{1}{1+e^{E_{\eta\sigma}/k_{\mathrm{B}}T}}\delta_{\eta\alpha}\delta_{\sigma\sigma'} \tag{4.10}$$

$$\left\langle \hat{\gamma}_{\eta\sigma}\hat{\gamma}_{\alpha\sigma'} \right\rangle = 0, \tag{4.11}$$

and the diagonalized Hamiltonian has a form

$$\hat{H}_{\mathrm{MF}} = E_g + \sum_{\eta\sigma} E_{\eta\sigma}\hat{\gamma}^\dagger_{\eta\sigma}\hat{\gamma}_{\eta\sigma}, \tag{4.12}$$

which can be rewritten in a commutation form

$$\left[\hat{H}_{\mathrm{MF}}, \hat{\gamma}_{\alpha\sigma'}\right] = -E_{\alpha\sigma'}\hat{\gamma}_{\alpha\sigma'}, \tag{4.13}$$

$$\left[\hat{H}_{\mathrm{MF}}, \hat{\gamma}^\dagger_{\alpha\sigma'}\right] = E_{\alpha\sigma'}\hat{\gamma}^\dagger_{\alpha\sigma'}. \tag{4.14}$$

These are the equations fixing the quasi-particle amplitudes. In order to derive the Bogoliubov-de Gennes equations we start by calculating the following commutator by inserting the mean-field Hamiltonian from equation (4.6)

$$\begin{aligned}\left[\hat{c}_{\uparrow k}, \hat{H}_{\mathrm{MF}}\right] = &- t_{\uparrow x,x+e_x}\hat{c}_{\uparrow k+e_x} - t_{\uparrow x,x-e_x}\hat{c}_{\uparrow k-e_x} - t_{\uparrow y,y+e_y}\hat{c}_{\uparrow k+e_y} \\ &- t_{\uparrow y,y-e_y}\hat{c}_{\uparrow k-e_y} + (V_{\uparrow k} - \mu_\uparrow)\,\hat{c}_{\uparrow k} + \Delta_k\hat{c}^\dagger_{\downarrow k}.\end{aligned} \tag{4.15}$$

The left-hand side of equation (4.15) can also be calculated using the Bogoliubov transformation of the creation and annihilation operators (4.7), and equations (4.13) and (4.14), to give

$$\left[\hat{c}_{\uparrow k}, \hat{H}_{\mathrm{MF}}\right] = \sum_{\eta} \left(u^{k}_{\eta\uparrow} \hat{\gamma}_{\eta\uparrow} E_{\eta\uparrow} + v^{k*}_{\eta\downarrow} \hat{\gamma}^{\dagger}_{\eta\downarrow} E_{\eta\downarrow} \right). \tag{4.16}$$

The Bogoliubov-de Gennes equations follow immediately by comparison of the coefficients. We could in a similar manner calculate $[\hat{c}_{k\downarrow}, \hat{H}_{\mathrm{MF}}]$ and would arrive at the second Bogoliubov-de Gennes equation for the spin-up state. The Bogoliubov-de Gennes equations then take the matrix form

$$\begin{pmatrix} \hat{L}_{\uparrow} & \hat{\Delta} \\ \hat{\Delta}^{*} & -\hat{L}^{*}_{\downarrow} \end{pmatrix} \begin{pmatrix} u^{i}_{\eta\uparrow} \\ v^{i}_{\eta\uparrow} \end{pmatrix} = E_{\eta\uparrow} \begin{pmatrix} u^{i}_{\eta\uparrow} \\ v^{i}_{\eta\uparrow} \end{pmatrix}, \tag{4.17}$$

where

$$\begin{aligned} \hat{L}_{\uparrow} u^{i}_{\eta\uparrow} = & - t_{\uparrow x, x+e_x} u^{i+e_x}_{\eta\uparrow} - t_{\uparrow x, x-e_x} u^{i-e_x}_{\eta\uparrow} \\ & - t_{\uparrow y, y+e_y} u^{i+e_y}_{\eta\uparrow} - t_{\uparrow y, y-e_y} u^{i-e_y}_{\eta\uparrow} + \left(V_{\uparrow i} - \mu_{\uparrow}\right) u^{i}_{\eta\uparrow}, \end{aligned} \tag{4.18}$$

and

$$\hat{\Delta} u^{i}_{\eta\uparrow} = \Delta_i u^{i}_{\eta\uparrow}. \tag{4.19}$$

We change notation which makes the structure of the Bogoliubov-de Gennes equations more transparent. This means that we use the following notation when writing the Bogoliubov-de Gennes equations

$$\sum_{j} \begin{pmatrix} L_{ij\uparrow} & \Delta_{ij} \\ \Delta^{*}_{ji} & -L^{*}_{ij\downarrow} \end{pmatrix} \begin{pmatrix} u^{j}_{\eta\uparrow} \\ v^{j}_{\eta\uparrow} \end{pmatrix} = E_{\eta} \begin{pmatrix} u^{i}_{\eta\uparrow} \\ v^{i}_{\eta\uparrow} \end{pmatrix}, \tag{4.20}$$

with $\Delta_{ij} = \Delta_i \delta_{ij}$ and

$$L_{ij\uparrow} = -t_{\uparrow i,j} \delta_{\langle ij \rangle} + \left(V_{\uparrow i} - \mu_{\uparrow}\right) \delta_{ij}. \tag{4.21}$$

Here we have introduced δ_{ij} and $\delta_{\langle ij\rangle}$ which are the Kronecker delta functions connecting on-site and nearest neighbor sites, respectively. The tunneling amplitude is given by

$$t_{\sigma i,j} = \begin{cases} t_{\sigma x,x+e_x} & \text{if } j = i + e_x \\ t_{\sigma x,x-e_x} & \text{if } j = i - e_x \\ t_{\sigma y,y+e_y} & \text{if } j = i + e_y \\ t_{\sigma y,y-e_y} & \text{if } j = i - e_y. \end{cases} \tag{4.22}$$

4.3.1 Duality of the solutions

It is sufficient to solve the Bogoliubov-de Gennes equations for the spin-up particles due to the duality of the spin-up and spin-down solutions, i.e.,

$$E_{\eta\sigma} \leftrightarrow -E_{\eta\bar{\sigma}}, \quad \begin{pmatrix} u^i_{\eta\sigma} \\ v^i_{\eta\sigma} \end{pmatrix} \leftrightarrow \begin{pmatrix} -v^{i*}_{\eta\bar{\sigma}} \\ u^{i*}_{\eta\bar{\sigma}} \end{pmatrix}. \tag{4.23}$$

We illustrate this by taking the Bogoliubov-de Gennes equations for the spin-up particles as our starting point and make the above substitutions to find that

$$\sum_j -L_{ij\uparrow} v^{j*}_{\eta\downarrow} + \Delta_i u^{i*}_{\eta\downarrow} = E_{\eta\downarrow} v^{i*}_{\eta\downarrow}, \tag{4.24}$$

$$\sum_j -L^*_{ij\downarrow} u^{j*}_{\eta\downarrow} - \Delta^*_i v^{i*}_{\eta\downarrow} = -E_{\eta\downarrow} u^{i*}_{\eta\downarrow}. \tag{4.25}$$

If we now complex conjugate both equations and multiply equation (4.25) by -1 we obtain the following equations

$$\sum_j -L^*_{ij\uparrow} v^{j}_{\eta\downarrow} + \Delta^*_i u^{i}_{\eta\downarrow} = E_{\eta\downarrow} v^{i}_{\eta\downarrow}, \tag{4.26}$$

$$\sum_j L_{ij\downarrow} u^{j}_{\eta\downarrow} + \Delta_i v^{i}_{\eta\downarrow} = E_{\eta\downarrow} u^{i}_{\eta\downarrow}, \tag{4.27}$$

which are recognized as the Bogoliubov-de Gennes equations of the spin-down particles.

4.4 Results

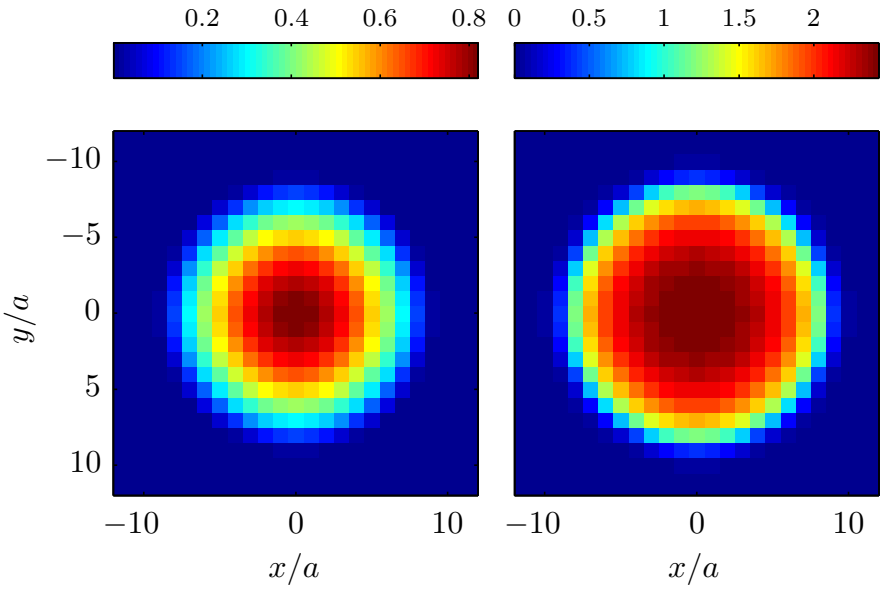

Figure 4.2 | Right: The on-site pairing order parameter. Left: The particle density for a balanced Fermi gas with $U/t = -6$, $\bar{\omega} = \sqrt{ma^2/t\omega} = 0.3$, $k_{\mathrm{B}}T/t = 10^{-5}$, and $N_\uparrow = N_\downarrow = 50$.

We choose the external potential to be a 2D harmonic trapping potential, since the lasers creating the optical lattice have a Gaussian profile and a confining harmonic trapping potential is often used in experiments. For simplicity, we choose an isotropic spin-independent trapping potential $\omega_{\uparrow x} = \omega_{\downarrow x} = \omega_{\uparrow y} = \omega_{\downarrow y} \equiv \omega$ and define $\bar{\omega} \equiv \sqrt{ma^2/t\omega}$. We also choose the tunneling amplitudes to be spin and direction independent (i.e. $t_{\uparrow x,x\pm e_x} = t_{\downarrow x,x\pm e_x} = t_{\uparrow y,y\pm e_y} = t_{\downarrow y,y\pm e_x} \equiv t$) in the following calculations. A numerical self-consistent calculation is performed using Broyden's algorithm keeping the number of particles in each spin state fixed and iterating with respect to Δ_i, $n_{\uparrow i}$, $n_{\downarrow i}$, $\mu_\uparrow$, and $\mu_\downarrow$.

Figure 4.2 (right) shows the on-site s-wave pairing order parameter, which is calculated by inserting the Bogoliubov transformation (4.7) into the expression for the pairing order parameter

$$\Delta_i = U \sum_\eta u^i_{\eta\uparrow} v^{i*}_{\eta\uparrow} f_{\eta\uparrow} \tag{4.28}$$

for a balanced Fermi gas with $U/t = -6$, $\bar{\omega} = \sqrt{ma^2/t}\omega = 0.3$, $k_\mathrm{B}T/t = 10^{-5}$, and $N_\uparrow = N_\downarrow = 50$. The sum is over positive and negative energies since we have made use of the duality relations (4.23). Figure 4.2 (left) shows the particle density calculated from the sum of

$$n_{\uparrow i} = \sum_\eta \left|u^i_{\eta\uparrow}\right|^2 f_{\eta\uparrow}, \tag{4.29}$$

$$n_{\downarrow i} = \sum_\eta \left|v^i_{\eta\uparrow}\right|^2 (1 - f_{\eta\uparrow}), \tag{4.30}$$

with the same parameters. As in (4.28) we have made use of the duality relations (4.23) and therefore perform the sum over positive as well as negative energies.

The equivalent calculations of the pairing order parameter have been performed for an imbalanced Fermi gas with $U/t = -4$, $\bar{\omega} = \sqrt{ma^2/t}\omega = 0.3$, $k_\mathrm{B}T/t = 10^{-5}$, $N_\downarrow = 55$, and $N_\uparrow = 40$, which is shown in figure 4.3 (right). This system is also studied in [48] for fermions in an optical lattice with harmonic confinement. It is seen that the sign of the pairing parameter oscillates in the radial direction for the imbalanced Fermi gas indicating a Fulde-Ferrell-Larkin-Ovchinnikov (FFLO) state. FFLO states have also been studied in lattice systems in [49]. Finally, figure 4.3 (left) shows the difference in the number of spin-up and spin-down particles $n_{\downarrow i} - n_{\uparrow i}$ on each lattice site for the imbalanced Fermi gas with the same parameters. We have furthermore shown a cut along the x-axis of the order parameters in figure 4.4 where it is very clear that the excess spin down particles are placed on a ring at the boundaries of the density cloud. This is also where we observe the oscillation in the s-wave pairing order parameter.

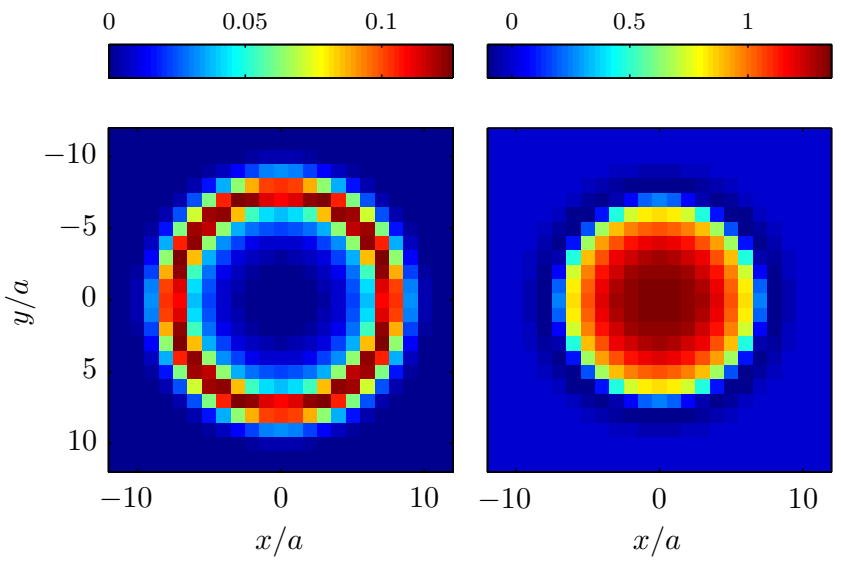

Figure 4.3 | Left: The density difference $\langle \hat{n}_{\downarrow i} - \hat{n}_{\uparrow i} \rangle$. Right: The pairing order parameter $\Delta_i = U \sum_\eta u^i_{\eta\uparrow} v^{i*}_{\eta\uparrow} f_{\eta\uparrow}$ for an imbalanced Fermi gas with $U/t = -4$, $\bar{\omega} = \sqrt{ma^2/t}\omega = 0.3$, $k_\mathrm{B}T/t = 10^{-5}$, $N_\uparrow = 40$, and $N_\downarrow = 55$.

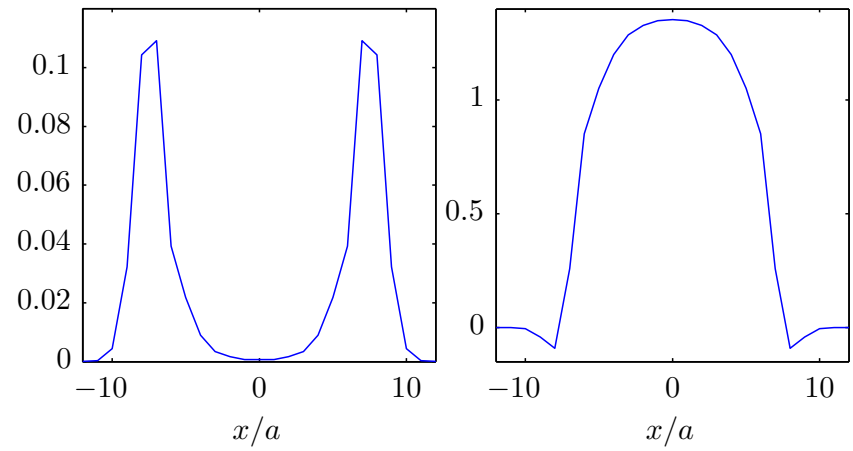

Figure 4.4 | Left: A cut along the x-axis of the density difference $\langle \hat{n}_{\uparrow i} - \hat{n}_{\downarrow i} \rangle$. Right: A cut along the x-axis of the pairing order parameter $\Delta_i = U \sum_\eta u^i_{\eta\uparrow} v^{i*}_{\eta\uparrow} f_{\eta\uparrow}$ for an imbalanced Fermi gas with $U/t = -4$, $\bar{\omega} = \sqrt{ma^2/t}\omega = 0.3$, $k_\mathrm{B}T/t = 10^{-5}$, $N_\uparrow = 40$, and $N_\downarrow = 55$.

4.5 A rotating Fermi gas

4.5.1 Introduction to vortices

Vortices exist on large as well as on small scales in nature, ranging from enormous tornadoes to microscopic quantized vortices in superfluids. The quantized vortices are direct evidence for superfluidity since they are a consequence of the macroscopic occupation of a single quantum state. These were observed by the group of Ketterle for a strongly interacting Fermi gas under rotation [50].

The superfluid velocity is given by $\boldsymbol{v}_\mathrm{s} = \frac{\hbar}{m_\mathrm{p}}\nabla\Theta$ [31], where Θ is the phase of the gap parameter $\Delta = |\Delta|\, e^{i\Theta}$, $m_\mathrm{p} = 2m$, and the mass of the fermions is denoted m. Since the velocity is proportional to the gradient of the phase, a superfluid velocity can only be present if the phase varies in space and is only well-defined when the gap parameter is well-defined. Also, since the velocity is the gradient of a scalar function, it is irrotational, that is, $\nabla \times \boldsymbol{v}_\mathrm{s} = 0$ in simply connected regions. Therefore, rotation can only take place in a multiply connected region. One way to create such a multiply connected region is to make a nodal line in the order parameter. The phase can then wind $n2\pi$ around the nodal line. This makes a vortex with winding number n. The circulation Γ describing the flow around a vortex is given by integrating the velocity around a closed loop in the superfluid

$$\Gamma = \oint \boldsymbol{v}_s \cdot d\boldsymbol{l} = \frac{\hbar}{m_\mathrm{p}} \oint \nabla\Theta(\boldsymbol{r}) \cdot d\boldsymbol{l} = n\frac{h}{m_\mathrm{p}} = n\Gamma_0, \tag{4.31}$$

where the winding number $n \in \mathbb{Z}$ is zero in a simply connected region. The consequences of this discrete circulation is that angular momentum can only enter the system in quantized units.

When fermions are placed in a rotating potential the Hamiltonian will take a form which is very similar to the Hamiltonian describing a charged particle in a magnetic field. This experiment can therefore be used to study a well-known problem in physics concerning charged particles moving through a lattice under an applied magnetic field. In a tight-binding description the band of the energy spectrum will split into magnetic bands forming the so-called Hofstadter butterfly spectrum. The energy gaps in

the spectrum lead to an insulating regime. For conventional superconductors, this insulating regime can be achieved only by applying very strong magnetic fields [36]. So one possibility to study this regime is by using fermions in rotating lattices. Rotation frequencies of up to 1kHz have been reached in [51]. A rotating quasi-2D optical lattice can be created by a rotating mask as in [52].

4.5.2 Unitary transformation to a co-rotating frame

To create vortices we set the system into rotation with frequency Ω around the z-axis and switch to a co-rotating frame where the Hamiltonian is time-independent in order to study thermodynamics. The co-rotating coordinates transform according to

$$|\boldsymbol{r}'\rangle = \hat{\mathcal{U}}\,|\boldsymbol{r}\rangle = e^{\frac{-i\Omega t\hat{L}_z}{\hbar}}\,|\boldsymbol{r}\rangle\,, \tag{4.32}$$

$$\langle\boldsymbol{r}'|\psi\rangle = \langle\boldsymbol{r}|\hat{\mathcal{U}}^\dagger|\psi\rangle = \langle\boldsymbol{r}|\psi_{\mathrm{rot}}\rangle\,. \tag{4.33}$$

So instead of rotating the coordinates we can think of it as rotating the state ket in the other direction. The Hamiltonian that describes the time-evolution of the state is then

$$\begin{aligned} i\hbar\frac{\partial}{\partial t}\,|\psi_{\mathrm{rot}}\rangle &= i\hbar\frac{\partial}{\partial t}\hat{\mathcal{U}}^\dagger\,|\psi\rangle = -\Omega\hat{L}_z\,|\psi_{\mathrm{rot}}\rangle + \hat{\mathcal{U}}^\dagger\hat{H}_{\mathrm{lab}}(t)\hat{\mathcal{U}}\hat{\mathcal{U}}^\dagger\,|\psi\rangle \\ &= -\Omega\hat{L}_z\,|\psi_{\mathrm{rot}}\rangle + \hat{H}_{\mathrm{lab}}\,|\psi_{\mathrm{rot}}\rangle = \hat{H}_{\mathrm{rot}}\,|\psi_{\mathrm{rot}}\rangle\,, \end{aligned} \tag{4.34}$$

where we have used that $\hat{\mathcal{U}}^\dagger\hat{H}_{\mathrm{lab}}(t)\hat{\mathcal{U}} = \hat{H}_{\mathrm{lab}}$. So $\hat{H}_{\mathrm{lab}}$ is now time-independent and corresponds to the time when the two coordinate systems are identical.

One immediately realizes that the energy in this rotating frame decreases with increasing rotation frequency when the angular momentum is non-zero and when the external rotation and the flow are parallel. It increases when the rotational flow is opposite to the external rotation. Also, at a certain critical velocity the state with a vortex becomes energetically favorable compared to the ground state of the non-rotating potential.

4.5.3 Rotation of a 2D optical lattice with harmonic confinement

The single-particle Hamiltonian of a particle in a 2D optical lattice with harmonic confinement rotating with frequency Ω around the z-axis reads

$$\begin{aligned} H &= \frac{\boldsymbol{p}^2}{2m} + \frac{1}{2}m\omega^2 r_i^2 - \Omega\hat{z}\cdot\boldsymbol{r}\times\boldsymbol{p} + \sum_{i=x,y} V_i^0 \sin^2(k_{\mathrm{L}}x_i) \\ &= \frac{(\boldsymbol{p} - m\Omega\hat{z}\times\boldsymbol{r})^2}{2m} + \frac{1}{2}m(\omega^2-\Omega^2)r_i^2 + \sum_{i=x,y} V_i^0 \sin^2(k_{\mathrm{L}}x_i). \end{aligned} \tag{4.35}$$

The Hamiltonian (4.35) has almost the same form as the Hamiltonian of a charged particle moving under the influence of a magnetic field directed along the z-axis. However, under closer inspection we see that (4.35) has an additional centrifugal term.

To incorporate the rotation into the mean-field Hubbard Hamiltonian (4.6) we use Peierls substitution [36]

$$\begin{aligned} \hat{H}_{\mathrm{MF}} = &\sum_{\sigma i}\left(-te^{-i\phi_{i,i+e_x}}\hat{c}^\dagger_{\sigma i}\hat{c}_{\sigma i+e_x} - te^{-i\phi_{i,i-e_x}}\hat{c}^\dagger_{\sigma i}\hat{c}_{\sigma i-e_x}\right) \\ &+ \sum_{\sigma i}\left(-te^{-i\phi_{i,i+e_y}}\hat{c}^\dagger_{\sigma i}\hat{c}_{\sigma i+e_y} - te^{-i\phi_{i,i-e_y}}\hat{c}^\dagger_{\sigma i}\hat{c}_{\sigma i-e_y}\right) \\ &+ \sum_{\sigma i}\left(\frac{1}{2}m(\omega^2-\Omega^2)r_i^2 - \mu_\sigma\right)\hat{c}^\dagger_{\sigma i}\hat{c}_{\sigma i} + \sum_i\left(\Delta_i\hat{c}^\dagger_{\uparrow i}\hat{c}^\dagger_{\downarrow i} + \Delta_i^*\hat{c}_{\downarrow i}\hat{c}_{\uparrow i}\right), \end{aligned} \tag{4.36}$$

where $\phi_{i,j} = \frac{m}{\hbar}\int_{\boldsymbol{r}_i}^{\boldsymbol{r}_j} d\boldsymbol{r}\cdot(\boldsymbol{\Omega}\times\boldsymbol{r})$ if we take $\Omega_\uparrow = \Omega_\downarrow \equiv \Omega$. For example, $\phi_{i,i+e_x} = -\alpha\bar{\omega}\bar{y}_i\sqrt{\pi^2 t/(2E_{\mathrm{R}})}$ can be expressed in terms of the recoil energy $E_{\mathrm{R}} = \frac{\hbar^2\pi^2}{2ma^2}$, a dimensionless length $\bar{y} = y/a$, and $\alpha = \Omega/\omega$. By approximating the Wannier functions by Gaussians we calculate the tunneling amplitude using [53]

$$t/E_{\mathrm{R}} = (V^0/E_{\mathrm{R}})^{3/4}\pi^{5/4}\left[1-(2/\pi)^2\right]\exp(-\pi^{3/2}\sqrt{V^0/E_{\mathrm{R}}}/4)/4. \tag{4.37}$$

We choose $V_0/E_{\mathrm{R}} = 5$ and obtain a tunneling amplitude of $t/E_{\mathrm{R}} = 0.09$, which is used in the following calculations. It is stressed that the frequency

of the trapping potential should be larger than the rotation frequency to have confinement.

4.5.4 Results

Solving the Bogoliubov-de Gennes equations self-consistently we find the pairing order parameter and the particle density of a balanced system with $U/t = -6$, $\bar{\omega} = 0.3$, $k_{\mathrm{B}}T/t = 10^{-4}$, $N_\uparrow = N_\downarrow = 85$, and $\alpha = 0.1$.

Figure 4.5 (right) shows the phase of the pairing order parameter $\Delta_i = U \sum_\eta u^i_{\eta\uparrow} v^{i*}_{\eta\uparrow} f_{\eta\uparrow}$ clearly illustrating the 2π phase winding associated with the vortex. Figure 4.5 (left) shows the density of particles $\langle \hat{n}_{\uparrow i} + \hat{n}_{\downarrow i} \rangle$.

In figure 4.6 we plot a cut along the x-axis of the same system. In the left figure we show again the density where the peak in the density is shown to be located at the central point (also observed for bosons in [54]). In the right figure we show the amplitude of the pairing order parameter where we see that there is a dip in the amplitude which together with the behavior of the phase provides evidence for the existence of the vortex in the system. We would expect the density to show no significant change in the presence of a vortex in accordance with [55]. However, we speculate that this is a lattice effect.

Figure 4.7 (right) shows a cut of the amplitude of the pairing order parameter along the x-axis for different interaction strengths for a system with $\bar{\omega} = 0.3$, $k_{\mathrm{B}}T/t = 10^{-4}$, $N_\uparrow = N_\downarrow = 85$, and $\alpha = 0.1$. The size of the vortex is characterized by the healing length which can be thought of as the length the pairing order parameter takes to heal from zero to its bulk value. For a bulk system it is given by $\xi = \frac{\hbar v_{\mathrm{F}}}{\pi \Delta}$ [35] where v_{F} is the Fermi velocity. We see in figure 4.7 that the healing length as expected increases with decreasing size of the interaction strength and therefore also with decreasing size of the pairing order parameter. We observe that when U becomes comparable to t the vortex starts to vanish which we would also expect since the interaction then becomes too weak to stabilize a vortex. This is also observed in the density shown for the same interaction strengths in figure 4.7 (left) where the peak in the density distribution vanishes for $U/t = -2$ and it becomes smooth.

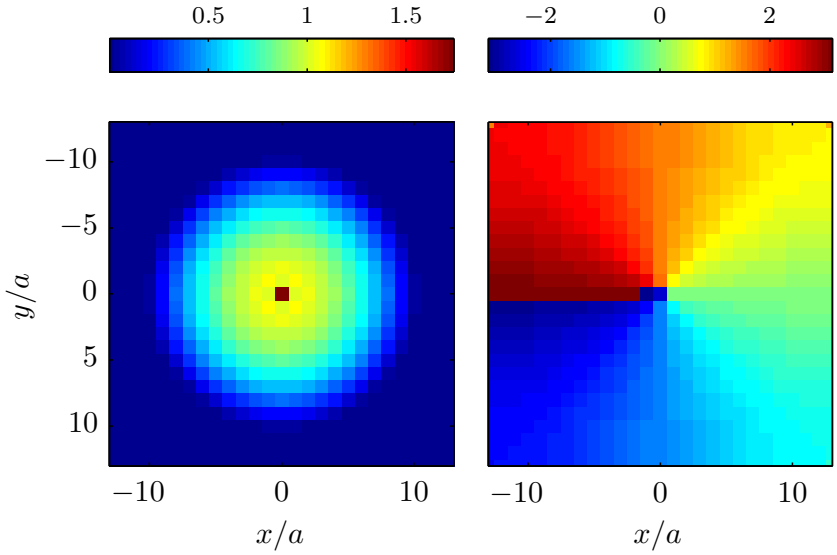

Figure 4.5 | Left: The total number density $\langle \hat{n}_{\uparrow i} + \hat{n}_{\downarrow i} \rangle$. Right: The phase of the pairing order parameter $\Delta_i = U \sum_\eta u^i_{\eta\uparrow} v^{i*}_{\eta\uparrow} f_{\eta\uparrow}$ for a balanced fermonic gas with $U/t = -6$, $\bar{\omega} = 0.3$, $k_B T/t = 10^{-4}$, $N_\uparrow = N_\downarrow = 85$, and $\alpha = 0.1$.

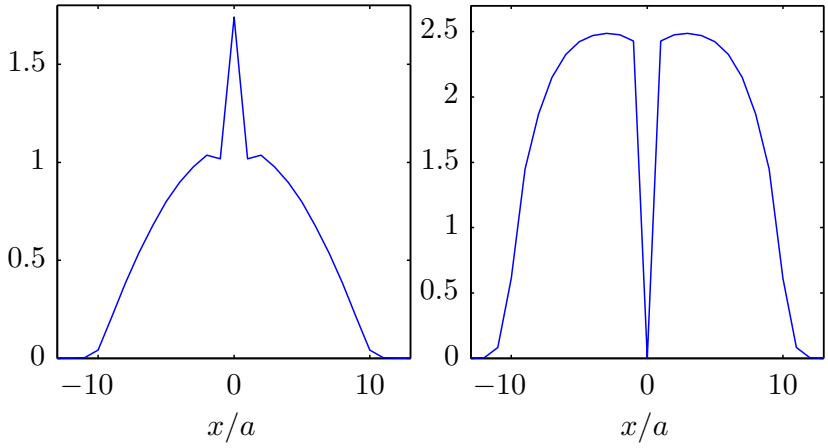

Figure 4.6 | Left: A cut along the x-axis of the total density $\langle \hat{n}_{\uparrow i} + \hat{n}_{\downarrow i} \rangle$. Right: A cut along the x-axis of the amplitude of the pairing order parameter $\Delta_i = U \sum_\eta u^i_{\eta\uparrow} v^{i*}_{\eta\uparrow} f_{\eta\uparrow}$ for a balanced fermonic gas with $U/t = -6$, $\bar{\omega} = 0.3$, $k_B T/t = 10^{-4}$, $N_\uparrow = N_\downarrow = 85$, and $\alpha = 0.1$.

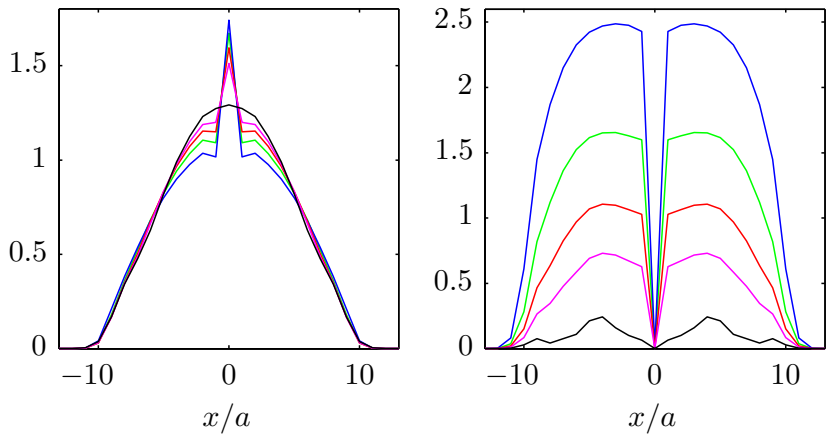

Figure 4.7 | Left: The total density $\langle \hat{n}_{\uparrow i} + \hat{n}_{\downarrow i} \rangle$. Right: The amplitude of the gap parameter for different interaction strengths with $\bar{\omega} = 0.3$, $k_B T/t = 10^{-4}$, $N_\uparrow = N_\downarrow = 85$, and $\alpha = 0.1$. Blue solid line corresponds to $U/t = -6$, green solid line $U/t = -4.5$, red solid line $U/t = -3.5$, pink solid line $U/t - 2.8$, and black solid line $U/t = -2$.

4.6 Superfluidity

4.6.1 Introduction to superfluidity

The first evidence of the existence of superfluidity of fermions in an optical lattice was found in [18]. Superfluidity was signaled by peaks in the interference patterns observed upon releasing the gas. However, when fermions are strongly interacting the peaks in the interference patterns can be smeared out. In order to circumvent this problem a magnetic field ramp was used in the experiment to increase the detuning from the Feshbach resonance, where the atomic scattering channel is degenerate with a bound molecular state. In this way they were able to decrease the interaction strength before turning off the confining potential.

The discrete version of the superfluid velocity of the paired fermions takes the following form

$$v_{\mathrm{s}}^{i} = \frac{\hbar}{m_{\mathrm{p}}} \nabla \Theta_i, \tag{4.38}$$

where i indicates the lattice site.

One model that is often considered is the two-fluid model consisting of a normal fluid with density n_{n} and velocity $\boldsymbol{v}_{\mathrm{n}}$ and a superfluid with density n_{s} and velocity $\boldsymbol{v}_{\mathrm{s}}$ introduced independently by Landau and Tisza. The normal component is restricted by certain boundary conditions, whereas the superfluid component is an independent thermodynamic variable and it is therefore possible to have a finite superfluid velocity with respect to the walls even if the normal fluid must come to rest with respect to the walls.

4.6.2 An analytical calculation of the superfluid density

If we impose twisted boundary conditions on the phase of the gap parameter it follows from equation (4.38), that a superfluid flow will be present with a corresponding kinetic energy. For a sufficiently small phase twist we can associate the change in the free energy of the ground state from the twisted to the untwisted system entirely to the kinetic energy of the flow.

We denote by F_Θ the free energy when the phase of the order parameter varies by $\delta\Theta$ between neighboring sites in the x-direction, and by F_0 the

free energy when there is no phase twist [56]. Associated with the phase twist, we define the site-dependent superfluid density $n^i_{\mathrm{s},x}$ by writing

$$F_\Theta - F_0 = \sum_i \frac{1}{2} n^i_{\mathrm{s},x} m^* {v_\mathrm{s}}^2 = \sum_i \frac{1}{4} t n^i_{\mathrm{s},x} \delta\Theta^2, \tag{4.39}$$

where $v_\mathrm{s} = \hbar\delta\Theta/2m^*a$ is the superfluid velocity of the Cooper pairs with mass $2m^*$. The effective mass for the dispersion $\epsilon_\mathbf{k} = -2t(\cos k_x a + \cos k_y a)$ is $m^* = \hbar^2/2ta^2$. A linear phase twist along the x-direction is equivalent to acting on the Hamiltonian with the gauge transformation

$$\hat{H}_\Theta = e^{-i\delta\theta\sum_l \hat{x}_l/a} \hat{H} e^{i\delta\theta\sum_l \hat{x}_l/a}, \tag{4.40}$$

where x_l is the x-coordinate of particle l [57]. We have $\delta\Theta = 2\delta\theta$ since the superfluid order parameter involves two particles so that the gauge transformation gives $\Delta_i \rightarrow \Delta_i \exp[2ix_i\delta\theta/a]$. The effect of the gauge transformation is to introduce a phase factor on the tunneling amplitudes $t\hat{c}^\dagger_i \hat{c}_{i\pm e_x} \rightarrow te^{\pm i\delta\theta}\hat{c}^\dagger_i \hat{c}_{i\pm e_x}$. Expanding to second order in $\delta\theta$, we obtain $\hat{H}_\Theta = \hat{H} + \hat{J} + \hat{T}$ with

$$\begin{aligned}
\hat{J} &= -i\delta\theta t \sum_{i\sigma} \left(\hat{c}^\dagger_{\sigma i} \hat{c}_{\sigma i+e_x} - \hat{c}^\dagger_{\sigma i} \hat{c}_{\sigma i-e_x} \right), \\
\hat{T} &= \frac{t}{2}\delta\theta^2 \sum_{i\sigma} \left(\hat{c}^\dagger_{\sigma i} \hat{c}_{\sigma i+e_x} + \hat{c}^\dagger_{\sigma i} \hat{c}_{\sigma i-e_x} \right).
\end{aligned} \tag{4.41}$$

Since the unitary transformation conserves particle number, we can take $F_\Theta - F_0 = \Omega_\Theta - \Omega_0$ where $\Omega = F - \mu N$ with N the total number of particles [58]. The grand canonical potential is found by using a linked cluster expansion

$$\begin{aligned}
\frac{Z}{Z_0} &= \frac{1}{Z_0} \mathrm{Tr}\left[e^{-\beta\hat{H}_\Theta} \right] = \frac{1}{Z_0} \mathrm{Tr}\left[e^{-\beta\hat{H}_0} e^{\beta\hat{H}_0} e^{-\beta\hat{H}_\Theta} \right] \\
&= \frac{1}{Z_0} \mathrm{Tr}\left[e^{-\beta\hat{H}_0} \left(1 + \beta\hat{H}_0 + \frac{1}{2}\beta^2\hat{H}_0^2 + ... \right) \left(1 - \beta\hat{H}_\Theta + \frac{1}{2}\beta^2\hat{H}_\Theta^2 - ... \right) \right] \\
&\approx 1 - \beta \langle \hat{H}_\Theta - \hat{H}_0 \rangle_0 + \frac{\beta^2}{2} \langle \left(\hat{H}_\Theta - \hat{H}_0 \right)^2 \rangle_0,
\end{aligned} \tag{4.42}$$

with $Z_0 = \mathrm{Tr}(e^{-\beta \hat{H}_0})$ the grand partition function for the untwisted system. $\langle \ldots \rangle_0$ denotes the thermal average with respect to the untwisted Hamiltonian. The last equality follows from cyclic permutation of the trace. From a Taylor expansion of the logarithm we get the following for the grand canonical potential (which only includes connected diagrams)

$$\begin{aligned}\Omega_\theta &= -\frac{1}{\beta}\ln\left(Z_0\frac{Z}{Z_0}\right) \\ &\approx \Omega_0 + \langle \hat{H}_\Theta - \hat{H}_0\rangle_0 - \frac{\beta}{2}\left[\langle\left(\hat{H}_\Theta - \hat{H}_0\right)^2\rangle_0 - \left(\langle \hat{H}_\Theta - \hat{H}_0\rangle_0\right)^2\right], \quad (4.43)\end{aligned}$$

which gives

$$\Omega_\Theta - \Omega_0 = \langle \hat{T}\rangle_0 - \frac{\beta}{2}\langle \hat{J}^2\rangle_0 \quad (4.44)$$

in accordance with the linked cluster expansion [59]. We have used that there is no current in the untwisted case, that is, $\langle \hat{J}\rangle_0 = 0$. Mean-field theory gives after some lengthy but straightforward algebra

$$\begin{aligned}\langle \hat{T}\rangle = &\frac{t}{2}\delta\theta^2\sum_{\eta,i}(u^{i*}_{\eta\uparrow}u^{i+e_x}_{\eta\uparrow} + u^{i*}_{\eta\uparrow}u^{i-e_x}_{\eta\uparrow})f_{\eta\uparrow} \\ &+ \frac{t}{2}\delta\theta^2\sum_{\eta,i}(v^{i}_{\eta\uparrow}v^{i+e_x*}_{\eta\uparrow} + v^{i}_{\eta\uparrow}v^{i-e_x*}_{\eta\uparrow})(1-f_{\eta\uparrow}) \quad (4.45)\end{aligned}$$

and

$$\begin{aligned}\langle \hat{J}^2\rangle = -t^2\delta\theta^2\sum_{ij}\sum_{\eta\alpha}\sum_{k,l=-1}^{1}[\; &u^{i*}_{\eta\uparrow}u^{j*}_{\alpha\uparrow}u^{j+ke_x}_{\eta\uparrow}u^{i+le_x}_{\alpha\uparrow}f_{\eta\uparrow}(1-f_{\alpha\uparrow}) \\ &- u^{i*}_{\eta\uparrow}v^{j}_{\eta\uparrow}u^{i+ke_x}_{\alpha\uparrow}v^{j+le_x*}_{\alpha\uparrow}f_{\eta\uparrow}(1-f_{\alpha\uparrow}) \\ &+ v^{i}_{\eta\uparrow}v^{j}_{\alpha\uparrow}v^{j+ke_x*}_{\eta\uparrow}v^{i+le_x*}_{\alpha\uparrow}f_{\alpha\uparrow}(1-f_{\eta\uparrow}) \\ &- v^{i}_{\eta\uparrow}u^{j*}_{\eta\uparrow}v^{i+ke_x*}_{\alpha\uparrow}u^{j+le_x}_{\alpha\uparrow}f_{\alpha\uparrow}(1-f_{\eta\uparrow})]. \quad (4.46)\end{aligned}$$

The duality of the BdG equations has been exploited in the above derivation, which means that the sums in equations (4.45) and (4.46) are taken over positive as well as negative energies. This gives a superfluid density of

$$
\begin{aligned}
n^i_{\mathrm{s},x} = & \frac{1}{2}\sum_{\eta}(u^{i*}_{\eta\uparrow}u^{i+e_x}_{\eta\uparrow} + u^{i*}_{\eta\uparrow}u^{i-e_x}_{\eta\uparrow})f_{\eta\uparrow} \\
& + \frac{1}{2}\sum_{\eta}(v^{i}_{\eta\uparrow}v^{i+e_x*}_{\eta\uparrow} + v^{i}_{\eta\uparrow}v^{i-e_x*}_{\eta\uparrow})(1-f_{\eta\uparrow}) \\
& + \frac{t\beta}{2}\sum_{j}\sum_{\eta\alpha}\sum_{k,l=-1}^{1} kl[u^{i*}_{\eta\uparrow}u^{j*}_{\alpha\uparrow}u^{j+ke_x}_{\eta\uparrow}u^{i+le_x}_{\alpha\uparrow}f_{\eta\uparrow}(1-f_{\alpha\uparrow}) \\
& - u^{i*}_{\eta\uparrow}v^{j}_{\eta\uparrow}u^{i+ke_x}_{\alpha\uparrow}v^{j+le_x*}_{\alpha\uparrow}f_{\eta\uparrow}(1-f_{\alpha\uparrow}) \\
& + v^{i}_{\eta\uparrow}v^{j}_{\alpha\uparrow}v^{j+ke_x*}_{\eta\uparrow}v^{i+le_x*}_{\alpha\uparrow}f_{\alpha\uparrow}(1-f_{\eta\uparrow}) \\
& - v^{i}_{\eta\uparrow}u^{j*}_{\eta\uparrow}v^{i+ke_x*}_{\alpha\uparrow}u^{j+le_x}_{\alpha\uparrow}f_{\alpha\uparrow}(1-f_{\eta\uparrow})].
\end{aligned} \tag{4.47}
$$

As is seen from (4.47) the superfluid density at the i'th lattice site depends on the amplitudes on the neighboring lattice sites along the x-direction.

4.6.3 Superfluidity in a 2D square lattice

To get a better understanding of the superfluid density we first consider the case of fermions in a 2D square lattice without a trap, which has also been studied in [60]. When fermions are placed in a lattice, Bloch's theorem states that the amplitudes can be expanded in a free wave basis, i.e.,

$$
u^i_{\eta\uparrow} = \frac{u_{\boldsymbol{k}\uparrow}e^{-i\boldsymbol{k}\cdot\boldsymbol{r}_i}}{\sqrt{N_{\mathrm{L}}}},\ v^i_{\eta\uparrow} = \frac{v_{\boldsymbol{k}\uparrow}e^{-i\boldsymbol{k}\cdot\boldsymbol{r}_i}}{\sqrt{N_{\mathrm{L}}}}. \tag{4.48}
$$

We consider a spin-balanced fermionic gas with $N_\uparrow = N_\downarrow$ and $\mu_\downarrow = \mu_\uparrow$. Note N_{L} is the number of lattice sites. Thus, $\langle\hat{T}\rangle$ reduces to

$$
\begin{aligned}
\langle\hat{T}\rangle = & \frac{t}{2}\delta\theta^2\sum_{\boldsymbol{k}}|u_{\boldsymbol{k}\uparrow}|^2e^{ik_xa}f_{\boldsymbol{k}\uparrow} + |u_{\boldsymbol{k}\uparrow}|^2e^{-ik_xa}f_{\boldsymbol{k}\uparrow} \\
& + \frac{t}{2}\delta\theta^2\sum_{\boldsymbol{k}}|v_{\boldsymbol{k}\uparrow}|^2e^{ik_xa}(1-f_{\boldsymbol{k}\uparrow}) + |v_{\boldsymbol{k}\uparrow}|^2e^{-ik_xa}(1-f_{\boldsymbol{k}\uparrow}) \\
= & 2t\delta\theta^2\sum_{\boldsymbol{k}}\cos(k_xa)n_{\boldsymbol{k}},
\end{aligned} \tag{4.49}
$$

where $\sum_{\boldsymbol{k}} n_{\boldsymbol{k}} = \sum_{\boldsymbol{k}} |u_{\boldsymbol{k}}|^2 f_{\boldsymbol{k}} + |v_{\boldsymbol{k}}|^2 (1 - f_{\boldsymbol{k}})$ and $f_{\mathbf{k}}$ is the Fermi-Dirac distribution. Similarly $\langle \hat{J}^2 \rangle$ reduces to

$$\langle \hat{J}^2 \rangle = 8t^2 \delta\theta^2 \sum_{\boldsymbol{k}} f_{\boldsymbol{k}}(1 - f_{\boldsymbol{k}}) \sin^2(k_x a). \tag{4.50}$$

Since the superfluid density is now a constant, we will define the superfluid fraction

$$f_{\mathrm{s}} = \frac{N_{\mathrm{L}} n_{\mathrm{s},x}}{N} = \frac{2}{N} \sum_{\boldsymbol{k}} \cos(k_x a) n_{\boldsymbol{k}} - \frac{4\beta t}{N} \sum_{\boldsymbol{k}} f_{\boldsymbol{k}}(1 - f_{\boldsymbol{k}}) \sin^2(k_x a), \tag{4.51}$$

where N is the total number of particles. The quasi-particle excitation energies are given by

$$E_{\boldsymbol{k}} = \sqrt{(\epsilon_{\boldsymbol{k}} - \mu)^2 + \Delta^2}, \tag{4.52}$$

and the amplitudes of the quasi-particle operators are of the form

$$u_{\boldsymbol{k}}^2 = \frac{1}{2}\left(1 + \frac{\epsilon_{\boldsymbol{k}} - \mu}{E_{\boldsymbol{k}}}\right), \; v_{\boldsymbol{k}}^2 = \frac{1}{2}\left(1 - \frac{\epsilon_{\boldsymbol{k}} - \mu}{E_{\boldsymbol{k}}}\right). \tag{4.53}$$

The superfluid fraction is now found in momentum space using the chemical potential and the pairing order parameter found from the self-consistent calculation in the discrete position space with periodic boundary conditions. Figure 4.8 shows the superfluid fraction calculated in momentum space from equation (4.51) and in position space from equation (4.47) as a function of temperature. As expected it is seen that there is extremely good agreement between the superfluid fraction calculated by the two methods. We notice that the superfluid fraction for fermions in an optical lattice does not approach 1 as the temperature goes to zero, which is caused by the localization in the wells of the optical lattice [61]. We note that the calculations are performed using mean-field theory but the critical temperature should in principle be calculated using BKT theory which would give a discontinuous drop to zero of the superfluid fraction at the BKT temperature T_{BKT}.

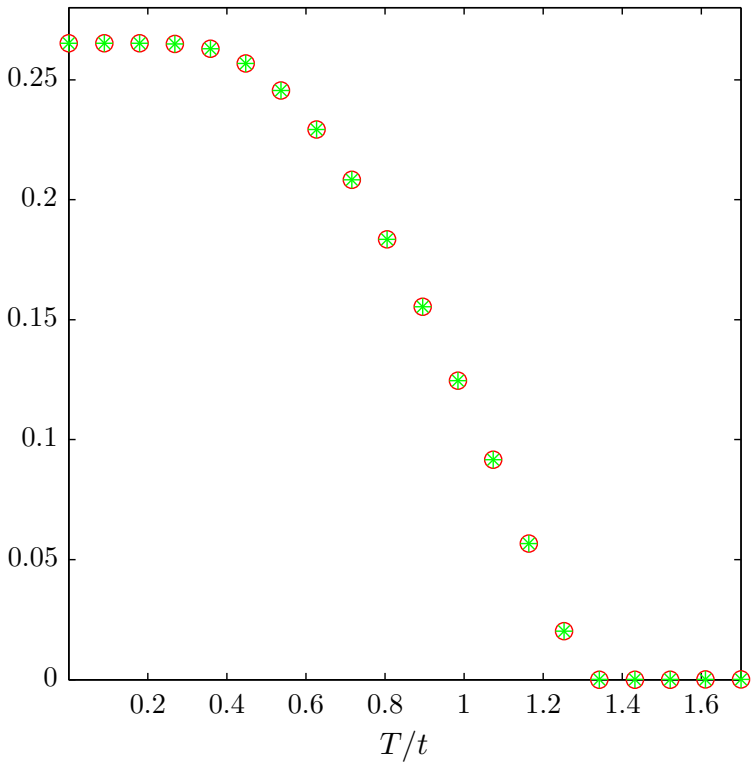

Figure 4.8 | The superfluid fraction calculated in momentum space and position space for a 15x15 lattice with $N_\uparrow = N_\downarrow = 113$ and $U/t = -6$. Red $\circ$'s (real space) and green $\star$'s (momentum space).

4.6.4 A calculation of the superfluid density in the local density approximation

When fermions are placed in an optical lattice with harmonic confinement, the discrete translational invariance breaks down. However, if the confining potential is sufficiently slowly varying, it can be approximated with a constant around each lattice site. This means that the global chemical potential, found from a self-consistent calculation for fermions with attractive interactions placed in an optical lattice with harmonic confinement, can be subtracted the local value of the confining potential to define

a local chemical potential $\mu \to \mu - V(x,y)$. The energies are then just the site-dependent versions of (4.52)

$$E_{\boldsymbol{k}}(x,y) = \sqrt{\xi_{\boldsymbol{k}}^2(x,y) + \Delta^2\,(x,y)}, \tag{4.54}$$

where $\xi_{\boldsymbol{k}}(x,y) = \epsilon_{\boldsymbol{k}} - (\mu - \frac{1}{2}m\omega^2x^2 - \frac{1}{2}m\omega^2y^2)$ and the quasi-particle amplitudes the site-dependent versions of (4.53)

$$u_{\boldsymbol{k}}(x,y)^2 = \frac{1}{2}\left(1 + \frac{\xi_{\boldsymbol{k}}(x,y)}{\sqrt{\xi_{\boldsymbol{k}}(x,y)^2 + \Delta(x,y)^2}}\right), \tag{4.55}$$

$$v_{\boldsymbol{k}}(x,y)^2 = \frac{1}{2}\left(1 - \frac{\xi_{\boldsymbol{k}}(x,y)}{\sqrt{\xi_{\boldsymbol{k}}(x,y)^2 + \Delta(x,y)^2}}\right). \tag{4.56}$$

The superfluid density will then take the following form

$$\begin{aligned} n_s(x,y) = &\frac{2}{N_{\boldsymbol{k},\mathrm{tot}}}\sum_{\boldsymbol{k}} n_{\boldsymbol{k}}(x,y)\cos(k_x a) \\ &- 4\frac{\beta t}{N_{\boldsymbol{k},\mathrm{tot}}}\sum_{\boldsymbol{k}} f_{\boldsymbol{k}}(x,y)(1 - f_{\boldsymbol{k}}(x,y))\sin^2(k_x a). \end{aligned} \tag{4.57}$$

Here $N_{\boldsymbol{k},\mathrm{tot}}$ is the number of $\boldsymbol{k}$-values we have put into the sum.

Figure 4.9 shows the superfluid density calculated on a 20×20 lattice with $N_\uparrow = N_\downarrow = 40$, $U/t = -6$, and $\bar{\omega} = 0.5$ for four selected temperatures decreasing from the upper left corner to the lower right corner. At zero temperature (shown in the upper left corner), the superfluid density is almost flat in the central part but decreases smoothly in the radial direction until it vanishes. At $T/t = 0.5$ the superfluid density is still significant and shows almost no deviation from the zero temperature superfluid density. However, at $T/t = 1$ the central part of the superfluid is less than half of the zero temperature value. At $T/t = 1.5$ the superfluid density has vanished completely. Figure 4.10 shows a cut of the superfluid density along the x-axis. From this figure the shape of the superfluid becomes more pronounced. We see that the shape of the superfluid density does not change significantly with temperature.

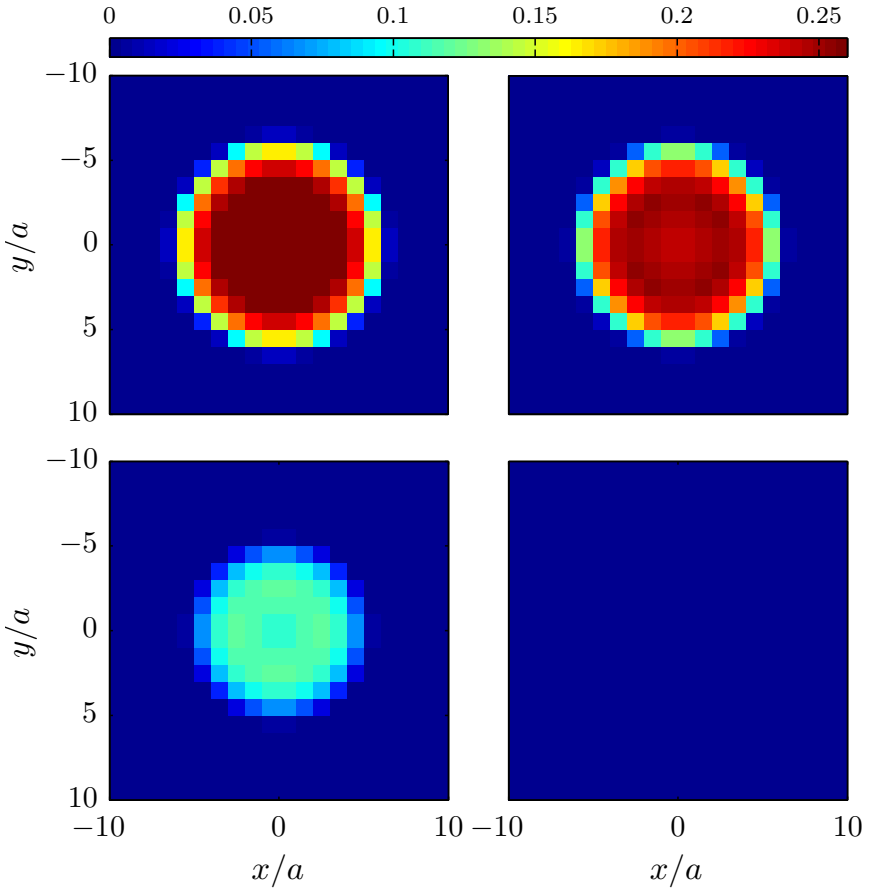

Figure 4.9 | The superfluid density as a function of temperature a 20x20 lattice with $N_\uparrow = N_\downarrow = 40$, $U/t = -6$, $\bar{\omega} = 0.5$. The upper left figure is for $T/t = 0$, the upper right figure for $T/t = 0.5$, the lower left figure for $T/t = 1$, and the lower right figure for $T/t = 1.5$.

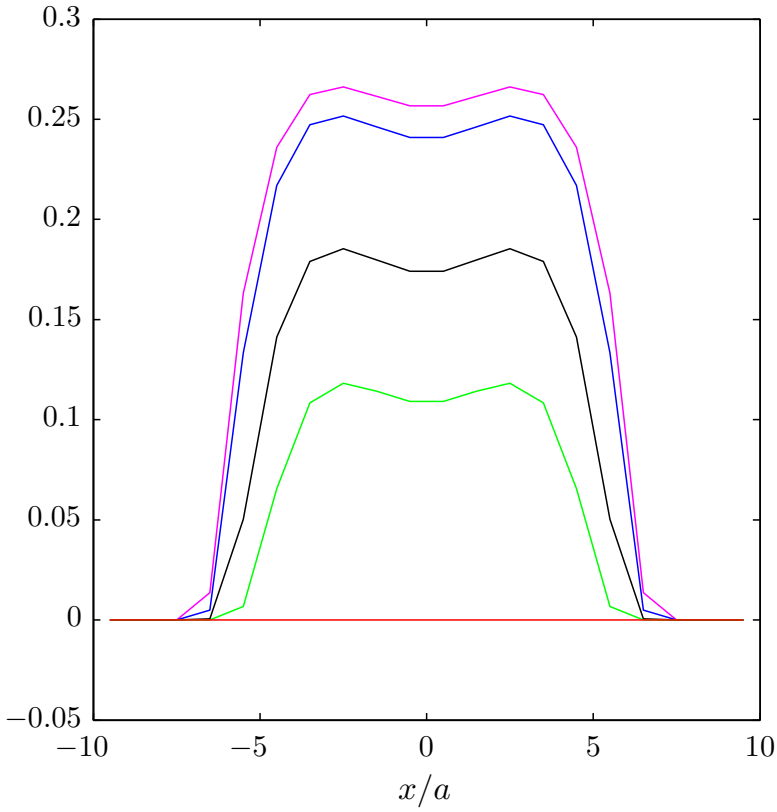

Figure 4.10 | A cut of the superfluid density along the x-axis as a function of temperature on a 20x20 lattice with $N_\uparrow = N_\downarrow = 40$, $U/t = -6$, $\bar{\omega} = 0.5$. The pink solid line is for $T/t = 0$, the blue solid line for $T/t = 0.5$, the black solid line for $T/t = 0.8$, the green solid line for $T/t = 1$, and the red solid line for $T/t = 1.5$.

Chapter

5 A simulation of high-T_C superconductivity

5.1 High-temperature superconductivity

The following chapter is based on the work from our recent paper [62].

The discovery of high-temperature superconductivity in 1986 [63] in cuprates triggered an experimental as well as theoretical effort to understand the mechanisms giving rise to this phenomenon. These high-T_c compounds consist of copper-oxygen layers with the parent compound showing an insulating behavior named the Mott-state. This term is given to systems which in principle should show metallic behavior in accordance to their band structure, but are insulators due to their strong repulsive forces. A generic phase-diagram for the cuprates is shown in figure 5.1 with the parent compound being La_2CuO_4 on the right hand side. When doping the system with Strontium(Sr), which is divalent in contrast to Lanthanum(La) which is trivalent the system becomes hole-doped. This corresponds to the right part of the phase-diagram where x denotes the hole-doping concentration. At zero doping the state is an anti-ferromagnet, corresponding to the spins being aligned antiparallel on neighboring lattice sites and tunneling virtually through the nearest neighbor site with a strength $J \simeq t^2/U$. Associated with this state is the Néel temperature which is around $T \simeq 300$K for this cuprate-type. When the hole-doping is increased the anti-ferromagnetic

state is replaced by a superconducting state with $d_{x^2-y^2}$ symmetry as evidenced from phase-sensitive experiments [64, 65]. The critical temperature T_c of this phase forms a dome-like structure and goes to zero around $x = 0.3$. The region of the phase-diagram above the critical temperature is often denoted the pseudo-gap phase and is associated with a loosely defined phase transition temperature T^*.

It is assumed that the essential physics of high-temperature superconductors can be understood within the framework of the doped antiferromagnet. A single-band Hubbard Hamiltonian in the strong-coupling limit, named the t-J model, gives the first platform to our understanding of the physics taking place. We will in this chapter only consider the hole-doped system. We take the Hubbard Hamiltonian as our starting point with a nearest neighbor hopping term. However, it is believed that the next-nearest neighbor hopping terms should be included to capture the physics giving rise to the anti-symmetry in the phase-diagram of the hole-doped and electron-doped parts of the phase-diagram.

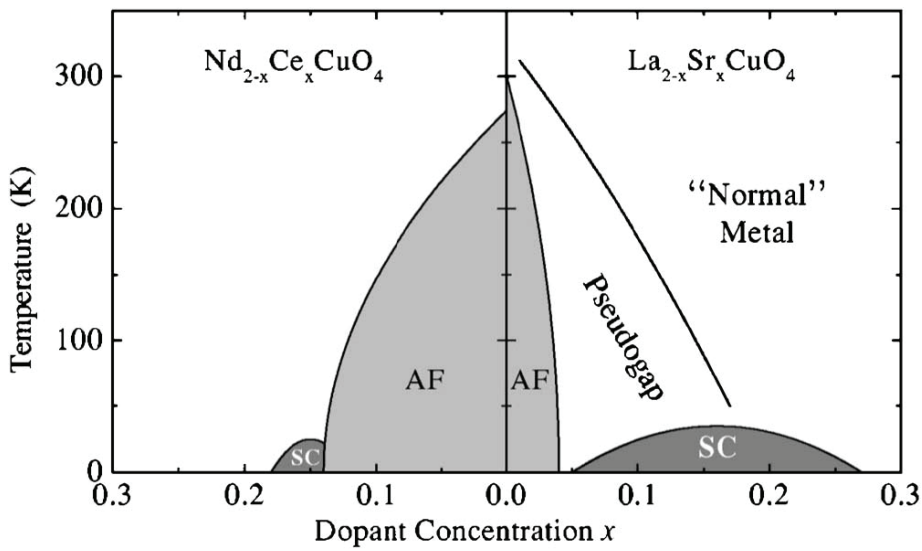

Figure 5.1 | A schematic phase-diagram of the parent compound La_2CuO_4 including the superconducting region with an associated critical temperature T_c, an antiferromagnetic region close to zero hole-doping with the so-called Néel temperature and a pseudo-gap region with the associated temperature T^* [21].

5.2 Motivation

The use of ultracold atoms allows for a thorough investigation of phenomena taking place in condensed matter systems. They embody very clean systems which can be tuned in a very precise and controlled manner from the weak to the strong coupling limit. This enables one to investigate a plethora of interesting phenomena ranging from the dynamics of strongly correlated bosons [7, 66] and fermions [67, 68] to quantum magnetism [69]. In particular, the fermionic Hubbard model has been realized for repulsive and attractive interactions. Fingerprints of the Mott state [70, 71] has already been observed in experiments. The challenge remains to access the Néel phase [72] in order to reveal the presence of high-temperature d-wave superfluidity close to half-filling [73]. Spin fluctuations, which are predicted to be the glue for d-wave superfluidity in the repulsive Hubbard model [20–23], have been studied experimentally in the context of BEC-BCS crossover [19]. In this chapter, we theoretically address the effect of the harmonic potential, which originates from the Gaussian profile of the laser beams generating the trap, on the d-wave superfluid phase of the Hubbard model. We explore the strongly repulsive limit which is realized in high-T_c superconductors [20–23]. The inhomogeneity of the trapping potential leads to a variation of the doping throughout the system. This allows us to map a great part of the phase-diagram of the untrapped system in the same system.

5.3 Basic formalism

We consider a strongly repulsive fermionic gas in a two-dimensional optical lattice confined by a harmonic trapping potential. To address the strongly repulsive regime, we consider the t-J Hamiltonian. The presence of the harmonic trapping potential enables the stabilization of co-existing and competing phases. In particular, at low temperatures, this allows the realization of a d-wave superfluid region surrounded by (gapless) normal edges. Solving the Bogoliubov-de Gennes equations and comparing with the local density approximation, we show that the proximity to the Mott insulator is revealed by a downturn of the Fermi liquid order parameter at the center of the trap where the d-wave gap has a maximum. The density

profile evolves linearly with distance. We consider relatively small fillings such that only a superfluid cloud is confined to the center of the trap and anti-ferromagnetism is hindered by the motion of atoms [74]. We investigate the co-existence between d-wave superfluidity and a normal phase at the boundaries applying an effective theory of a doped Mott insulator. More precisely, we start from the t-J Hamiltonian and apply a low-energy (superfluid) theory that allows us to describe the proximity to the Mott insulator [38, 75, 76].

5.3.1 Derivation of the t-J model

The t-J model applies to strongly interacting systems. A simple way of obtaining this model is by considering only a single spin-up and a single spin-down particle on two lattice sites. The generalization to larger lattice systems then follows immediately. We consider fermions with strongly repulsive on-site interactions in a one-dimensional (1D) lattice of two lattice sites with $U/t \gg 1$. For a system of i lattice sites the lowest band Hubbard Hamiltonian reads

$$\hat{H} = -t \sum_{\langle ij \rangle \sigma} \hat{c}^{\dagger}_{i\sigma} \hat{c}_{j\sigma} + \text{h.c.} + U \sum_{i} \hat{n}_{i\uparrow} \hat{n}_{i\downarrow} = \hat{H}_{\text{t}} + \hat{H}_{\text{int}}, \tag{5.1}$$

with U the on-site interaction strength, t the tunneling amplitude, $\langle ij \rangle$ denoting a sum over nearest neighbors, and $\hat{c}^{\dagger}_{i\sigma}$ the creation operator, creating a particle with spin σ at the i'th lattice site. We divide our space into subspaces consisting of singly occupied states and states which have at least one doubly occupied site and perform a unitary transformation. When expanding in the small parameter t/U, perturbation theory gives us

$$\hat{H} \to \hat{H}' \equiv e^{it\hat{O}} \hat{H} e^{-it\hat{O}} = \hat{H} + it[\hat{O}, \hat{H}] + \frac{i^2 t^2}{2} [\hat{O}, [\hat{O}, \hat{H}]] + ... \tag{5.2}$$

We choose the operator $\hat{O}$ of the form $i\hat{O} = -\frac{1}{tU}[\hat{P}_{\text{s}} \hat{H}_{\text{t}} \hat{P}_{\text{d}} - \hat{P}_{\text{d}} \hat{H}_{\text{t}} \hat{P}_{\text{s}}]$ such that the first order terms in t/U effectively vanish, that is, $\hat{H}_{\text{t}} - it[\hat{H}_{\text{int}}, \hat{O}] = 0$, where $\hat{P}_{\text{s}}$ projects onto the singly occupied subspace and $\hat{P}_{\text{d}}$ projects onto the doubly occupied subspace. We have exploited the fact that $\hat{P}_{\text{s}} \hat{H}_{\text{int}} = 0$ in the above derivation. The Hamiltonian then reduces to

$$\begin{aligned}\hat{H}' &\approx \hat{H}_{\mathrm{t}} + \hat{H}_{\mathrm{int}} + it[\hat{O}, \hat{H}_{\mathrm{t}}] + it[\hat{O}, \hat{H}_{\mathrm{int}}] - \frac{t^2}{2}[\hat{O}, [\hat{O}, \hat{H}_{\mathrm{int}}]] + \hat{O}(t^3) \\ &\approx \hat{H}_{\mathrm{int}} + \frac{it}{2}[\hat{O}, \hat{H}_{\mathrm{t}}]. \end{aligned} \tag{5.3}$$

Projection of the Hamiltonian onto the singly occupied space results in

$$\begin{aligned}\hat{P}_{\mathrm{s}}\hat{H}'\hat{P}_{\mathrm{s}} &= \hat{P}_{\mathrm{s}}\left(\hat{H}_{\mathrm{int}} - \frac{it}{2}[\hat{H}_{\mathrm{t}}, \hat{O}]\right)\hat{P}_{\mathrm{s}} \\ &= \hat{P}_{\mathrm{s}}\left(\frac{t}{2}\left(-\hat{H}_{\mathrm{t}}\frac{1}{tU}\hat{P}_{\mathrm{d}}\hat{H}_{\mathrm{t}} - \frac{1}{tU}\hat{H}_{\mathrm{t}}\hat{P}_{\mathrm{d}}\hat{H}_{\mathrm{t}}\right)\right)\hat{P}_{\mathrm{s}} \\ &= \frac{-1}{U}\hat{P}_{\mathrm{s}}\hat{H}_{\mathrm{t}}\hat{P}_{\mathrm{d}}\hat{H}_{\mathrm{t}}\hat{P}_{\mathrm{s}} = J(\boldsymbol{S}_1 \cdot \boldsymbol{S}_2 - \frac{1}{4}), \end{aligned} \tag{5.4}$$

where $J = 4t^2/U$ and $\boldsymbol{S}_i = 1/2\sum_{\sigma\sigma'}\hat{c}^\dagger_{i\sigma}\sigma^i_{\sigma\sigma'}\hat{c}_{i\sigma'}$ is the spin-operator. The virtual tunneling processes associated with the spin-spin term favor antiferromagnetic ordering of spins on neighboring lattice sites. This mechanism is denoted the super-exchange process and the corresponding Hamiltonian of this correlated magnetic insulator named the Heisenberg Hamiltonian. When the system is shifted away from half-filling we obtain the t-J Hamiltonian.

5.3.2 The trapped t-J model

In the following we consider the t-J model but include the effect of a harmonic trapping potential. A representation of the system of interest is shown in figure 5.2. The Hamiltonian reads

$$\hat{H}_{\text{t-J}} = -t\sum_{\langle ij\rangle\sigma}\left[\hat{c}^\dagger_{i\sigma}\hat{c}_{j\sigma} + \text{h.c.}\right] + \sum_{i\sigma}V_i\hat{c}^\dagger_{i\sigma}\hat{c}_{i\sigma} + J\sum_{\langle ij\rangle}\boldsymbol{S}_i \cdot \boldsymbol{S}_j. \tag{5.5}$$

Here t, the tunneling amplitude, is chosen to be spin and direction independent, and V_i denotes an isotropic and spin independent external trapping potential, $V(x, y) = (m/2)\omega^2(x^2 + y^2)$ evaluated at the i'th lattice site. The number of fermions per site is assumed to be less than one.

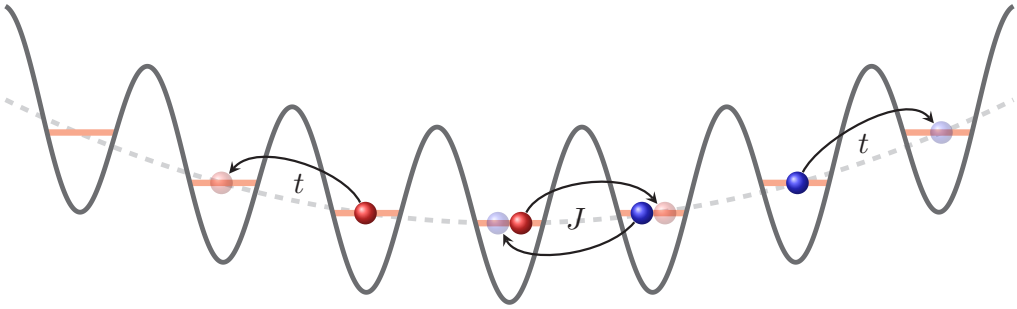

Figure 5.2 | Illustration of the harmonically trapped lattice system of a two-component fermionic gas. t denotes the tunneling amplitude and J denotes the exchange interaction. Blue and red illustrate the two spin-components.

The ground state properties can be analyzed using a projected Bardeen-Cooper-Schrieffer (BCS) state taking into account that double occupancy is forbidden for large interactions, $\hat{P}_{\mathrm{G}} |\mathrm{BCS}\rangle$ where $\hat{P}_{\mathrm{G}} = \prod_i (1 - \hat{n}_{i\uparrow}\hat{n}_{i\downarrow})$ [23, 38, 39]. The projection can be incorporated into the Hamiltonian through the Gutzwiller renormalization factors which link the expectation values in the projected state to the expectation values in the unprojected state with a weight factor. We account for the strong repulsion by projecting onto the states with site-population less than or equal to unity which is done by introducing the site-dependent Gutzwiller factors [38]:

$$g_{\mathrm{t}}^{ij} = \sqrt{g_{\mathrm{t}}^{i} g_{\mathrm{t}}^{j}} = \sqrt{2\delta^i/(1+\delta^i)}\sqrt{2\delta^j/(1+\delta^j)}, \tag{5.6}$$
$$g_{\mathrm{s}}^{ij} = \sqrt{g_{\mathrm{s}}^{i} g_{\mathrm{s}}^{j}} = \sqrt{4/(1+\delta^i)^2}\sqrt{4/(1+\delta^j)^2},$$

where we denote the deviation from half-filling $\delta^i = 1 - \langle \hat{n}_i \rangle$ with $\langle \hat{n}_i \rangle = \sum_\sigma \langle \hat{n}_{i\sigma} \rangle$ representing the total number of particles on site i (refer to appendix A for further details). This is justified by choosing a small curvature of the external trapping potential compared to the hopping amplitude. This procedure is shown to be in good agreement with variational Monte Carlo calculations for the projected d-wave state [77]. The renormalized Hamiltonian then takes the form

$$\hat{H} = -t \sum_{\langle ij \rangle \sigma} \left[g_{\mathrm{t}}^{ij} \hat{c}_{i\sigma}^\dagger \hat{c}_{j\sigma} + \mathrm{h.c.} \right] + \sum_{i\sigma} V_i \hat{c}_{i\sigma}^\dagger \hat{c}_{i\sigma} + J \sum_{\langle ij \rangle} g_{\mathrm{s}}^{ij} \boldsymbol{S}_i \cdot \boldsymbol{S}_j, \tag{5.7}$$

where g_{s}^{ij} works as to enhance spin-spin correlations since $g_{\mathrm{s}}^{ij} \geq 1$ and g_{t}^{ij} suppresses the tunneling term since $g_{\mathrm{t}}^{ij} \leq 1$ and goes to zero when the doping goes to zero. This resembles the suppression of the kinetic energy in the Mott insulating state.

5.3.3 Mean-field theory

In order to solve this many-body Hamiltonian we introduce the Fermi liquid order parameter, χ_{ij}, and the pairing order parameter, Δ_{ij}, with the following averages [38]

$$\begin{aligned} \chi_{ij} &= \frac{3}{4} g_{\mathrm{s}}^{ij} J \sum_{\sigma} \langle \hat{c}_{i\sigma}^{\dagger} \hat{c}_{j\sigma} \rangle \,, \\ \Delta_{ij} &= \frac{3}{4} g_{\mathrm{s}}^{ij} J \sum_{\sigma\sigma'} \epsilon_{\sigma\sigma'} \langle \hat{c}_{i\sigma} \hat{c}_{j\sigma'} \rangle \,, \end{aligned} \tag{5.8}$$

where $\epsilon_{\uparrow\downarrow} = 1 = -\epsilon_{\downarrow\uparrow}$ and $\epsilon_{\uparrow\uparrow} = 0 = \epsilon_{\downarrow\downarrow}$ and i and j are nearest neighbors. At a general level, spin fluctuations not too far from half-filling will favor d-wave superfluidity. We then obtain the mean-field Hamiltonian

$$\begin{aligned} \hat{H} = &- \sum_{\langle ij \rangle \sigma} \left[\left(t g_{\mathrm{t}}^{ij} + \frac{\chi_{ji}}{2} \right) \hat{c}_{i\sigma}^{\dagger} \hat{c}_{j\sigma} + \mathrm{h.c.} \right] - \mu \sum_{i\sigma} \hat{c}_{i\sigma}^{\dagger} \hat{c}_{i\sigma} \\ &+ \sum_{i\sigma} V_i \hat{c}_{i\sigma}^{\dagger} \hat{c}_{i\sigma} + \sum_{\langle ij \rangle} \left[\frac{\Delta_{ij}}{2} \left(\hat{c}_{i\uparrow}^{\dagger} \hat{c}_{j\downarrow}^{\dagger} - \hat{c}_{i\downarrow}^{\dagger} \hat{c}_{j\uparrow}^{\dagger} \right) + \mathrm{h.c.} \right], \end{aligned} \tag{5.9}$$

where we now work in the grand-canonical ensemble and therefore introduce the chemical potential μ since the number of particles is no longer conserved. We have in the above expression assumed that the potential is slowly varying so that $\langle \hat{c}_{i\uparrow} \hat{c}_{j\downarrow} \rangle = \langle \hat{c}_{j\uparrow} \hat{c}_{i\downarrow} \rangle$. Furthermore, we have exploited the fact that the additional term to the tunneling amplitude is spin-independent $\langle \hat{c}_{i\uparrow}^{\dagger} \hat{c}_{j\uparrow} \rangle = \langle \hat{c}_{i\downarrow}^{\dagger} \hat{c}_{j\downarrow} \rangle$ under our present assumptions.

In the following sections, we show that the pairing order parameter depends strongly on the position in the trap. It converges to the untrapped case in the center of the trap where it is maximal, which reflects the emergence of superfluidity induced by the pairing term. We confirm the coexistence of a d-wave superfluid domain and a gapless edge region. Before

considering the trapped system we start by considering a simpler system with no external trapping potential and derive the phase-diagram for this system.

5.4 The untrapped system

We first study the untrapped system for which we find the phase-diagram of the order parameters as a function of the doping concentration. This is most easily solved in momentum space due to the discrete translational invariance of the system.

5.4.1 Transformation of the Hamiltonian to momentum space

The Hamiltonian is found in Fourier space by writing the creation and annihilation operators as $\hat{c}_{j\sigma} = 1/N_{\mathrm{L}} \sum_{\boldsymbol{k}} e^{-i\boldsymbol{k}\cdot\boldsymbol{j}} \hat{c}_{\boldsymbol{k}\sigma}$ and assume real values for the order parameters. Here the sum is performed over the first Brillouin zone and N_{L} denotes the number of lattice sites going into the sum. The Hamiltonian takes the following form

$$H = \sum_{\boldsymbol{k}\sigma} \xi_{\mathbf{k}} c^{\dagger}_{\mathbf{k}\sigma} c_{\mathbf{k}\sigma} + \sum_{\mathbf{k}} \Delta_{\mathbf{k}} \left(c^{\dagger}_{\mathbf{k}\uparrow} \hat{c}^{\dagger}_{-\mathbf{k}\downarrow} + \mathrm{h.c.} \right), \tag{5.10}$$

where the pairing order parameter is $\Delta_{\mathbf{k}} = \Delta(\cos(k_x a) - \cos(k_y a))$ in accordance with the d-wave symmetry of the order parameter and with $\Delta = 3/4 g_{\mathrm{s}} J \sum_{\sigma\sigma'} \epsilon_{\sigma\sigma'} \langle \hat{c}_{i\sigma} \hat{c}_{j\sigma'} \rangle$. The Fermi liquid order parameter is $\chi = 3/4 g_{\mathrm{s}} J \sum_{\sigma} \langle \hat{c}^{\dagger}_{i\sigma} \hat{c}_{j\sigma} \rangle$ and the energies $\xi_{\mathbf{k}} = -(2t g_{\mathrm{t}} + \chi)(\cos(k_x a) + \cos(k_y a)) - \mu$. This Hamiltonian is diagonalized by making a Bogoliubov transformation of the creation and annihilation operators. The creation and annihilation operators are then linear combinations of new fermionic quasi-particle operators

$$\begin{pmatrix} \hat{c}_{\mathbf{k}\uparrow} \\ \hat{c}^{\dagger}_{-\mathbf{k}\downarrow} \end{pmatrix} = U_{\mathbf{k}} \begin{pmatrix} \hat{\gamma}_{\mathbf{k}\uparrow} \\ \hat{\gamma}^{\dagger}_{-\mathbf{k}\downarrow} \end{pmatrix} = \begin{pmatrix} u_{\mathbf{k}} & -v_{\mathbf{k}} \\ v_{\mathbf{k}} & u_{\mathbf{k}} \end{pmatrix} \begin{pmatrix} \hat{\gamma}_{\mathbf{k}\uparrow} \\ \hat{\gamma}^{\dagger}_{-\mathbf{k}\downarrow} \end{pmatrix}. \tag{5.11}$$

The eigenvalues are given by

$$E_{\mathbf{k}\pm} = \pm\sqrt{\xi_{\mathbf{k}}^2 + \Delta_{\mathbf{k}}^2} \tag{5.12}$$

and the corresponding quasi-particle amplitudes are

$$u_{\mathbf{k}} = \frac{1}{\sqrt{2}}\sqrt{1 + \frac{\xi_{\mathbf{k}}}{E_{k+}}},\ v_{\mathbf{k}} = \frac{1}{\sqrt{2}}\sqrt{1 - \frac{\xi_{\mathbf{k}}}{E_{\mathbf{k}+}}}, \tag{5.13}$$

with $u_{\mathbf{k}}v_{\mathbf{k}} = \Delta_{\mathbf{k}}/2E_{\mathbf{k}+}$. In the following we define $E_{\mathbf{k}+} \equiv E_{\mathbf{k}}$, which naturally means that $E_{\mathbf{k}-} = -E_{\mathbf{k}}$.

5.4.2 Self-consistent equations

Self-consistency of the untrapped system is obtained from

$$\begin{aligned}
\chi &= \frac{-3}{4N_{\mathrm{L}}} g_{\mathrm{s}} J \sum_{\boldsymbol{k}} \left(\cos(k_x a) + \cos(k_y a)\right) \tanh\left(\frac{E_{\boldsymbol{k}}}{2k_{\mathrm{B}}T}\right) \frac{\xi_{\boldsymbol{k}}}{2E_{\boldsymbol{k}}}, \\
\delta &= \frac{1}{N_{\mathrm{L}}} \sum_{\boldsymbol{k}} \tanh\left(\frac{E_{\boldsymbol{k}}}{2k_{\mathrm{B}}T}\right) \frac{\xi_{\boldsymbol{k}}}{E_{\boldsymbol{k}}}, \\
\Delta &= \frac{3}{4N_{\mathrm{L}}} g_{\mathrm{s}} J \sum_{\boldsymbol{k}} \left(\cos(k_x a) - \cos(k_y a)\right) \tanh\left(\frac{E_{\boldsymbol{k}}}{2k_{\mathrm{B}}T}\right) \frac{\Delta_{\boldsymbol{k}}}{2E_{\boldsymbol{k}}}.
\end{aligned} \tag{5.14}$$

These equations are solved self-consistently for $T/J = 0$ and $t/J = 5$ as a function of doping and the corresponding result is shown in figure 5.3. The Fermi liquid order parameter is plotted with green $\star$'s and the pairing order parameter with blue $\circ$'s. It is seen that the pairing order parameter vanishes when the doping is around 0.3. The Fermi liquid order parameter, on the other hand, is almost unaffected by the doping concentration in the region of our interest. The Fermi liquid order parameter can be physically interpreted as a measure of how localized the particles are and should be zero in the anti-ferromagnetic state.

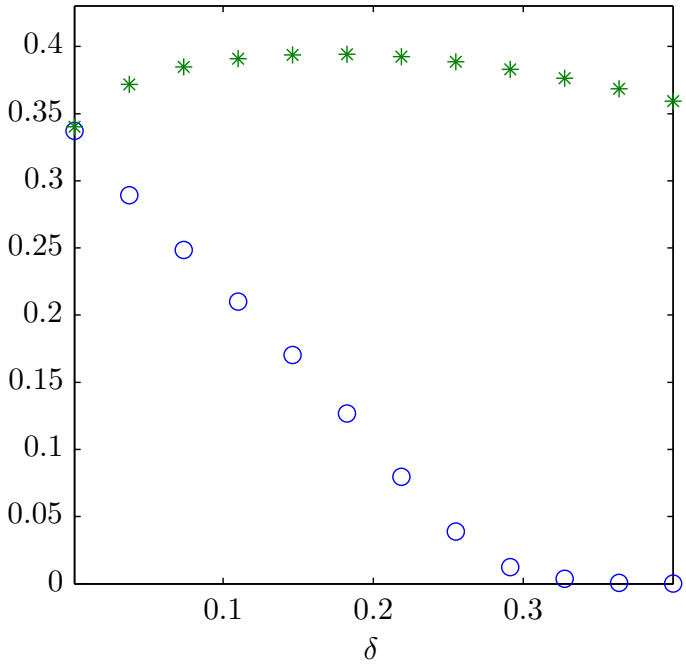

Figure 5.3 | The Fermi liquid order parameter χ (green $\star$'s) and the pairing order parameter Δ (blue $\circ$'s) in units of $3/4g_sJ$ for $T/J = 0$ and $t/J = 5$.

5.5 The trapped system

In the following we add the effect of a harmonic trapping potential and compare numerical results from solving the BdG equations in real space with results from a local density approximation.

5.5.1 Bogoliubov-de Gennes equations

Since the trap breaks the discrete translational invariance, we first find the d-wave pairing order parameter, the Fermi liquid order as well as the density profile by solving the BdG equations. We diagonalize the renormalized mean-field Hamiltonian by making a unitary Bogoliubov-Valatin transformation of the creation and annihilation operators, expanding them

on a complete basis of quasi-particle modes annihilated by the fermionic mode operators $\hat{\gamma}_{\eta\sigma}$ as in (4.7).

The self-consistent equations of the mean-field parameters take the following form in terms of the quasi-particle amplitudes

$$\begin{aligned}
\Delta_{ij} &= \frac{3g_{\mathrm{s}}^{ij}J}{4}\sum_{\eta}\left[u_{\eta\uparrow}^{i}v_{\eta\uparrow}^{j*}\left(1-f_{\eta\uparrow}\right)-u_{\eta\uparrow}^{j}v_{\eta\uparrow}^{i*}f_{\eta\uparrow}\right],\\
\chi_{ij} &= \frac{3g_{\mathrm{s}}^{ij}J}{4}\sum_{\eta}\left[u_{\eta\uparrow}^{i*}u_{\eta\uparrow}^{j}f_{\eta\uparrow}+v_{\eta\uparrow}^{i}v_{\eta\uparrow}^{j*}\left(1-f_{\eta\uparrow}\right)\right],\\
\delta^{i} &= 1-\sum_{\eta}\left[|u_{\eta\uparrow}^{i}|^{2}f_{\eta\uparrow}+|v_{\eta\uparrow}^{i}|^{2}\left(1-f_{\eta\uparrow}\right)\right].
\end{aligned} \tag{5.15}$$

In the above expression the duality of the spin-up and spin-down solutions has been exploited to transform the sum into a sum over positive as well as negative energies for spin-up particles only.

5.5.2 The local density approximation

Assuming a small curvature of the harmonic trapping potential, it is possible to approximate the potential with a constant in the vicinity of each lattice site and replace the eigenstates with plane wave states in accordance with Subsection 4.6.4. Assuming a large number of particles in each cell of constant potential, we define a local Fermi sea. This consists in defining a local chemical potential in each cell $\mu\left(\boldsymbol{r}\right)=\mu-V(x,y)$ and letting

$$u_{\eta\uparrow}(\boldsymbol{r})=\frac{u_{\boldsymbol{k}\uparrow}\left(\boldsymbol{r}\right)e^{-i\boldsymbol{k}\cdot\boldsymbol{r}}}{\sqrt{N_{\mathrm{L}}}},\ v_{\eta\uparrow}(\boldsymbol{r})=\frac{v_{\boldsymbol{k}\uparrow}\left(\boldsymbol{r}\right)e^{-i\boldsymbol{k}\cdot\boldsymbol{r}}}{\sqrt{N_{\mathrm{L}}}}, \tag{5.16}$$

where $u_{\boldsymbol{k}}(\boldsymbol{r})$ and $v_{\boldsymbol{k}}(\boldsymbol{r})$ are solutions of the homogeneous system with $\mu(\boldsymbol{r})=\mu-V(x,y)$ [78] and N_{L} is the number of lattice sites. Below, we introduce the local variables

$$\begin{aligned}
\Delta(x,y) &= \Delta_{i}=\frac{1}{N_{\mathrm{N}}}\sum_{\hat{a}}\alpha_{\hat{a}}\Delta_{i,i+\hat{a}},\\
\chi(x,y) &= \chi_{i}=\frac{1}{N_{\mathrm{N}}}\sum_{\hat{a}}\chi_{i,i+\hat{a}},\\
\delta(x,y) &= \delta^{i},
\end{aligned} \tag{5.17}$$

where $\hat{a}$ denotes the nearest neighbors, N_{N} is the number of nearest neighbors, and $\alpha_{e_x} = \alpha_{-e_x} = -\alpha_{e_y} = -\alpha_{-e_y} = 1$. Here, e_x denotes one lattice step in the x-direction. Within this local density approximation the self-consistent equations take the form

$$\begin{aligned}\chi(x,y) = &-\frac{3g_{\mathrm{s}}(x,y)J}{4N_{\mathrm{L}}}\sum_{\boldsymbol{k}}\left(\cos(k_x a)+\cos(k_y a)\right)\\ &\times\tanh\left(\frac{E_{\boldsymbol{k}}(x,y)}{2k_{\mathrm{B}}T}\right)\frac{\xi_{\boldsymbol{k}}(x,y)}{2E_{\boldsymbol{k}}(x,y)},\end{aligned} \tag{5.18}$$

$$\delta(x,y) = \frac{1}{N_{\mathrm{L}}}\sum_{\boldsymbol{k}}\tanh\left(\frac{E_{\boldsymbol{k}}(x,y)}{2k_{\mathrm{B}}T}\right)\frac{\xi_{\boldsymbol{k}}(x,y)}{E_{\boldsymbol{k}}(x,y)}, \tag{5.19}$$

$$\begin{aligned}\Delta(x,y) = &\frac{3g_{\mathrm{s}}(x,y)J}{4N_{\mathrm{L}}}\sum_{\boldsymbol{k}}\left(\cos(k_x a)-\cos(k_y a)\right)\\ &\times\tanh\left(\frac{E_{\boldsymbol{k}}(x,y)}{2k_{\mathrm{B}}T}\right)\frac{\Delta_{\boldsymbol{k}}(x,y)}{2E_{\boldsymbol{k}}(x,y)},\end{aligned} \tag{5.20}$$

which are simply the site-dependent versions of the order parameters for the untrapped system (5.14). Here the sum is performed over the first Brillouin zone and

$$\begin{aligned}E_{\boldsymbol{k}}(x,y) = &\sqrt{\xi_{\boldsymbol{k}}(x,y)^2+\Delta_{\boldsymbol{k}}(x,y)^2},\\ \xi_{\boldsymbol{k}}(x,y) = &-\left(2tg_t(x,y)+\chi(x,y)\right)\left[\cos(k_x a)+\cos(k_y a)\right],\\ &-\mu(x,y)\\ \Delta_{\boldsymbol{k}}(x,y) = &\Delta(x,y)\left[\cos(k_x a)-\cos(k_y a)\right].\end{aligned} \tag{5.21}$$

Above, we have neglected the variation in chemical potentials on neighboring lattice sites and approximated the renormalization factors with their value on the i'th lattice site, for example $g_{\mathrm{s}}(x,y) = 4/(1+\delta(x,y))^2$. This is justified when the curvature of the harmonic potential is small compared to the tunneling amplitude. In the absence of the harmonic trap, these equations and their solutions agree with well-known results; see for example Ref. [76].

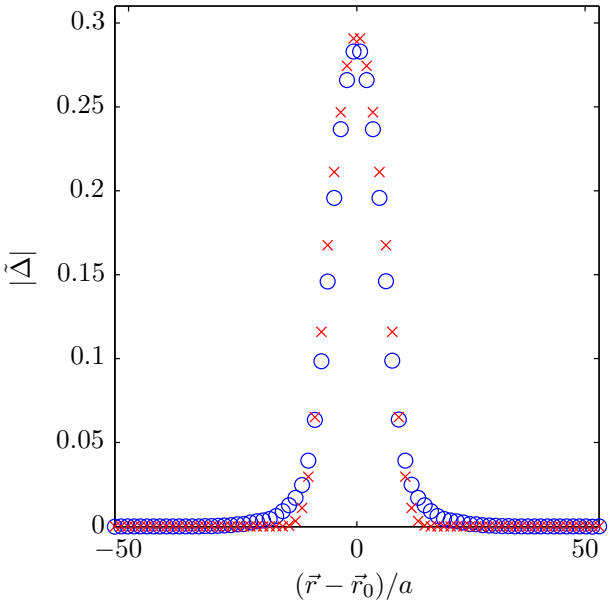

Figure 5.4 | A diagonal cross-section of $|\tilde{\Delta}(\mathbf{r})|$ of the trapped system with 76×76 lattice sites, as a function of the distance from the center of the trap $\mathbf{r}_0$. $t/J = 5$, $\mu/J = -0.1$, $T/J = 0$, and $\tilde{\omega} = \sqrt{ma^2/J}\omega = 0.16$. BdG (circles) and LDA (crosses).

5.6 Results for the trapped system

We now compare the local density approximation calculation to the BdG calculation of the site-dependent values of $|\tilde{\Delta}_i|$, $\tilde{\chi}_i$ and $\langle \hat{n}_i \rangle$; note that the tilde values mean that the mean-field order parameters are expressed in units of $3/4g_{\mathrm{s}}^{ii}J$. For large interactions, we check that the order parameters are controlled by the super-exchange J. We expect that the critical distance at which $|\tilde{\Delta}_i|$ will be zero is given by the position with a doping corresponding to the critical "doping" from the homogeneous calculation which lies around $\delta = 0.35$ [76] if one assumes the LDA is correct. Remarkably, we obtain a very good quantitative agreement between the LDA approximation and the BdG calculation as shown in figures 5.4, 5.5, and 5.6. We corroborate the co-existence of d-wave superfluidity and normal edges in accordance with results from a calculation on a similar system sufficiently away from half-filling in the weakly interacting limit [74]. In

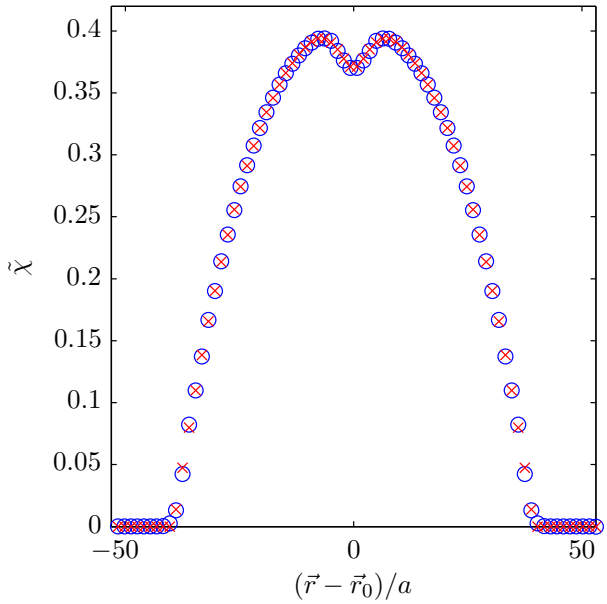

Figure 5.5 | A diagonal cross-section of $\tilde{\chi}(\mathbf{r})$ of the trapped system with 76×76 lattice sites, as a function of the distance from the center of the trap $\mathbf{r}_0$. $t/J = 5$, $\mu/J = -0.1$, $T/J = 0$, and $\tilde{\omega} = \sqrt{ma^2/J}\omega = 0.16$. BdG (circles) and LDA (crosses).

addition, the downturn of $\tilde{\chi}_i$ in the center of the trap is reminiscent of the Mott state. We note that our mean-field calculation breaks down at zero doping since we do not include the terms leading to anti-ferromagnetic ordering.

5.6.1 The local density approximation in small systems

We expect the local density approximation to be less accurate for smaller system sizes with larger trapping frequency. We therefore perform similar calculations on a lattice with 24×24 lattice sites and a trapping frequency of $\tilde{\omega} = \sqrt{ma^2/J}\omega = 0.48$.

Figure 5.7 shows the Fermi liquid order parameter in the trap at zero temperature. It is seen that the result obtained in the local density approximation deviates from the result obtained in real space in the center as well as at the boundary. We expect the LDA to be most accurate for the

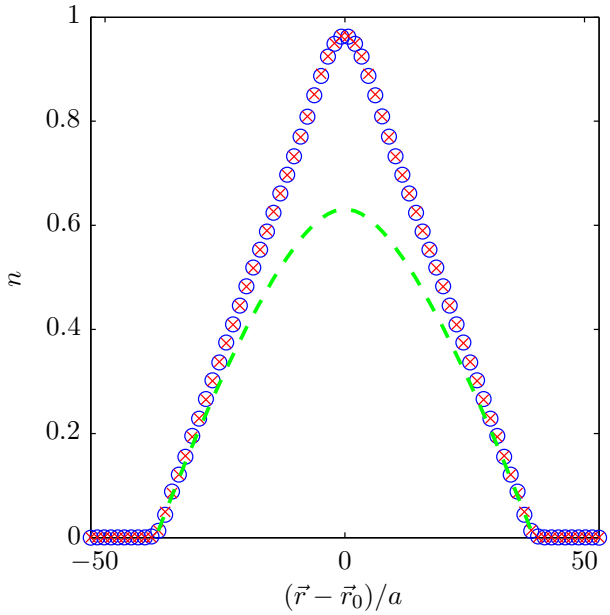

Figure 5.6 | A diagonal cross-section of $\langle\hat{n}(\mathbf{r})\rangle$ of the trapped system with 76×76 lattice sites, as a function of the distance from the center of the trap $\mathbf{r}_0$. $t/J = 5$, $\mu/J = -0.1$, $T/J = 0$, and $\tilde{\omega} = \sqrt{ma^2/J}\omega = 0.16$. BdG (circles), LDA (crosses) and analytical (dashed).

Fermi liquid order parameter when the average distance between particles scaling as $1/k_{\mathrm{F}}$ is much smaller than the oscillator length $a_{\mathrm{osc}} = \sqrt{\hbar/m\omega}$. Indeed we see that at the boundaries where the density is very small the LDA calculation breaks down. We notice that the LDA also breaks down in the center of the trap but here we expect this is caused due to the fast variation of the order parameter $\tilde{\chi}(\mathbf{r})$ where another physical length scale comes into play.

In figure 5.8 we plot a cut of the pairing order parameter $|\tilde{\Delta}(\mathbf{r})|$. We here expect that the validity of the LDA is for the coherence length $\xi = \frac{\hbar v_{\mathrm{F}}}{\pi|\tilde{\Delta}(\mathbf{r})|}$ much smaller than a_{osc}. Accordingly, we see that the results from the BdG calculation and the LDA calculation differ relatively much at the boundaries where the pairing order parameter is small. On the contrary the result of the density profile in the local density approximation and the result obtained in real space figure 5.9 seem to agree closely.

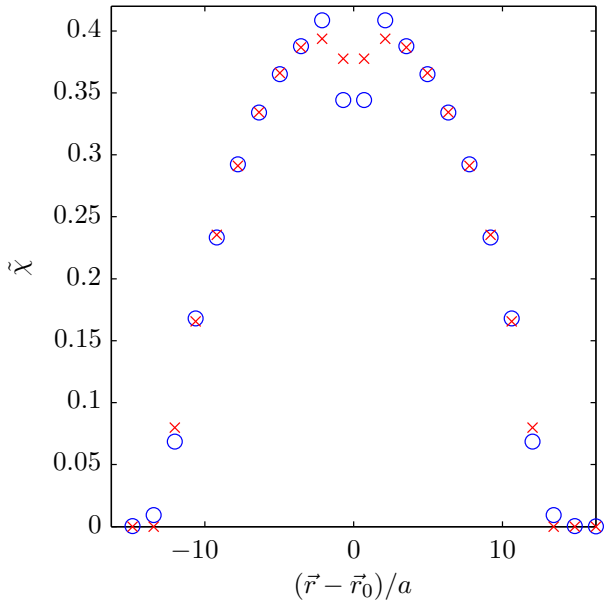

Figure 5.7 | A diagonal cut of $\tilde{\chi}(\mathbf{r})$ of the trapped system with 24×24 lattice sites, as a function of the distance from the center of the trap $\mathbf{r}_0$. $t/J=5$, $\mu/J=-0.1$, $T/J=0$, and $\tilde{\omega}=\sqrt{ma^2/J}\omega=0.48$. BdG (circles) and LDA (crosses).

5.6.2 The density profile

In the following we derive an analytical expression for the doping close to the boundary of the density profile defined as the circle in the xy-plane with radius R where $\delta(x,y)$ reaches unity in the local density approximation. This circle is only well-defined in the continuous system but becomes sufficiently well-defined for large lattices. In the vicinity of the density boundary the pairing order parameter has vanished, $\chi(x,y)$ is so small that we ignore it and at the boundary the chemical potential $\mu(R)$ is equal to $-4t$ which is the bottom of the energy band. At the boundary we find from equation (5.19) the doping at zero temperature

$$\delta(R)=\frac{1}{N_\mathrm{L}}\sum_{\boldsymbol{k}}\frac{\xi_{\boldsymbol{k}}(R)}{E_{\boldsymbol{k}}(R)}=\frac{1}{N_\mathrm{L}}\sum_{\boldsymbol{k}}\mathrm{sgn}\left[\xi_{\boldsymbol{k}}(R)\right]. \tag{5.22}$$

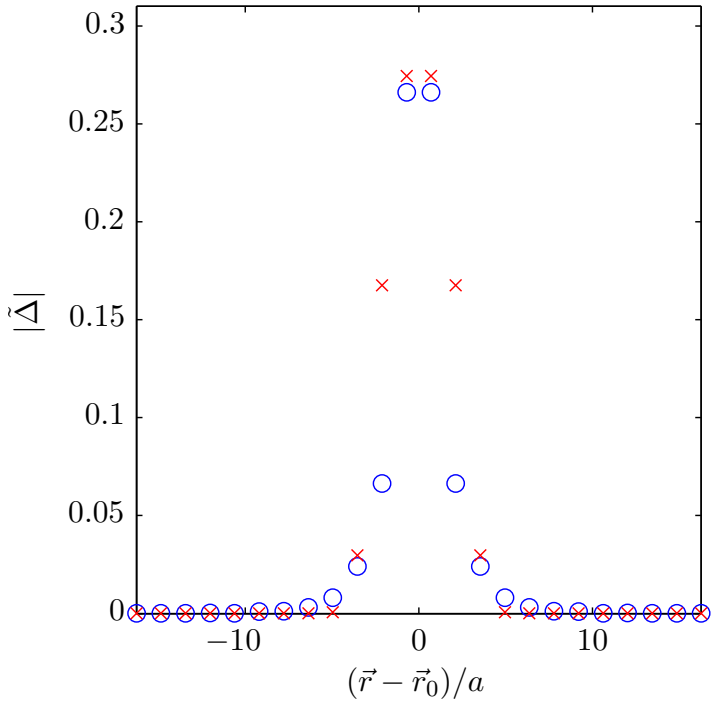

Figure 5.8 | A diagonal cut of $|\tilde{\Delta}(\mathbf{r})|$ of the trapped system with 24×24 lattice sites, as a function of the distance from the center of the trap $\mathbf{r}_0$. $t/J = 5$, $\mu/J = -0.1$, $T/J = 0$, and $\tilde{\omega} = \sqrt{ma^2/J}\omega = 0.48$. BdG (circles) and LDA (crosses).

For $\delta(R)$ to be unity we must have $\xi_{\boldsymbol{k}}(x,y) > 0$ for all quasi-momenta which is the case when the chemical potential is less than $-4t$. In a small region close to $\delta(R) = 1$ the terms in the sum which contribute to a lowering of the doping concentration will form a circle in $\boldsymbol{k}$-space. Hence, we make a Taylor expansion of the cosine terms in $\boldsymbol{k}$-space at site i with coordinates (x,y) to find the radius ka corresponding to the change of sign in $\xi_{\boldsymbol{k}}(x,y)$

$$\begin{aligned}\xi_{\boldsymbol{k}}(x,y) &= -2tg_{\mathrm{t}}(x,y)(\cos(k_x a) + \cos(k_y a)) - \mu(x,y) \\ &\approx -2tg_{\mathrm{t}}(x,y)(2 - 1/2\left[(k_x a)^2 + (k_y a)^2\right]) - \mu(x,y) \\ &= -2tg_{\mathrm{t}}(x,y)(2 - 1/2(ka)^2) - \mu(x,y) = 0, \end{aligned} \tag{5.23}$$

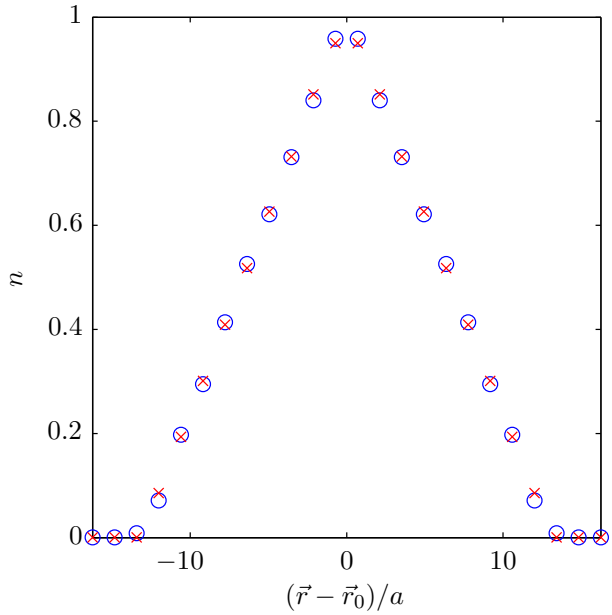

Figure 5.9 | A diagonal cut of $n(\mathbf{r})$ of the trapped system with 24×24 lattice sites, as a function of the distance from the center of the trap $\mathbf{r}_0$. $t/J=5$, $\mu/J=-0.1$, $T/J=0$, and $\tilde{\omega}=\sqrt{ma^2/J}\omega=0.48$. BdG (circles) and LDA (crosses).

which corresponds to a radius of $(ka)^2=\frac{\mu(x,y)}{tg_t(x,y)}+4$. The doping will then be given by

$$\begin{aligned}\delta(x,y)&=\frac{1}{N_L}\sum_{\boldsymbol{k}}\mathrm{sgn}\left[\xi_{\boldsymbol{k}}(x,y)\right]\\&=\frac{4\pi^2-2\pi(ka)^2}{4\pi^2}=1-\frac{\frac{\mu(x,y)}{tg_t(x,y)}+4}{2\pi}\\&=1-\frac{2}{\pi}-\frac{\mu(x,y)}{4\pi t\delta(x,y)}-\frac{\mu(x,y)}{4\pi t}\\&=\frac{1}{2}-\frac{1}{\pi}\left[\frac{\mu(x,y)}{8t}+1\right]\\&+\frac{\sqrt{\left(1-\frac{2}{\pi}\left(\frac{\mu(x,y)}{8t}+1\right)\right)^2-\frac{\mu(x,y)}{\pi t}}}{2},\end{aligned}\tag{5.24}$$

with $\mu(x,y) = \mu - V(x,y)$ the local chemical potential when realizing that one must subtract the area corresponding to the negative contribution twice. The analytical result obtained above is shown as the dashed line in figure 5.6

One can use the expression for the chemical potential at the boundaries $\mu(R) = \mu - 1/2m\omega^2 R^2 = -4t$ to obtain the associated radius

$$R = \sqrt{2\left(4t + \mu\right) / \left(m\omega^2\right)}, \tag{5.25}$$

which corresponds to a radius of $R = 39.5a$ when $t/J = 5$, $T/J = 0$, $\mu/J = -0.1$, and $\tilde{\omega} = 0.16$ which is shown to be correct in figure 5.6.

Due to the isotropy of the harmonic potential the expression for the doping is assumed to have no angular dependence as in the continuous case and the expression for the density, which looks linear in the gapless region, can be Taylor expanded around R to first order in x to give $n(x,0) = -0.024(x/a - 39.5)$. We note that the shape of the density profile is almost unaffected by the presence of the pairing order parameter since it is very small and continuously goes to zero.

5.6.3 Finite temperature effects

In figure 5.10 we plot the amplitude of the pairing order parameter $|\tilde{\Delta}_i|$ as a function of temperature. We note that we cannot distinguish between the pseudo-gap and the superfluid regions since we do not provide any information about the phase of the pairing order parameter. We observe that the height and the width of $|\tilde{\Delta}_i|$ decreases with increasing temperature whereas the shape does not change significantly. As is seen in figure 5.10 the amplitude of the pairing order parameter becomes very small when $T/J = 0.6$ with only a small gap in the center of the trap. The untrapped expression for the critical temperature is doping-dependent and we would therefore also expect a critical temperature which depends on the position in the trap.

To summarize, we have shown that a harmonic trapping potential can simulate the effect of inhomogeneous doping allowing to stabilize a novel d-wave superfluid phase for fermions with gapless edge states. In the context of strongly repulsive fermions, we have found that at the center of the trap

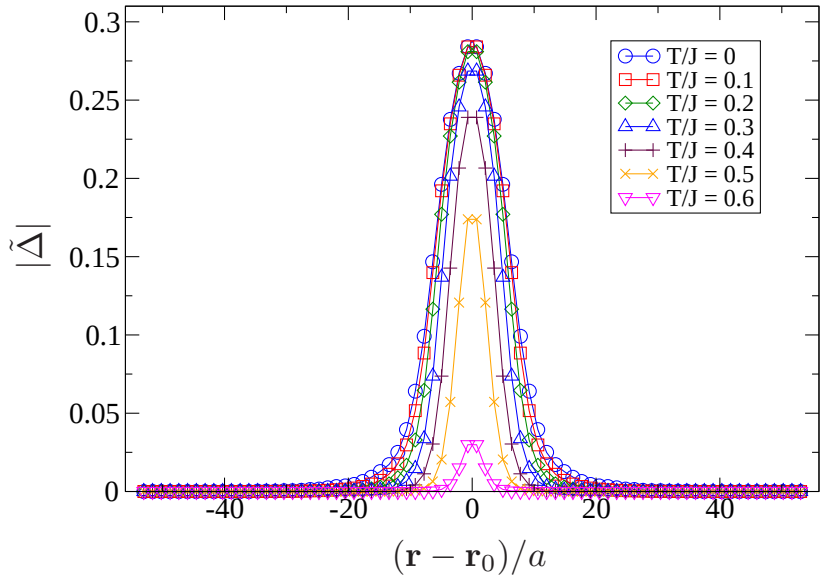

Figure 5.10 | A diagonal cross-section of $|\tilde{\Delta}(\boldsymbol{r})|$ of the trapped system with 76×76 lattice sites, as a function of the distance from the center of the trap $\boldsymbol{r}_0$. $t/J = 5$, $\mu/J = -0.1$, and $\tilde{\omega} = \sqrt{ma^2/J}\omega = 0.16$. BdG (circles) and LDA (crosses) [62].

the downturn of the Fermi liquid order parameter is reminiscent of the Mott insulating state, whereas the d-wave gap is maximal. The proximity to the Mott insulating state at the center of the trap should affect the double occupancy. The d-wave symmetry of the pairing can be detected through the bunching which is maximal along the x and y-directions and minimal along $x = \pm y$. The pairing should be maximal around the Fermi surface. Phase sensitive measurements could also be performed [79]. The superfluid fraction can be determined experimentally through simulation of rotation by the use of a vector potential as in [80]. We found a linear profile of the fermion density close to the boundaries. When decreasing the density, one might observe magnetic real-space shell structures competing with the superfluid phase [74].

Chapter

6 Trapped dipolar fermions in 2D square lattices at zero temperature

In this chapter we consider harmonically trapped dipolar fermions in a two-dimensional (2D) square lattice. The chapter is based on [81]. The anisotropy of the dipolar interaction combined with the lattice leads to transitions between phases with density orders of different symmetry. For experimentally realistic systems, we demonstrate the existence of competing phases with density order of checkerboard or stripe symmetry, and superfluid order. We show that the attractive part of the dipolar interaction results in a superfluid phase which is suppressed by density order. The trapping potential is demonstrated to make the different phases co-exist, forming ring and island structures. However, the phases with density and superfluid order can overlap forming regions with supersolid order. The harmonic potential, which is always present in trapped atomic/molecular systems, is included exactly, since the characteristic lengths of the ordered phases can be comparable to the system size for experimentally realistic systems. This means that one cannot simply resort to the local density approximation.

6.1 Experiments

An increasing number of experimental groups are trapping and cooling atoms or molecules with a permanent magnetic or electric dipole moment. Bose-Einstein condensates of ^{52}Cr atoms [24, 25] and of ^{164}Dy atoms [26] with large magnetic dipole moments have been realized. The former atomic species with a dipole moment of $\mu = 6\mu_B$ and the latter with a dipole moment of $\mu = 10\mu_B$. Fermionic gases of ^{40}K^{87}Rb [27, 28] and ^{23}Na^{6}Li [29] molecules with an electric dipole moment have been created, and the first steps toward the formation of fermionic ^{23}Na^{40}K molecules have been reported [82]. The ^{40}K^{87}Rb [27, 28] molecules have a permanent dipole moment of $d = 0.57$D, which in the absence of an external electric field is zero in the laboratory frame. However, by applying an electric field the accessible induced electric dipole moments are in the range $0 - 0.22$D with $1\text{D} = 3.336 \cdot 10^{-30}$Cm [28]. Table 6.1 shows the coupling strength $g = D^2/ta^3$ for lattice depth $V_0 = 5E_R$ with V_0 calculated from equation (4.37). Note, $D^2 = d^2/4\pi\epsilon_0$ for electric dipoles and $D^2 = \mu^2\mu_0/4\pi$ for magnetic dipoles. We use the ground state dipole moments of ^{23}Na^{40}K and ^{23}Na^{6}Li to estimate the coupling strengths in the table. This means that we have used $d = 0.5$D and $d = 2.72$D for the $X^1\Sigma^+$ ground states of ^{23}Na^{6}Li for ^{23}Na^{40}K, respectively.

atom/molecule	dipole moment	$g = D^2/ta^3$
^{164}Dy	$10\mu_B$	0.09
^{52}Cr	$6\mu_B$	0.01
^{23}Na^{6}Li	0.5D	0.46
^{23}Na^{40}K	2.72D	29.5
^{40}K^{87}Rb	0.22D	0.39

Table 6.1 | Electric and magnetic coupling strengths.

Also, experimental progress toward realizing dipolar molecules in an optical lattice have recently been presented [83]. The anisotropy of the dipole interaction offers unique opportunities for exploring novel few-body [84–87] and many-body quantum systems [88, 89]. Attention has been drawn toward the dipolar physics first of all due to the progress in cooling exper-

iments but also due to the new and interesting physics resulting from the long-range anisotropic behavior of these gases. The orientation control of the dipoles means that one can have both attractive and repulsive regions in the same system depending on the polarization of the dipole moment of the particles. The dipolar interaction potential can stem from the particles having either magnetic dipole moments or electric dipole moments, the latter generally being much larger than the former.

We can determine the relative strength from a simple estimate. From a first estimate we take a typical size of the electric dipole moment in an atomic or molecular system which is on the order of the Bohr radius times the typical charge ea_0. Since the typical magnetic dipole moment is the Bohr magneton μ_B our simple estimate gives us for the relative strength of the dipolar interactions

$$\frac{\mu_\mathrm{B}^2 \mu_0 \epsilon_0}{e^2 a_0^2} = \mu_0 \epsilon_0 \frac{\left(\frac{e\hbar}{2m_e}\right)^2}{e^2 \left(\frac{4\pi\epsilon_0 \hbar^2}{m_e e}\right)^2} = \alpha^2, \tag{6.1}$$

where $\alpha \approx 1/137$ is the fine-structure constant [90].

The anisotropy of the dipole interaction results in many intriguing effects. In a two-dimensional lattice, the existence of density ordered phases with a complicated unit cell [91], liquid crystal phases [92], and a supersolid phase [93] have been predicted when the dipole moments are perpendicular to the lattice plane. Tilting the dipoles toward the lattice plane leads to density order with different symmetry, superfluidity and bond-solid order at zero temperature [94, 95].

6.2 Basic formalism

The fermions have mass m and dipole moment $\mathbf{d}$ which is aligned by an external field forming the angle θ_P with the z-axis perpendicular to the lattice (xy) plane and the azimuthal angle ϕ_P with respect to one of the lattice vectors parallel to the x-axis, see figure 6.1. In the lowest band approximation, this system is described by the extended Hubbard model

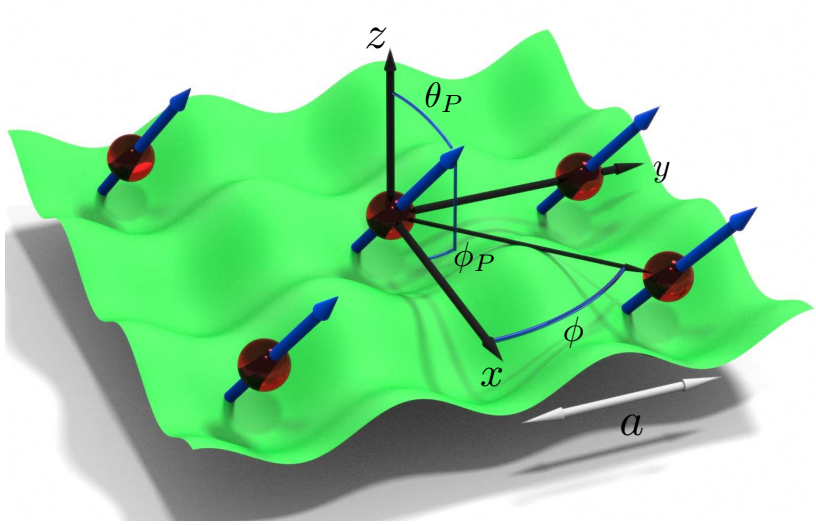

Figure 6.1 | We consider dipoles in a square 2D lattice in the xy-plane. The dipoles are aligned forming an angle θ_P with the z-axis and the azimuthal angle ϕ_P with the x-axis which is parallel to one of the lattice vectors.

with the Hamiltonian $\hat{H} = \hat{H}_0 + \hat{V}$ where

$$\hat{H}_0 = -t \sum_{\langle ij \rangle} \left(\hat{c}_i^\dagger \hat{c}_j + \text{h.c.} \right) + \sum_i \left(\frac{1}{2} m\omega^2 r_i^2 - \mu \right) \hat{n}_i \tag{6.2}$$

and

$$\hat{V} = \frac{1}{2} \sum_{i \neq j} V_D(\mathbf{r}_{ij}) \hat{n}_i \hat{n}_j, \tag{6.3}$$

with $\mathbf{r}_{ij} = \mathbf{r}_i - \mathbf{r}_j$. Here, $\hat{c}_i$ removes a dipole at site i with position $\mathbf{r}_i$, $\hat{n}_i = \hat{c}_i^\dagger \hat{c}_i$, μ is the chemical potential, t is the hopping matrix element between nearest neighbor sites $\langle ij \rangle$, and $i \neq j$ since we are considering identical fermions. The trapping frequency is ω and the interaction between

two dipoles separated by $\mathbf{r}$ is

$$V_D(\mathbf{r}) = \frac{D^2}{r^3}\left[1 - 3\cos^2(\theta_{rd})\right]$$
$$= \frac{D^2}{r^3}\left[1 - 3\cos^2(\phi_P - \phi)\sin^2(\theta_P)\right], \tag{6.4}$$

with $D^2 = d^2/4\pi\epsilon_0$ for electric dipoles and θ_{rd} denoting the angle between $\mathbf{d}$ and $\mathbf{r} = r(\cos\phi, \sin\phi, 0)$, see figure 6.1. The dipolar interaction is symmetric under parity inversion.

Since the dipolar interaction (6.4) has both attractive and repulsive regions, the system exhibits both pairing and density instabilities depending on (θ_P, ϕ_P). To model this complex behavior, we decouple the interaction $\hat{V}$ using the mean-field approximation which yields

$$\hat{V}_{\mathrm{MF}} = \sum_{i\neq j} V_D(\mathbf{r}_{ij})\left(\langle\hat{n}_j\rangle\hat{n}_i - \frac{1}{2}\langle\hat{n}_j\rangle\langle\hat{n}_i\rangle\right)$$
$$+ \sum_{i\neq j}\frac{V_D(\mathbf{r}_{ij})}{2}\left(\langle\hat{c}_j\hat{c}_i\rangle\,\hat{c}_i^\dagger\hat{c}_j^\dagger + \mathrm{h.c.} - |\,\langle\hat{c}_j\hat{c}_i\rangle\,|^2\right), \tag{6.5}$$

where $\langle\hat{c}_j\hat{c}_i\rangle$ is the pairing order parameter which is odd under parity inversion. Even though fluctuations are important in 2D, we expect mean-field theory to capture the existence and competition between different ordered phases at $T = 0$. Indeed, mean-field theory is widely used in the high-T_{c} community to describe the competition between e.g. anti-ferromagnetic and superfluid ordering [96–99]. We have not included the Fock term in the mean-field Hamiltonian (6.5), since one dipole interacts with many others making the problem similar to a high dimensional one, for which the Hartree term dominates [100]. The Fock term has recently been shown to lead to bond-solid order phases at half-filling [94].

The mean-field Hamiltonian $\hat{H}_0 + \hat{V}_{\mathrm{MF}}$ is diagonalized by the Bogoliubov transformation $\hat{c}_i = \sum_{E_\eta>0}(u_\eta^i\hat{\gamma}_\eta + v_\eta^{i*}\hat{\gamma}_\eta^\dagger)$ which is the single-spin version of (4.7), where $\hat{\gamma}_\eta$ are fermionic operators annihilating a quasi-particle with energy E_η. The wave functions u_η^i and v_η^i satisfy the Bogoliubov-de Gennes equations

$$\sum_j \begin{pmatrix} L_{ij} & \Delta_{ij} \\ \Delta_{ji}^* & -L_{ij} \end{pmatrix}\begin{pmatrix} u_\eta^j \\ v_\eta^j \end{pmatrix} = E_\eta \begin{pmatrix} u_\eta^i \\ v_\eta^i \end{pmatrix}, \tag{6.6}$$

with $\Delta_{ij} = V_D(\mathbf{r}_{ij})\langle \hat{c}_j \hat{c}_i \rangle$ and

$$L_{ij} = -t\delta_{\langle ij \rangle} + (\sum_k V_D(\mathbf{r}_{ik})\langle n_k \rangle + \frac{m}{2}\omega^2 r_i^2 - \mu)\delta_{ij}. \tag{6.7}$$

Here δ_{ij} and $\delta_{\langle ij \rangle}$ are the Kronecker delta functions defined in Section 4.3 and the quasi-particle amplitudes satisfy the duality relations, in analogy to the case of two spin-components (4.23) with

$$\begin{pmatrix} u_\eta^i \\ v_\eta^i \end{pmatrix} \leftrightarrow \begin{pmatrix} v_\eta^{i*} \\ u_\eta^{i*} \end{pmatrix} \tag{6.8}$$

and $E_\eta \leftrightarrow -E_\eta$ since

$$\begin{aligned} &\sum_j L_{ij} v_\eta^{j*} + \Delta_{ij} u_\eta^{j*} = \sum_j L_{ij} v_\eta^{j*} - \Delta_{ji} u_\eta^{j*} \\ &= \sum_j (L_{ij} v_\eta^j - \Delta_{ji}^* u_\eta^j)^* = -E_\eta v_\eta^{i*}, \end{aligned} \tag{6.9}$$

$$\begin{aligned} &\sum_j -L_{ij} u_\eta^{j*} + \Delta_{ji}^* v_\eta^{j*} = \sum_j -L_{ij} u_\eta^{j*} - \Delta_{ij}^* v_\eta^{j*} \\ &= \sum_j (-L_{ij} u_\eta^j - \Delta_{ij} v_\eta^j)^* = -E_\eta u_\eta^{i*}. \end{aligned} \tag{6.10}$$

Self-consistency is obtained iteratively through the usual relations for the order parameters:

$$\langle \hat{n}_i \rangle = \sum_{E_\eta > 0} \left[(1 - f_\eta) |v_\eta^i|^2 + f_\eta |u_\eta^i|^2 \right] \tag{6.11}$$

and

$$\langle \hat{c}_i \hat{c}_j \rangle = \sum_{E_\eta > 0} [u_\eta^i v_\eta^{j*} (1 - f_\eta) + v_\eta^{i*} u_\eta^j f_\eta], \tag{6.12}$$

which reduce to $\langle \hat{n}_i \rangle = \sum_{E_\eta > 0} |v_\eta^i|^2$ and $\langle \hat{c}_i \hat{c}_j \rangle = \sum_{E_\eta > 0} u_\eta^i v_\eta^{j*}$ at zero temperature.

6.3 No trapping potential

We first consider a system with no trapping potential. To get a better understanding of the nature of the dipolar interaction we Fourier expand it for $(\theta_P, \phi_P) = (\pi/2, 0)$ and $(\theta_P, \phi_P) = (0, 0)$, with $\tilde{V}_D(\mathbf{k}) = \sum_i \exp(-i\mathbf{k} \cdot \mathbf{r}_i) V_D(\mathbf{r}_i)$ and $k_x, k_y \in [-\frac{\pi}{a}, \frac{\pi}{a}[$. The Fourier expansion of the potential in units of g with $(\theta_P, \phi_P) = (\pi/2, 0)$ is shown in figure 6.2 (left) and the Fourier expansion of the dipolar potential in units of g with $(\theta_P, \phi_P) = (0, 0)$ showing no angular dependence is shown in figure 6.2 (right).

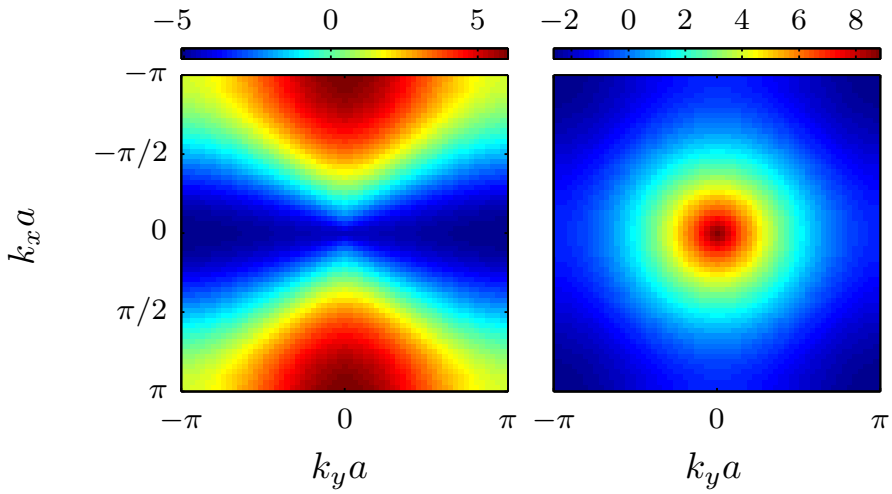

Figure 6.2 | Fourier transform of the interaction potential in units of g. Left: $(\theta_P, \phi_P) = (\pi/2, 0)$. Right: $\theta_P = 0$.

6.3.1 The striped phase at half-filling

We first study the untrapped system at half-filling, $f = N_{\mathrm{L}}^{-1} \sum_i \langle \hat{n}_i \rangle = 1/2$ with the density order $\langle \hat{n}_i \rangle = \left[1 + M(-1)^{y_i/a}\right]/2$ for $M \in [0, 1]$. For an illustration of this phase see the lower right inset in figure 6.3. This phase corresponds to the dipoles forming stripes along the x-direction. When the dipoles are oriented perpendicularly to the $x - y$ plane the dipolar interaction is isotropic and repulsive. This alignment favors a checkerboard density order, see the upper left inset in figure 6.3. However, when tilting

the dipoles toward the lattice plane along for example along the x-axis the dipolar potential becomes anisotropic and eventually attractive in a sliver along the x-direction. The density order must therefore be of the checkerboard form at half-filling for strong interactions and small θ_P, but when tilting the dipoles sufficiently it eventually becomes favorable to form stripes hereby minimizing the energy.

For the untrapped system the Hamiltonian of the striped phase takes the following form in $\mathbf{k}$-space when summing over the positive values of k_y in the first Brillouin zone

$$\begin{aligned}\hat{H} = &\sum_{k_y>0} \left(\nu_{\mathbf{k}} - 2t\cos(k_y a)\right) \hat{c}^\dagger_{\mathbf{k}} \hat{c}_{\mathbf{k}} \\ &+ \sum_{k_y>0} \left(\nu_{\mathbf{k}} + 2t\cos(k_y a)\right) \hat{c}^\dagger_{\mathbf{k}+(0,\pi/a)} \hat{c}_{\mathbf{k}+(0,\pi/a)} \\ &+ \sum_{k_y>0} \frac{\tilde{V}_D(0,\pi/a)M}{2} \hat{c}^\dagger_{\mathbf{k}} \hat{c}_{\mathbf{k}+(0,\pi/a)} + \frac{\tilde{V}_D(0,\pi/a)M}{2} \hat{c}^\dagger_{\mathbf{k}+(0,\pi/a)} \hat{c}_{\mathbf{k}}, \end{aligned} \tag{6.13}$$

where $\nu_{\mathbf{k}} = -2t\cos(k_x a) - \mu + \frac{\tilde{V}_D(0,0)}{2}$. The Hamiltonian may be diagonalized

$$\hat{H} = \sum_{k_y>0} \left[E_{1\mathbf{k}} \gamma^\dagger_{1\mathbf{k}} \gamma_{1\mathbf{k}} + E_{2\mathbf{k}} \gamma^\dagger_{2\mathbf{k}} \gamma_{2\mathbf{k}} \right] \tag{6.14}$$

by a unitary transformation of the creation and annihilation operators

$$\hat{\boldsymbol{c}} = \begin{pmatrix} \hat{c}_{\mathbf{k}} \\ \hat{c}_{\mathbf{k}+(0,\pi/a)} \end{pmatrix} = \begin{pmatrix} u_{\mathbf{k}} & -v_{\mathbf{k}} \\ v_{\mathbf{k}} & u_{\mathbf{k}} \end{pmatrix} \begin{pmatrix} \hat{\gamma}_{1\mathbf{k}} \\ \hat{\gamma}_{2\mathbf{k}} \end{pmatrix} \tag{6.15}$$

with the single-particle energies

$$E_{1\mathbf{k}} = \nu_{\mathbf{k}} + \sqrt{(2t\cos(k_y a))^2 + [\tilde{V}_D(0,\pi/a)M/2]^2}. \tag{6.16}$$

The energy $E_{2\mathbf{k}}$ is given by equation (6.16) with a minus-sign in front of the square root. Self-consistency is obtained through

$$1 = \frac{1}{N_{\mathrm{L}}} \sum_{k_y>0} \frac{\tilde{V}_D(0,\pi/a)\left(f_{1\mathbf{k}} - f_{2\mathbf{k}}\right)}{\sqrt{4t^2\cos^2(k_y a) + [\tilde{V}_D(0,\pi/a)M/2]^2}}. \tag{6.17}$$

6.3.2 The checkerboard phase at half-filling

We next study the untrapped system at half-filling, $f = N_{\mathrm{L}}^{-1}\sum_i \langle \hat{n}_i \rangle = 1/2$ with the density order $\langle \hat{n}_i \rangle = 1/2\left[1 + M(-1)^{x_i/a + y_i/a}\right]$ associated with the checkerboard phase as illustrated in the upper left inset in figure 6.3. The interplay between the kinetic energy and the dipolar interaction determines the size of the order parameter M which becomes 1 for optimal polarization angles when $g/t \gg 1$.

The Hamiltonian of this phase is as for the striped phase (6.13) found in $\mathbf{k}$ space as

$$\begin{aligned}\hat{H} = &\sum_{k_y>0}\left(\epsilon_{\mathbf{k}} - \mu + \frac{\tilde{V}_D(0,0)}{2}\right)\hat{c}^\dagger_{\mathbf{k}}\hat{c}_{\mathbf{k}} \\ &+ \sum_{k_y>0}\left(-\epsilon_{\mathbf{k}} - \mu + \frac{\tilde{V}_D(0,0)}{2}\right)\hat{c}^\dagger_{\mathbf{k}+(\pi/a,\pi/a)}\hat{c}_{\mathbf{k}+(\pi/a,\pi/a)} \\ &+ \sum_{k_y>0}\frac{\tilde{V}_D(\pi/a,\pi/a)M}{2}\hat{c}^\dagger_{\mathbf{k}}\hat{c}_{\mathbf{k}+(\pi/a,\pi/a)} + \frac{\tilde{V}_D(\pi/a,\pi/a)M}{2}\hat{c}^\dagger_{\mathbf{k}+(\pi/a,\pi/a)}\hat{c}_{\mathbf{k}}.\end{aligned} \tag{6.18}$$

Again we make a unitary transformation of the creation and annihilation operators in order to diagonalize the Hamiltonian

$$\hat{\boldsymbol{c}} = \begin{pmatrix}\hat{c}_{\mathbf{k}} \\ \hat{c}_{\mathbf{k}+(\pi/a,\pi/a)}\end{pmatrix} = \begin{pmatrix}u_{\mathbf{k}} & -v_{\mathbf{k}} \\ v_{\mathbf{k}} & u_{\mathbf{k}}\end{pmatrix}\begin{pmatrix}\hat{\gamma}_{\mathbf{k}+} \\ \hat{\gamma}_{\mathbf{k}-}\end{pmatrix}, \tag{6.19}$$

where $\hat{\gamma}_{\mathbf{k}-}$ and $\hat{\gamma}_{\mathbf{k}+}$ are again fermionic quasi-particle operators with the single particle energies

$$E_{\mathbf{k}\pm} = -\mu + \frac{\tilde{V}_D(0,0)}{2} \pm \sqrt{\epsilon^2_{\mathbf{k}} + \left[\tilde{V}_D(\pi/a,\pi/a)M/2\right]^2}. \tag{6.20}$$

Analogous to the striped phase, self-consistency is obtained from

$$1 = \frac{1}{N_{\mathrm{L}}}\sum_{k_y>0}\frac{\tilde{V}_D(\pi/a,\pi/a)\left(f_{1\mathbf{k}} - f_{2\mathbf{k}}\right)}{\sqrt{\epsilon^2_{\mathbf{k}} + \left[\tilde{V}_D(\pi/a,\pi/a)M/2\right]^2}}. \tag{6.21}$$

6.3.3 The p-wave pairing case

When $\theta_P \geq \arcsin(1/\sqrt{3}) \approx 0.2\pi$, the interaction has attractive regions. A phase with a p wave pairing order parameter [101] will then compete with the striped phase being favorable for certain interaction strengths. In the following we take into account the pairing in the system and assume to be in a regime where the striped density order is absent.

Thus, the Hamiltonian takes the form

$$\hat{H} = \sum_{\mathbf{k}} \xi_{\mathbf{k}} \hat{c}^\dagger_{\mathbf{k}} \hat{c}_{\mathbf{k}} + \frac{\Delta_{-\mathbf{k}}}{2} \hat{c}^\dagger_{\mathbf{k}} \hat{c}^\dagger_{-\mathbf{k}} + \text{h.c.}, \tag{6.22}$$

with $\xi_{\mathbf{k}} = -2t(\cos k_x a + \cos k_y a) - \mu + \tilde{V}_D(0,0)\langle \hat{n} \rangle$ and $\Delta_{\mathbf{k}} = 1/N_{\mathrm{L}} \sum_{ij} V_D(\mathbf{r}_{ij}) \Delta_{ij} e^{-i\mathbf{k}(r_i - r_j)}$. Diagonalization of the Hamiltonian results in the quasi-particle energies $E_{\mathbf{k}} = \pm\sqrt{\xi^2_{\mathbf{k}} + \Delta^2_{\mathbf{k}}}$ and the amplitudes

$$u^2_{\mathbf{k}} = \frac{1}{2}\left(1 + \frac{\xi_{\mathbf{k}}}{\sqrt{\xi^2_{\mathbf{k}} + \Delta^2_{\mathbf{k}}}}\right), \qquad v^2_{\mathbf{k}} = \frac{1}{2}\left(1 - \frac{\xi_{\mathbf{k}}}{\sqrt{\xi^2_{\mathbf{k}} + \Delta^2_{\mathbf{k}}}}\right). \tag{6.23}$$

with $u_{\mathbf{k}} v_{\mathbf{k}} = -\Delta_{\mathbf{k}}/2E_{\mathbf{k}}$. Self-consistency is obtained through the finite temperature relations

$$\langle \hat{n} \rangle = \frac{1}{2}\left(1 - \frac{1}{N_{\mathrm{L}}} \sum_{\mathbf{k}} \frac{\xi_{\mathbf{k}}}{E_{\mathbf{k}}} \tanh\left(\frac{E_{\mathbf{k}}}{2k_{\mathrm{B}}T}\right)\right), \tag{6.24}$$

$$\Delta_{\mathbf{k}} = -\frac{1}{N_{\mathrm{L}}} \sum_{\mathbf{k}'} \tilde{V}_D(\mathbf{k} - \mathbf{k}') \frac{\Delta_{\mathbf{k}'}}{2E_{\mathbf{k}}} \tanh\left(\frac{E_{\mathbf{k}'}}{2k_{\mathrm{B}}T}\right). \tag{6.25}$$

6.3.4 Results

We plot in figure 6.3 the ground state as a function of the dipolar angles (θ_P, ϕ_P) in the limit of strong interactions $g/t = 16$ with $g = D^2/a^3$. Note, that the results are obtained by solving the Bogoliubov-de Gennes equations (6.6). The filling fraction is $f = N_{\mathrm{L}}^{-1} \sum_i \langle \hat{n}_i \rangle = 1/2$. We consider two possible ground states: One with the checker-board density order and

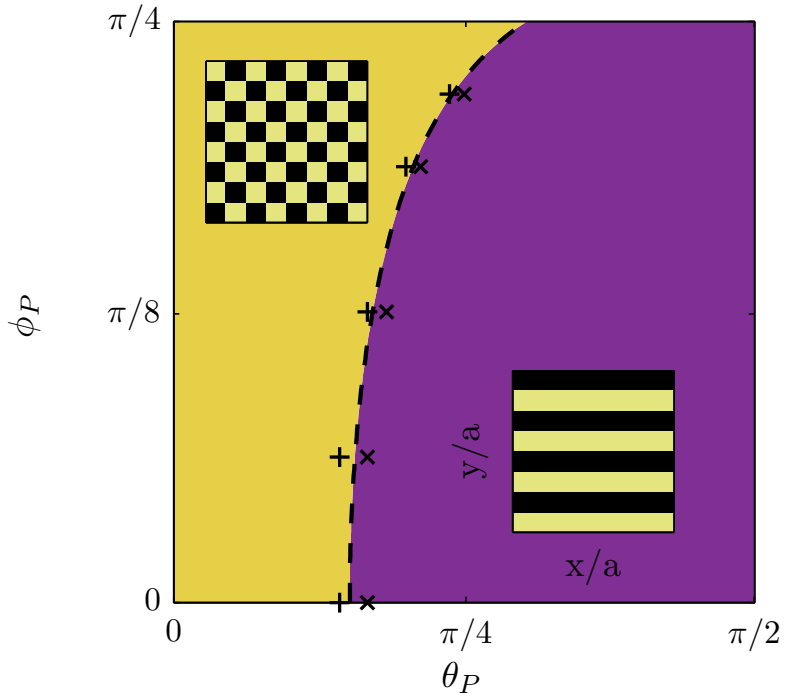

Figure 6.3 | The phase-diagram for an untrapped system for strong coupling $g/t = 16$ and half-filling. The dashed line shows the boundary between the checker-board and the striped phase.

one with the striped density order, discussed in Subsection 6.3.1 and Subsection 6.3.2. The + and × symbols indicate when mean-field theory on a 26×26 lattice predicts the checker-board and striped phase to have the lowest energy, respectively. In order to take into account the long-range nature of the dipolar interaction we have calculated the Hartree term by duplicating the 26×26 lattice so that it constitutes a lattice of $9 \cdot 26 \times 9 \cdot 26$ sites.

For small θ_P the checker-board phase is favored, whereas for larger θ_P a phase with stripes along the x-direction has the lowest energy. This is easily understood for $\phi_P = 0$, where the dipoles are aligned head-to-tail in this phase which clearly minimizes the interaction energy. When $\phi_P > 0$, the alignment is not perfect by stripe formation along the x-axis, but the interaction energy is still minimized although it requires larger tilting angles

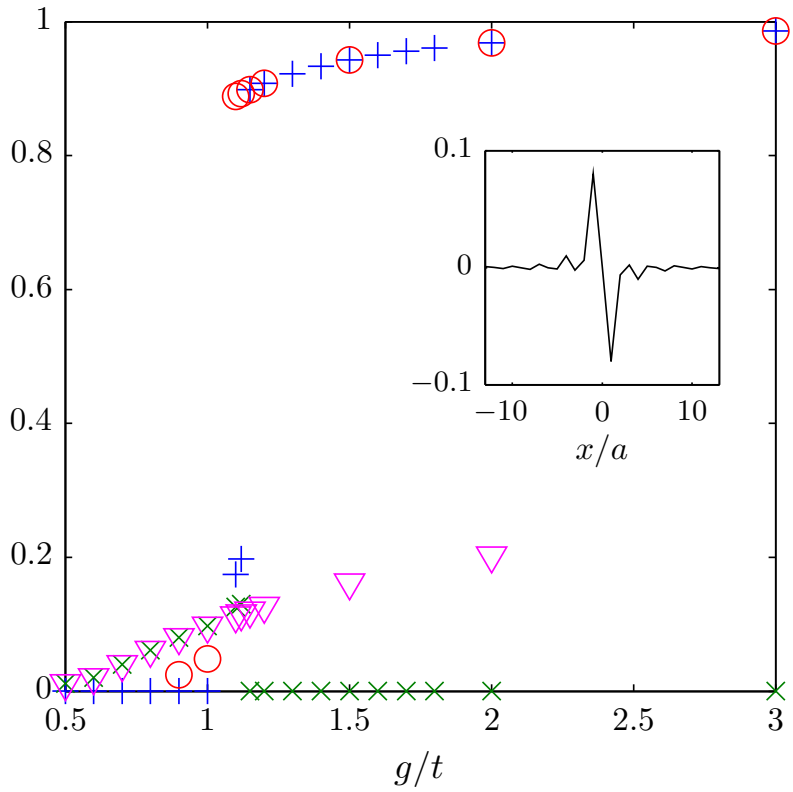

Figure 6.4 | The nearest neighbor pairing $|\langle \hat{c}_{i+e_x} \hat{c}_i \rangle|$ ($\times$'s) and stripe order $|\langle \hat{n}_i - \hat{n}_{i+e_y} \rangle|$ ($+$'s) as a function of g/t with $(\theta_P, \phi_P) = (\pi/2, 0)$. The $\circ$'s show $|\langle \hat{n}_i - \hat{n}_{i+e_y} \rangle|$ when we take the gap to be zero. The ∇'s show $|\langle \hat{c}_{i+e_x} \hat{c}_i \rangle|$ when the density is taken to be homogeneous. The inset shows a cut of $\langle \hat{c}_{i+e_x} \hat{c}_i \rangle$ along the x-axis when $g/t = 0.9$.

θ_P as expected. This is illustrated further by the dashed line separating the checker-board phase from the striped phase, which is a result of comparing the classical interaction energy in the two phases. The good agreement between the numerics and this calculation demonstrates that for strong coupling $g/t \gg 1$ the kinetic energy can be neglected, and the problem becomes classical.

When $\theta_P \geq \arcsin(1/\sqrt{3}) \approx 0.2\pi$, the interaction has attractive regions as pointed out in Subsection 6.3.3, and we now examine the competition between the resulting pairing instability and the instability toward density order. In figure 6.4, we plot as $\times$'s the largest value of the nearest neigh-

bor pairing $|\langle \hat{c}_{i+e_x} \hat{c}_i \rangle|$ as a function of the coupling strength g/t. We have chosen $(\theta_P, \phi_P) = (\pi/2, 0)$ and $f = 1/3$. The calculations are performed on a 27×27 lattice. For weak coupling, the ground state is a superfluid. The cut along the x-axis of the pair wave function $\langle \hat{c}_j \hat{c}_i \rangle$ with $\mathbf{r}_i = (0, 0)$ plotted in the inset, illustrates that it is odd under inversion as for the homogeneous case [101, 102]. For simplicity, we refer to this as p-wave symmetry in the following, even though the pair wave function in general contains higher odd components of angular momenta. For stronger coupling, the pairing vanishes as the striped phase emerges. The stripe order defined as $\langle \hat{n}_i - \hat{n}_{i+e_y} \rangle$, with e_y a unit vector along the y direction so that $\langle \hat{n}_i \rangle$ and $\langle \hat{n}_{i+e_y} \rangle$ give the densities for a site in the stripe and next to the stripe respectively, is plotted as $+$'s in figure 6.4. We also plot as $\circ$'s the stripe order parameter when pairing is not included in the calculation, and as ∇'s the pairing order parameter when the stripe formation is not included. This demonstrates that the stripe order is insensitive to pairing since the critical coupling strength for the formation of stripes essentially does not change when pairing is included. The pairing on the other hand does not vanish with increasing coupling if the stripes are suppressed. We therefore conclude that it is the pairing which is suppressed by the stripe formation and not the other way around. We see that the critical coupling strength where the striped phase dominates over the superfluid state is $g/t > 1.15$.

More complicated density order with larger unit cells can appear for untrapped systems, as has recently been demonstrated for $\theta_P = 0$ [91]. Here, we focus on the experimentally most relevant orders with the smallest unit cell, since the trapping potential will complicate the observation of orders with a large unit cells.

6.4 Trapped case

We now examine the interplay between the harmonic trapping potential and the competition between density and pairing instabilities.

6.4.1 Angle $\theta_P = 0$

Consider first the case when the dipolar orientation is perpendicular to the lattice so that the interaction is purely repulsive. Figure 6.5 shows the

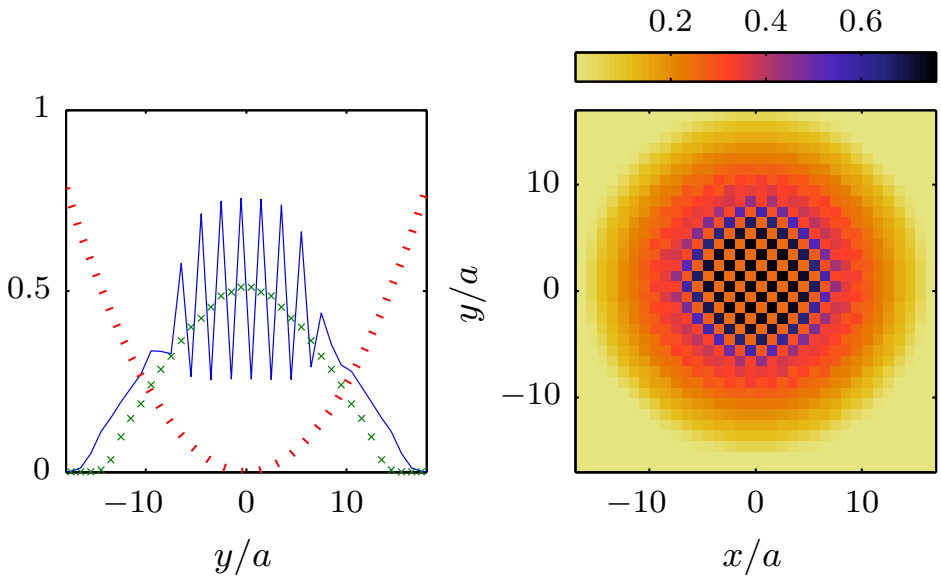

Figure 6.5 | Left: The density profile through the center of the trap. The blue solid line is for $g/t = 1$ and 207 particles trapped and the green crosses are for $g/t = 0.5$ and 144 particles trapped. The red dotted line indicates the trapping potential in units of 2.5t with $\tilde{\omega} = 0.24$. Right: 2D plot of the density in the lattice plane for the $g/t = 1$ case.

density profile for trapped dipoles with $\tilde{\omega} = \omega a\sqrt{m/t} = 0.24$ which is a relatively weak trapping potential so that there are regions with phases resembling those for the case with no trapping potential. For $g/t = 0.5$ and 144 particles, there is no density order whereas for stronger coupling $g/t = 1$ and 207 particles, the system exhibits a checker-board density profile in the center of the trap. In this region, $f \simeq 1/2$ which is optimal for the checker-board phase [91]. The checker-board phase is surrounded by a normal phase with a lower density. Experimentally, similar shell structures have been observed for atoms with a short range interaction [103].

6.4.2 Angles $(\theta_P, \phi_P) = (\pi/2, 0)$

Consider next the case when the dipoles are aligned in the plane along the x-axis ($\phi_P = 0$). There is then a competition between density and pairing order. In figure 6.6, we plot the density and the nearest neighbor

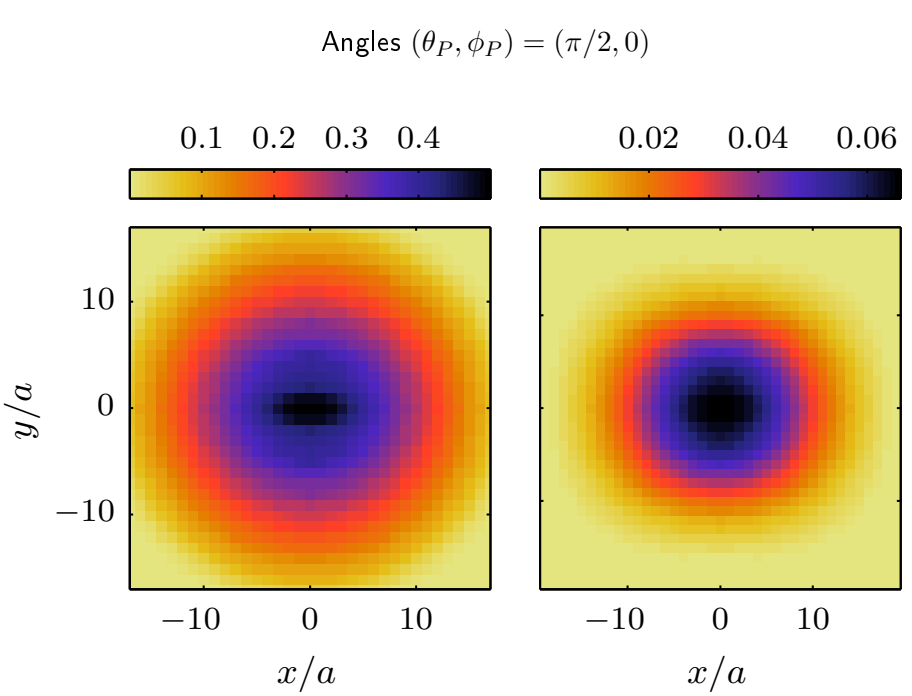

Figure 6.6 | Left: The particle density for 205 dipoles with $\theta_P = \pi/2$, $g/t = 0.85$, and $\tilde{\omega} = 0.11$. Right: The nearest neighbor pairing $(|\langle \hat{c}_{i+e_x} \hat{c}_i \rangle| + |\langle \hat{c}_{i-e_x} \hat{c}_i \rangle|)/2$.

pairing $(|\langle \hat{c}_{i+e_x} \hat{c}_i \rangle| + |\langle \hat{c}_{i-e_x} \hat{c}_i \rangle|)/2$ (symmetrized to reduce trap effects) for $g/t = 0.85$, $\tilde{w} = 0.11$ and 205 dipoles trapped in a 39×39 lattice. For this set of parameters, there is no density order since the density is low and the interaction weak. This results in p-wave pairing throughout most of the cloud. The cloud profile is slightly elongated in the x-direction due to the anisotropy of the dipolar interaction in analogy with what has been observed for dipolar condensates [89].

Figure 6.7 depicts the density and the nearest neighbor pairing for a stronger coupling strength $g/t = 1$ with $\tilde{w} = 0.11$ and 180 dipoles trapped on a 39×39 lattice. There is a pronounced stripe order in the center of the trap with an average filling fraction $f \simeq 1/2$ which squeezes the pairing away from the center into two islands centered at $x = 0$. This intriguing island structure is a consequence of the anisotropy of the interaction. Since the interaction is attractive when the dipoles are aligned head-to-tail (x-direction) and repulsive when they are side-by-side (y-direction), the average interaction for a given radius is attractive in the regions close to the y-axis whereas it is repulsive in the regions close to the x-axis. Thus, pair-

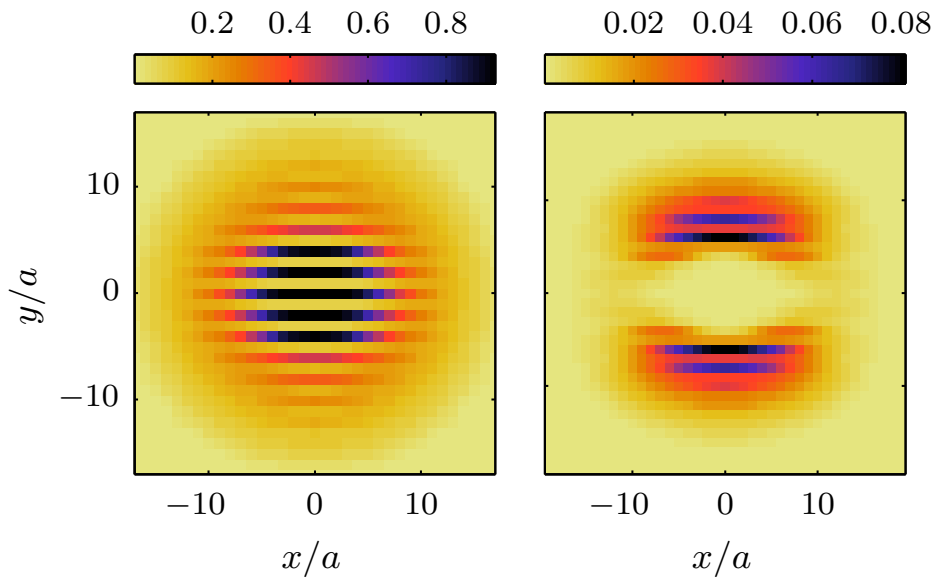

Figure 6.7 | Left: The density profile for 180 dipoles with $\theta_P = \pi/2$, $g/t = 1$, and $\tilde{\omega} = 0.11$. Right: The nearest neighbor pairing $(|\langle \hat{c}_{i+e_x} \hat{c}_i \rangle| + |\langle \hat{c}_{i-e_x} \hat{c}_i \rangle|)/2$.

ing can exist in the islands around $x = 0$ away from the center where stripe order dominates, whereas it is suppressed in the regions around $y = 0$. These islands of pairing should be compared with the ring structures predicted for a two-component trapped Fermi gas with a short range isotropic repulsive interaction where anti-ferromagnetic order competes with d-wave pairing [74]. Remarkably, the stripe order is not completely suppressed in the two islands of pairing. The pairing in fact oscillates *in-phase* with the stripe order. This indicates that the trapping potential induces regions of pairing co-existing with density order as in a supersolid. A phase which has been subject to intense investigations since its theoretical prediction long ago [104–109].

The lattices considered here have experimentally realistic sizes, and with electric dipole moments up to several Debye for the experimentally relevant KRb, RbCs, and LiCs molecules [27, 28, 110–112], one can easily reach the strong-coupling regime with $g/t \gg 1$ using typical values for an optical lattice. The density ordering can be observed directly by in-situ imaging [113, 114] or by time-of-flight experiments which also can detect

pairing correlations [74, 115].

Chapter

7 Trapped dipolar fermions in 2D square lattices at non-zero temperature

7.1 Introduction

In this chapter, we examine fermionic dipoles in a 2D square lattice including the presence of a harmonic trapping potential. The chapter is based on [116]. Focus is on the effects of a non-zero temperature and the melting of density ordered and superfluid phases. We determine the critical temperature for the density ordered phases and find that it is proportional to the interaction strength in the strong coupling regime. For the superfluid phase, we calculate the superfluid fraction and the Berezinskii-Kosterlitz-Thouless (BKT) transition temperature, which is proportional to the hopping matrix element in the strong coupling limit. We analyze the effects of an external trapping potential showing that for experimentally realistic systems, the ordered phases exist in the center of the trap with melting temperatures close to that which can be obtained from a local density approximation.

7.2 Model

We now extend the analysis of the trapped dipolar fermions to finite temperature. As in the zero-temperature calculation we must solve the

Bogoliubov-de Gennes equations [81]

$$\sum_j \begin{pmatrix} L_{ij} & \Delta_{ij} \\ \Delta_{ji}^* & -L_{ij} \end{pmatrix} \begin{pmatrix} u_\eta^j \\ v_\eta^j \end{pmatrix} = E_\eta \begin{pmatrix} u_\eta^i \\ v_\eta^i \end{pmatrix}, \tag{7.1}$$

where $\Delta_{ij} = V_D(\mathbf{r}_{ij})\langle \hat{c}_j \hat{c}_i \rangle$ and

$$L_{ij} = -t\delta_{\langle ij \rangle} + (\sum_k V_D(\mathbf{r}_{ik})\langle n_k \rangle + \frac{m}{2}\omega^2 r_i^2 - \mu)\delta_{ij}. \tag{7.2}$$

Self-consistency is now obtained iteratively through the self-consistent finite temperature relations (6.11) and (6.12).

7.3 Stripe melting at half filling

We first analyze the case of no trapping potential and half filling, $f = N_{\mathrm{L}}^{-1} \sum_i \langle \hat{n}_i \rangle = 1/2$. When the dipoles are perpendicular to the lattice, it follows from the perfect nesting of the Fermi surface that a phase with checkerboard density order persists down to $g/t \to 0$ for $T = 0$ [91]. In the limit of strong interaction $g/t \gg 1$ where the kinetic energy can be neglected and the problem becomes classical, it was shown in the previous chapter that the checkerboard phase is replaced by a striped phase when the dipoles are tilted at a sufficiently large angle θ_P. We now examine the melting of these density ordered phases at a non-zero temperature. The melting is in the Ising universality class due to the discreteness of the lattice, and we therefore expect mean-field theory to yield a qualitatively correct value for the transition temperature. In the following we set $k_{\mathrm{B}} = 1$.

For the case of stripes along the x-direction, we obtain the self-consistent equation for the order parameter from equation (6.17) In the limit of strong interaction, $g/t \gg 1$, this yields

$$T_{\mathrm{c}}^{\mathrm{st}} = -\frac{1}{4}\tilde{V}_D(0, \pi/a). \tag{7.3}$$

When the dipoles are aligned in the lattice plane with $(\theta_P, \phi_P) = (\pi/2, 0)$, equation (7.3) gives $T_{\mathrm{c}}^{\mathrm{st}} \approx 1.27g$. A similar analysis for the checkerboard phase yields $T_{\mathrm{c}}^{\mathrm{cb}} = -\tilde{V}_D(\pi/a, \pi/a)/4$ in the strong coupling limit, which gives $T_{\mathrm{c}}^{\mathrm{cb}} \approx 0.66g$ for $\theta_P = 0$ [91].

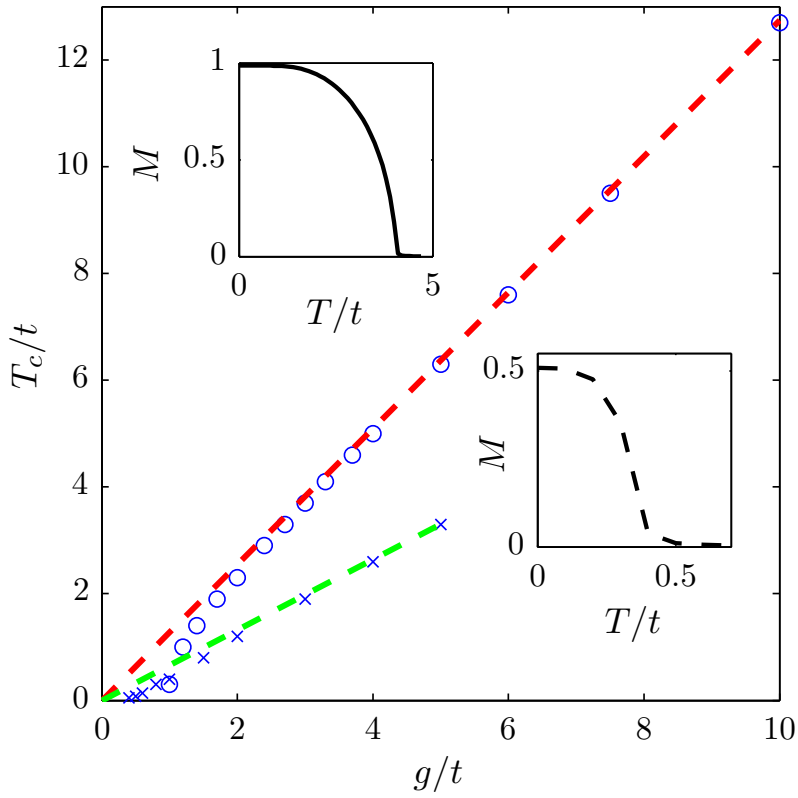

Figure 7.1 | The critical temperature of the striped phase for $(\theta_P, \phi_P) = (\pi/2, 0)$ ($\circ$'s) and of the checkerboard phase for $\theta_P = 0$ ($\times$'s) as a function of coupling strength for half filling obtained from a numerical calculation on 30×30 lattice sites. The dashed lines give the strong coupling results $T_c^{\mathrm{st}} = -\tilde{V}_D(0, \pi/a)/4$ with $(\theta_P, \phi_P) = (\pi/2, 0)$ and $T_c^{\mathrm{cb}} = -\tilde{V}_D(\pi/a, \pi/a)/4$ with $\theta_P = 0$. The upper left inset shows the striped order parameter M for $g/t = 3.3$ as a function of T for $(\theta_P, \phi_P) = (\pi/2, 0)$. The lower right inset shows the checkerboard order parameter M for $g/t = 1$ as a function of T for $\theta_P = 0$.

Figure 7.1 shows the critical temperature as a function of the interaction strength for the checkerboard phase with $\theta_P = 0$ and for the striped phase with $(\theta_P, \phi_P) = (\pi/2, 0)$. The $\circ$'s and $\times$'s are numerical results for the stripe and checkerboard phases respectively, obtained from solving the BdG equations (7.1), and the lines the analytical results for the strong coupling limit discussed above. Finite size effects of the system are eliminated by

neglecting the high temperature tail of the order parameter. For example, for the lower right inset in figure 7.1 the elimination of the high temperature tail gives the critical temperature $T_{\rm c}^{\rm cb}/t = 0.4$. We see that the numerical results agree well with the strong coupling results for $g/t \gg 1$ whereas the critical temperature becomes exponentially suppressed in the weak coupling limit. Note that the critical temperature of the striped phase is almost twice that of the checkerboard phase, which makes it easier to observe experimentally. The upper left inset shows how the striped order parameter M decreases with T for $(\theta_P, \phi_P) = (\pi/2, 0)$ and $g/t = 3.3$, and the lower right inset shows the checkerboard order parameter M as a function of T for $\theta_P = 0$ and $g/t = 1$.

Figure 7.2 shows the critical temperature of the striped and the checkerboard phase as a function of (θ_P, ϕ_P) in the strong coupling regime. It is obtained from $\max[-\tilde{V}(0, \pi/a)/4, -\tilde{V}(\pi/a, \pi/a)/4]$. For most orientations of the dipoles, the critical temperature of the striped phase exceeds that of the checkerboard phase. We note that the upper right corner in the phase-diagram shows a negative critical temperature which indicates that none of the two phases we explore are stable in this region.

7.4 Stripe and superfluid melting at one third filling

For smaller filling fractions, the system can be in a superfluid state with p-wave symmetry for large enough θ_P [81, 94]. This leads to a competition between density and superfluid order in analogy with dipoles moving in a 2D plane without a lattice [101, 117–121]. As an example, we now consider the melting of the superfluid and the striped phase for the filling fraction $f = 1/3$ and $(\theta_P, \phi_P) = (\pi/2, 0)$. As we saw in Chapter 6, mean-field theory predicts the system to be superfluid for $g/t \leq 1.15$ and to exhibit stripe order for $g/t > 1.15$ at $T = 0$.

For the 2D system considered here, the melting of the superfluid phase is of the BKT type as discussed in Chapter 3 with a transition temperature as determined by the phase stiffness of the order parameter [32–34, 44]. The phase stiffness $J_x^{\rm XY}$ associated with a phase twist of the superfluid

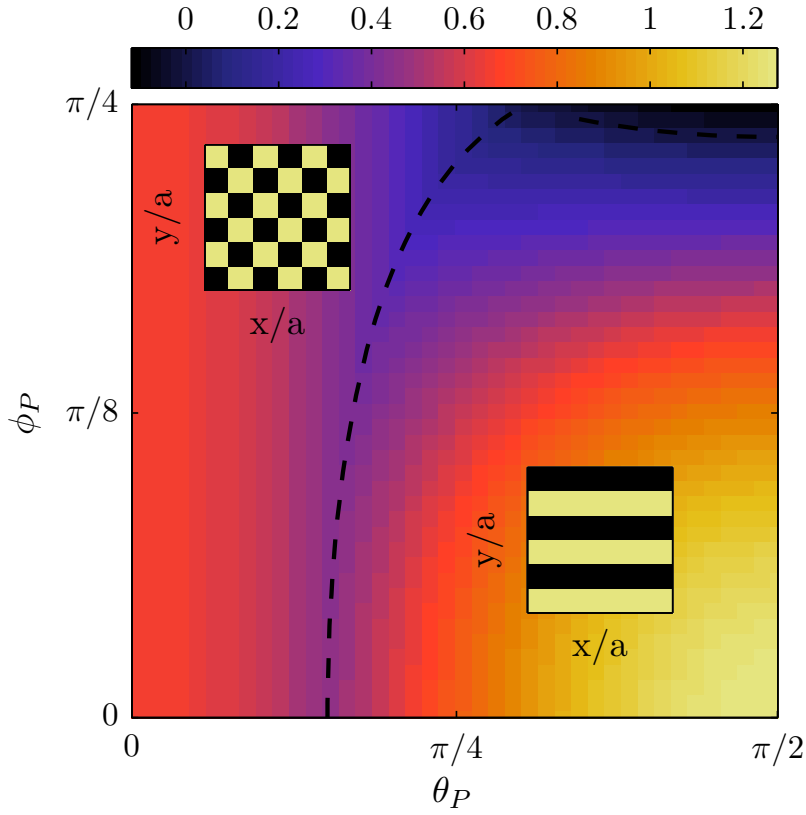

Figure 7.2 | The critical temperature in units og g of the striped and checkerboard phases as a function of the dipole orientation (θ_P, ϕ_P) for half filling. A dashed line marks the boundary between the stripe and checkerboard phases, and the region with no density order is bounded by another dashed line.

order parameter in the x-direction is determined from the energy cost

$$F_\Theta - F_0 \simeq \frac{J_x^{\mathrm{XY}}}{2} \sum_i \delta\Theta^2. \tag{7.4}$$

Here, F_Θ is the free energy when the phase of the order parameter varies by $\delta\Theta$ between neighboring sites in the x-direction and F_0 is the free energy when there is no phase twist [56]. In analogy with the derivation of the superfluid density in Section 4.6, we define the superfluid fraction $\rho_{\mathrm{s},x}$

associated with this phase twist

$$F_\Theta - F_0 = \frac{N}{2}\rho_{\mathrm{s},x} m^* {v_\mathrm{s}}^2 = \frac{N}{4} t \rho_{\mathrm{s},x} \delta\Theta^2. \tag{7.5}$$

Similar expressions hold for the phase stiffness J_y^{XY} and the superfluid fraction $\rho_{\mathrm{s},y}$ for the y-direction. Note that the superfluid fraction is dimensionless.

As in equation (4.40) we perform the gauge transformation corresponding to a phase twist along the x-direction

$$\hat{H}_\Theta = e^{-i\delta\theta \sum_l \hat{x}_l/a} \hat{H} e^{i\delta\theta \sum_l \hat{x}_l/a}. \tag{7.6}$$

The gauge transformation gives $\Delta_{ij} \rightarrow \Delta_{ij} \exp[i(x_i + x_j)\delta\theta/a]$ and only effects the tunneling amplitudes so that $t\hat{c}_i^\dagger \hat{c}_{i\pm e_x} \rightarrow t e^{\pm i\delta\theta} \hat{c}_i^\dagger \hat{c}_{i\pm e_x}$. Expanding the Hamiltonian to second order in $\delta\theta$, we get $\hat{H}_\Theta = \hat{H} + \hat{J} + \hat{T}$ with

$$\begin{aligned} \hat{J} &= -i\delta\theta t \sum_i \left(\hat{c}_i^\dagger \hat{c}_{i+e_x} - \hat{c}_i^\dagger \hat{c}_{i-e_x} \right), \\ \hat{T} &= \frac{t}{2} \delta\theta^2 \sum_i \left(\hat{c}_i^\dagger \hat{c}_{i+e_x} + \hat{c}_i^\dagger \hat{c}_{i-e_x} \right). \end{aligned} \tag{7.7}$$

which differs from the expression for $\hat{J}$ and $\hat{T}$ in Section 4.6, since we are now dealing with a single spin-component. Again, we can take $F_\Theta - F_0 = \Omega_\Theta - \Omega_0$ since the unitary transformation conserves particle number. As seen in equation (4.44) we get

$$\Omega_\Theta - \Omega_0 = \langle \hat{T} \rangle_0 - \frac{\beta}{2} \langle \hat{J}^2 \rangle_0, \tag{7.8}$$

where we have exploited that there is no current in the untwisted case, i.e. $\langle \hat{J} \rangle_0 = 0$ as in the two-component case in Section 4.6. The Bogoliubov transformations can now be inserted to give

$$\langle \hat{T} \rangle = \frac{t}{2} \delta\theta^2 \sum_{\eta,i} (u_\eta^{i*} u_\eta^{i+e_x} + u_\eta^{i*} u_\eta^{i-e_x}) f_\eta \tag{7.9}$$

and

$$\begin{aligned} \left\langle J^2 \right\rangle = -t^2 \delta\theta^2 \sum_{ij} \sum_{\eta\alpha} \sum_{k,l=-1}^{1} kl \left[u_\eta^{i*} u_\alpha^{j*} u_\eta^{j+ke_x} u_\alpha^{i+le_x} \right. \\ \left. \times f_\eta (1 - f_\alpha) - u_\eta^{i*} v_\eta^j u_\alpha^{i+ke_x} v_\alpha^{j+le_x *} f_\eta (1 - f_\alpha) \right]. \end{aligned} \tag{7.10}$$

The sums in equations (7.9) and (7.10) are taken over positive as well as negative energies, and we have made use of the duality $(u_\eta, v_\eta, E_\eta) \leftrightarrow (v_\eta^*, u_\eta^*, -E_\eta)$ of the Bogoliubov-de Gennes equations.

When there is no trap, the Bogoliubov-de Gennes equations are straightforward to solve and equations (7.5), (7.9), and (7.10) yield

$$\rho_{\mathrm{s},x} = \frac{1}{N}\sum_{\mathbf{k}}\left[n_{\mathbf{k}}\cos k_x a - \frac{2t}{T}f_{\mathbf{k}}(1-f_{\mathbf{k}})\sin^2 k_x a\right]. \tag{7.11}$$

Here $E_{\mathbf{k}}$ are the BCS quasi-particle energies for the p-wave paired state, and $n_{\mathbf{k}} = u_{\mathbf{k}}^2 f_{\mathbf{k}} + v_{\mathbf{k}}^2(1-f_{\mathbf{k}})$. This has the same form as for the two-component fermionic gas explored in Section 4.6 except for the factor of two, since we are now dealing with a single spin-component. In the continuum limit $a \to 0$ keeping the density $N/N_{\mathrm{L}}a^2$ constant, this reduces to the usual expression

$$\rho_{\mathrm{s},x} = 1 + (3m^*n)^{-1}(2\pi)^{-3}\int d^3k\,\partial_E f_{\mathbf{k}} k^2 \tag{7.12}$$

for a single component superfluid [122].

From the phase stiffness, we can extract the transition temperature as $T_{\mathrm{BKT}} = \pi\bar{J}^{\mathrm{XY}}/2$ [32–34, 44] where we have taken the average $\bar{J}^{\mathrm{XY}} = (J_x^{\mathrm{XY}} + J_y^{\mathrm{XY}})/2$ to account for the anisotropy of the p-wave pairing. Equations (7.4) and (7.5) give $\bar{J}^{\mathrm{XY}} = N\bar{\rho}_{\mathrm{s}}t/2N_{\mathrm{L}}$ with $\bar{\rho}_{\mathrm{s}} = (\rho_{\mathrm{s},x} + \rho_{\mathrm{s},y})/2$, and we finally obtain

$$T_{\mathrm{BKT}} = \frac{\pi}{4}\frac{N}{N_{\mathrm{L}}}\bar{\rho}_{\mathrm{s}}t = \frac{\pi}{8}\frac{\bar{n}_{\mathrm{s}}}{m^*}, \tag{7.13}$$

with the superfluid density defined as $\bar{n}_{\mathrm{s}} = N\bar{\rho}_{\mathrm{s}}/N_{\mathrm{L}}a^2$ which is now a density and not dimensionless as in (4.39).

In figure 7.3, we plot T_{BKT} as a function of the coupling strength obtained from equation (7.13). For comparison, we plot the mean-field superfluid transition temperature T^*. We also plot the critical temperature $T_{\mathrm{c}}^{\mathrm{st}}$ for the stripe phase which is the ground state for $g/t > 1.15$. For weak coupling, the T_{BKT} approaches T^* as expected [123], whereas it is significantly lower for stronger coupling. For strong coupling, it follows from equation (7.13) that the critical temperature will saturate at $T_{\mathrm{BKT}} \sim t$. Indeed, the numerical results yield $T_{\mathrm{BKT}} \simeq 0.12t$ for $g/t \gg 1$ as can be

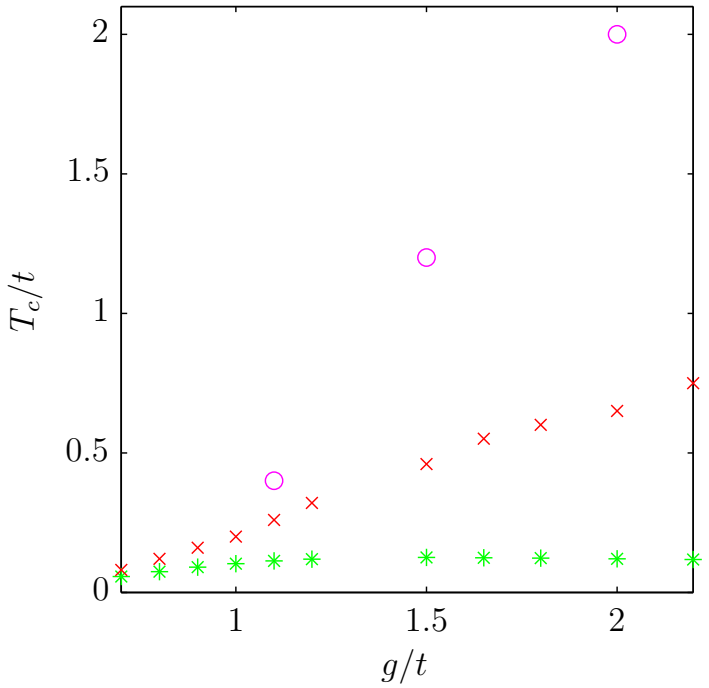

Figure 7.3 | The critical temperature for the superfluid phase ($*$'s) and the striped phase ($\circ$'s) for $(\theta_P, \phi_P) = (\pi/2, 0)$ as a function of coupling strength for one third filling obtained from a numerical calculation on a 27×27 lattice site. The $\times$'s give the mean-field superfluid transition temperature T^*. For illustrative purposes, we plot the critical temperature of the superfluid phase even for $g/t > 1.15$, where stripe order suppresses superfluidity.

seen from figure 7.3. Note however that stripe order sets in for $g/t > 1.15$ which suppresses the superfluid order. Like the case for half filling, we have $T_c^{\mathrm{st}} \sim g$ for the critical temperature for the striped phase, which is a higher temperature than the superfluid transition temperature. It is interesting that both critical temperatures, $T_{\mathrm{BKT}} \sim t$ and $T_c^{\mathrm{st}} \sim g$, can be much higher than that of the anti-ferromagnetic phase for atoms in a 3D lattice, which scales as $T_{\mathrm{N}} \sim t^2/U$ in the strong coupling limit with $U \gg t$ the on-site interaction [124–126].

In figure 7.4, we plot the superfluid fraction and the nearest neighbor order parameter as a function of T for various coupling strengths. As usual

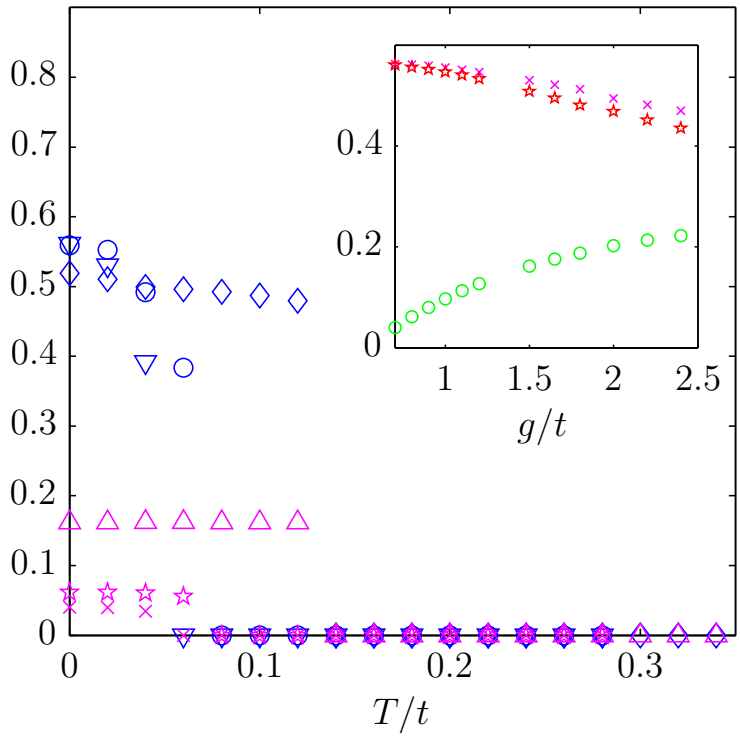

Figure 7.4 | The superfluid fraction $\bar{\rho}_s$ and the nearest neighbor pairing $|\langle \hat{c}_{i+e_x} \hat{c}_i \rangle|$ as a function of T for various coupling strengths. $|\langle \hat{c}_{i+e_x} \hat{c}_i \rangle|$: Pink $\times$'s for $g/t = 0.7$, pink $\star$'s for $g/t = 0.8$, and pink $\triangle$'s for $g/t = 1.5$. $\bar{\rho}_s$: Blue $\triangledown$'s for $g/t = 0.7$, blue $\circ$'s for $g/t = 0.8$, and blue $\diamond$'s for $g/t = 1.5$. The numerical calculations are performed on a 27×27 lattice with one third filling. Inset: The nearest neighbor pairing $|\langle \hat{c}_{i+e_x} \hat{c}_i \rangle|$ (green $\circ$'s) and the superfluid fractions $\rho_{s,x}$ (pink $\times$'s) and $\rho_{s,y}$ (red $\star$'s) as a function of g for $T = 0$.

for a 2D system, the superfluid fraction is discontinuous at the critical temperature. Contrary to a translationally invariant system, the superfluid fraction is less than 1, even for $T = 0$ [127]. In the inset, we plot the superfluid fraction and the nearest neighbor pairing as a function of coupling strength for $T = 0$. We see that $\rho_{\mathrm{s},x} \neq \rho_{\mathrm{s},y}$, which follows from the anisotropy of the p-wave paring. Note that the superfluid fraction behaves very differently from the pairing as a function of the coupling strength [60].

We expect correlation effects to decrease the transition temperatures of

the ordered phases from what is predicted in the present work. Even so, we believe that our results are qualitatively correct due to the long range nature of the interaction. This includes the scaling of T_{BKT}, $T_{\mathrm{c}}^{\mathrm{st}}$, and $T_{\mathrm{c}}^{\mathrm{cb}}$ for strong coupling. Our results therefore present a useful first analysis of the ordered phases of fermionic dipoles in a lattice at non-zero temperature.

7.5 Trapped system

The harmonic trapping potential is always present in atomic gas experiments. For $T = 0$, this leads to the co-existence of superfluid and density ordered phases forming ring and island structures as seen in Chapter 6. We now investigate these effects at a non-zero temperature.

Figure 7.5 (top) shows the density and the checkerboard order parameter as a function of temperature for the dipoles aligned perpendicularly to the lattice plane with $(\theta_P, \phi_P) = (0, 0)$. We have chosen $\tilde{\omega} = \omega a\sqrt{m/t} = 0.24$, $g/t = 1$, and $\mu/t = 4.23$ for the numerical calculations, giving $N = 207 - 210$ dipoles trapped and an average filling fraction close to $1/2$ in the center of trap. For these parameters, there is a large region in the center of the trap with checkerboard density order for $T = 0$. With increasing temperature, the radius of the checkerboard phase in the center shrinks and it melts completely for $T/t \simeq 0.4$. In figure 7.5 (bottom), we compare the central value of the density order parameter with that of an untrapped system at half-filling performed on a 30×30 lattice with the same interaction strength. We see that the critical temperature of the trapped system is close to that of an untrapped system. This shows that the system essentially behaves according to the local density approximation.

In figure 7.6 (top), we plot the density and the stripe order parameter for the case where the dipoles are aligned along the x-axis with $(\theta_P, \phi_P) = (\pi/2, 0)$. The coupling strength is $g/t = 1$, $\tilde{w} = 0.11$, and $\mu/t = -2$ giving $179 - 190$ dipoles trapped with the average filling $f = 0.5$ in the center of trap. For this set of parameters, the center of the trap is in the striped phase for $T = 0$. The stripe order disappears with increasing temperature. Interestingly, the melting is anisotropic in the sense that the stripe order disappears first in the y-direction. The stripe order is completely gone for $T/t \simeq 0.3$. Again, we see from figure 7.6 (bottom) that the density order in the center of the trap agrees well with that of an untrapped system with

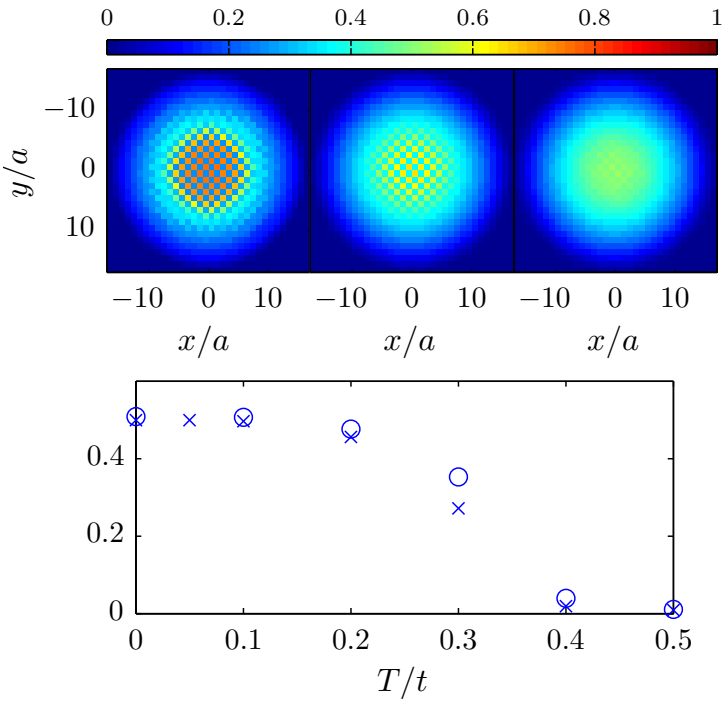

Figure 7.5 | Top: The density for $T/t = 0$ (left), $T/t = 0.3$ (middle), and $T/t = 0.4$ (right) for $g/t = 1$, $\tilde{\omega} = 0.24$, $\theta_P = 0$, and $207 - 210$ dipoles trapped. Bottom: $\times$'s are the checkerboard order parameter $|\langle \hat{n}_i - \hat{n}_{i+e_y} \rangle|$ in the center of the trap as a function of T and $\circ$'s are the checkerboard order parameter performed on the untrapped system at half-filling with the same parameters.

the same parameters.

Finally, we plot in figure 7.7 the pairing order parameter as a function of temperature for $\mu/t = -1.72$ with $(\theta_P, \phi_P) = (\pi/2, 0)$, $g/t = 0.85$, $\tilde{\omega} = 0.11$, and $205 - 207$ dipoles trapped. Since the coupling is weak, the system is superfluid for $T = 0$ and there is no stripe order. As expected, the pairing decreases with increasing T and it disappears for $T/t \simeq 0.11$. The critical temperature is calculated using mean-field theory. We expect corrections to mean-field theory to be small since the critical temperature is so small. The pairing increases slightly with increasing T at low temperature. This is because we for simplicity keep the chemical potential fixed in the numerical

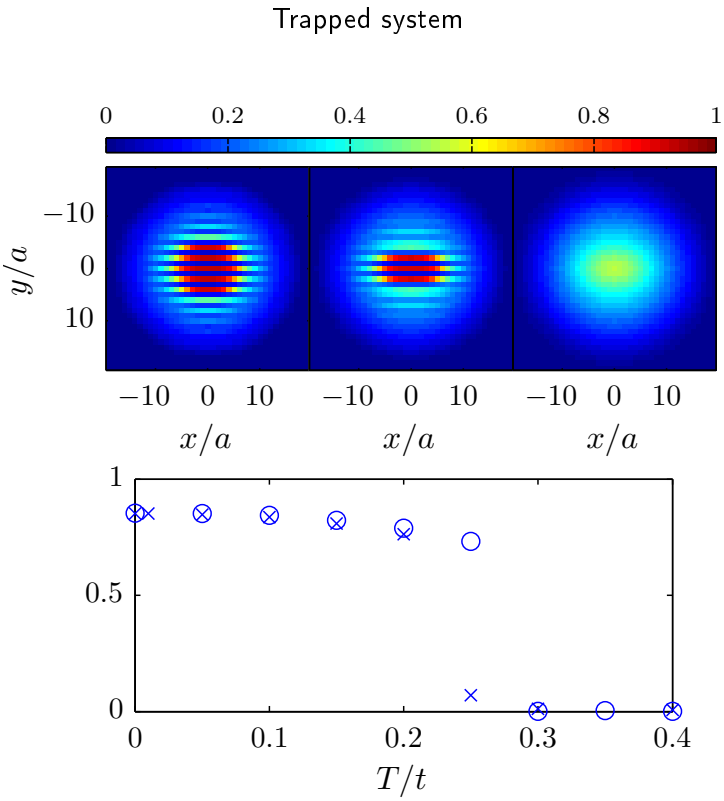

Figure 7.6 | Top: The density for $T/t = 0$ (left), $T/t = 0.1$ (middle), and $T/t = 0.3$ (right) for $g/t = 1$, $\tilde{\omega} = 0.11$, $(\theta_P, \phi_P) = (\pi/2, 0)$, and $179 - 190$ dipoles trapped. Bottom: $\times$'s are the stripe order parameter $|\langle \hat{n}_i - \hat{n}_{i+e_y} \rangle|$ in the center of the trap as a function of T and $\circ$'s are the stripe order parameter of an untrapped system at half filling with the same parameters.

calculations leading to an increased density with increasing T. A number conserving calculation would yield a monotonically decreasing pairing with increasing T.

These results illustrate that even in the presence of a trap, one can observe the superfluid and density ordered phases predicted for the infinite lattice systems, provided the system is large enough. In particular, the transition temperature is determined by the parameters in the center of the trap, and the results for a system with no trap can be used.

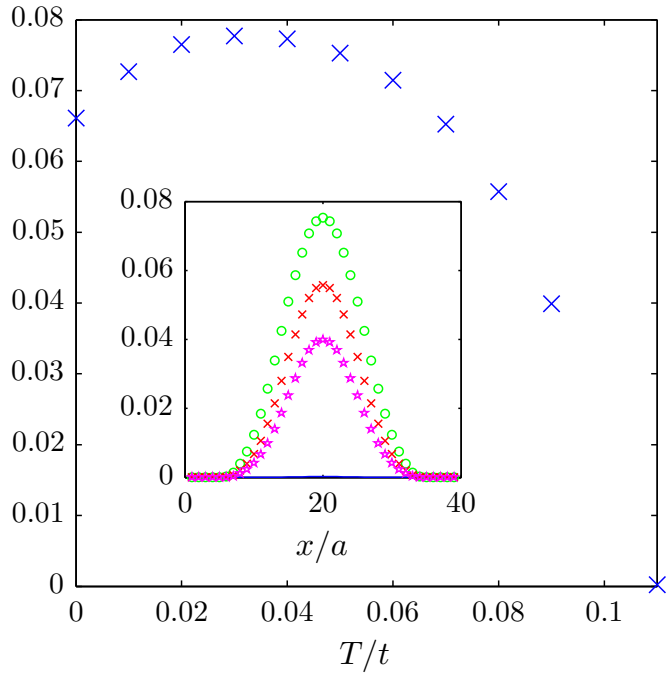

Figure 7.7 | The pairing order parameter $(|\langle \hat{c}_{i+e_x} \hat{c}_i \rangle| + |\langle \hat{c}_{i-e_x} \hat{c}_i \rangle|)/2$ in the center for $\mu = -1.72$ with $\theta_P = \pi/2$, $g/t = 0.85$, and $\tilde{\omega} = 0.11$ as a function of T. There are $205 - 207$ dipoles trapped. The inset shows a diagonal cross section of the pairing order parameter. Green $\circ$'s are $T/t = 0.05$, red $\times$'s are $T/t = 0.08$, pink $\star$'s are $T/t = 0.09$, and blue solid line is for $T/t = 0.11$.

Chapter

8 Conclusion and outlook

This thesis examined a fermionic gas in a 2D optical lattice with harmonic confinement from a mean-field perspective. We started by deriving the mean-field Hubbard Hamiltonian for a two-component system with on-site interactions. This was diagonalized by a Bogoliubov transformation leading to the Bogoliubov-de Gennes equations. By performing a self-consistent calculation of the attractive case we found the on-site pairing order parameter and particle density for a balanced and imbalanced system, respectively. We then extended the model to account for a rotating potential introducing the rotation into the Hubbard Hamiltonian using Peierls substitution. Here, we found that the gap parameter had a central vortex. Finally, we derived an analytical expression of the superfluid density by imposing twisted boundary conditions on the phase of the gap parameter. The superfluid density was then calculated for a Fermi gas in an optical lattice and compared to an expression obtained in momentum space for different temperatures (also done in [60]). To calculate the superfluid density of a Fermi gas in a 2D optical lattice with harmonic confinement we used the local density approximation.

The analysis of trapped fermions in 2D square lattices was then extended to strongly repulsive interactions. The physics of this system was studied using the t-J model which is appropriate in the strongly repulsive

regime. This system was first studied at zero temperature where we found the phase-diagram of the homogeneous system. We then introduced the trapping potential leading to a co-existence of phases in one system with a central d-wave pairing order parameter and normal edges. For illustrative purposes we also considered the finite temperature regime, where we do not believe the method to be sufficient to describe the system accurately.

In the last part of the thesis we studied dipolar fermions, hereby introducing the possibility of anisotropic interactions. We considered the competition of phases as a function of polarization angle and interaction strength. By introducing a trapping potential we found the co existence of a striped ordered density and a p-wave pairing order parameter in the same system. They even had a small overlapping region which could be interpreted as a supersolid region. The final section of the dipolar chapter was dedicated to finite temperature calculations using the Berezinskii-Kosterlitz-Thouless theory. We gave a short introduction to the theory and then proceeded to calculate the critical temperature of the superfluid phase.

A natural continuation of the work presented in this thesis would be to study dipolar fermions with an effective attractive dipolar interaction as has been done in [128] for an untrapped system. It would be interesting to see if the observed topological $p_x + ip_y$ superfluid phase is stable in the trapped system.

So far we have studied a single layer of dipolar fermions with tunable dipole orientation. Adding more layers to the system will introduce even more symmetries and it would be fascinating to consider these possible symmetries as well as a possible interlayer pairing.

Also, the physics of fermions in lattices of different symmetries could be explored. The group of Tilman Esslinger at ETH are working on band-structure engineering forming Dirac bands and manipulating these. I will in the fall 2012 work as a postdoc at ETH where theoretical studies of these systems will play a central role.

Appendix

A Gutzwiller renormalization

Here, we briefly discuss how the Gutzwiller renormalization factors needed in Chapter 5, Subsection 5.3.2, are derived, using simple counting arguments as in [129] neglecting correlations in the wave-functions. We incorporate the projection into the Hamiltonian using the Gutzwiller renormalization factors. These are found by linking the expectation values in the projected state $|\Psi\rangle$ to the expectation values in the unprojected state $|\Psi_0\rangle$

$$\frac{\langle\Psi_0|P_{\mathrm{G}}\hat{O}P_{\mathrm{G}}|\Psi_0\rangle}{\langle\Psi_0|P_{\mathrm{G}}^2|\Psi_0\rangle} \approx g_{\mathrm{O}}\frac{\langle\Psi_0|\hat{O}|\Psi_0\rangle}{\langle\Psi_0|\Psi_0\rangle}, \tag{A.1}$$

with the projection operator $P_{\mathrm{G}} = \prod_i(1-\hat{n}_{i\downarrow}\hat{n}_{i\uparrow})$. We proceed and obtain

$$g_{\mathrm{O}} \approx \frac{\langle\hat{O}\rangle_{\Psi}}{\langle\hat{O}\rangle_{\Psi_0}}. \tag{A.2}$$

We first consider the hopping term, which in the projected state can be rewritten as

$$\langle\hat{c}_{i\uparrow}^{\dagger}\hat{c}_{j\uparrow}\rangle_{\Psi} = \langle(1-\hat{n}_{i\downarrow})\hat{c}_{i\uparrow}^{\dagger}(1-\hat{n}_{j\downarrow})\hat{c}_{j\uparrow}\rangle_{\Psi}\,. \tag{A.3}$$

We only get a contribution from the ket state when there is a single spin-up particle on the j'th lattice site and no particle on the i'th lattice site. For the bra we only get a contribution when there is a single spin-up particle on the i'th lattice site and no particle at the j'th lattice site. The ratio of the expectation value of the operator $(1-\hat{n}_{i\downarrow})\hat{c}^{\dagger}_{i\uparrow}(1-\hat{n}_{j\downarrow})\hat{c}_{j\uparrow}$ in the projected and the unprojected state is then

$$\tilde{g}_{\mathrm{t}} = \frac{(n_{i\uparrow}(1-n_j))^{1/2}(n_{j\uparrow}(1-n_i))^{1/2}}{(n^0_{i\uparrow}(1-n^0_{i\downarrow})(1-n^0_{j\downarrow})(1-n^0_{j\uparrow}))^{1/2}(n^0_{j\uparrow}(1-n^0_{j\downarrow})(1-n^0_{i\downarrow})(1-n^0_{i\uparrow}))^{1/2}}. \tag{A.4}$$

However, since we are interested in the weight factor associated with the hopping term $\hat{c}^{\dagger}_{i\uparrow}\hat{c}_{j\uparrow}$ we proceed and obtain

$$\begin{aligned}\langle \hat{c}^{\dagger}_{i\uparrow}\hat{c}_{j\uparrow}\rangle_{\Psi} &= \langle (1-\hat{n}_{i\downarrow})\hat{c}^{\dagger}_{i\uparrow}(1-\hat{n}_{j\downarrow})\hat{c}_{j\uparrow}\rangle_{\Psi} \\ &\approx \tilde{g}_t(1-n^0_{i\downarrow})(1-n^0_{j\downarrow})\,\langle \hat{c}^{\dagger}_{i\uparrow}\hat{c}_{j\uparrow}\rangle_{\Psi_0}\,. \end{aligned} \tag{A.5}$$

Finally, the renormalization factor takes the form

$$g^{ij}_{\mathrm{t}} = \frac{2\delta_j^{1/2}\delta_i^{1/2}}{(1+\delta_j)^{1/2}(1+\delta_i)^{1/2}}, \tag{A.6}$$

when taking $n_{i\uparrow} = n_{i\downarrow} = n_i/2$ and for simplicity assuming $n^0_i = n_i$ and with $\delta_i = 1 - n_i$ defined in Chapter 5. A similar factor for the spin-spin term can be calculated. A simple way to do this is by rewriting the spin-spin term in terms of its components

$$\mathbf{S}_i \cdot \mathbf{S}_j = \hat{S}^z_i\hat{S}^z_j + \frac{1}{2}\left(\hat{S}^+_i\hat{S}^-_j + \hat{S}^-_i\hat{S}^+_j\right). \tag{A.7}$$

Firstly, we consider the $+/-$-component. By arguments similar to the arguments in the calculation of the renormalization factor on the hopping term we find the renormalization factors associated with the $+/-$-terms

$$
\begin{aligned}
g_{\mathrm{s}}^{\pm} &= \frac{\sqrt{n_{i\downarrow} n_{j\uparrow} n_{i\uparrow} n_{j\downarrow}}}{\sqrt{n_{i\uparrow}^0 \left(1-n_{i\downarrow}^0\right) n_{j\downarrow}^0 \left(1-n_{j\uparrow}^0\right) n_{i\downarrow}^0 \left(1-n_{i\uparrow}^0\right) n_{j\uparrow}^0 \left(1-n_{j\downarrow}^0\right)}} \\
&= \frac{1}{(1-n_i^0/2)(1-n_j^0/2)} \\
&= \frac{4}{(1+\delta_i)(1+\delta_j)}.
\end{aligned} \tag{A.8}
$$

Secondly, we find the factor corresponding to the z-term

$$
g_{\mathrm{s}}^{z} = \frac{\langle \hat{S}_i^z \hat{S}_j^z \rangle_{\Psi}}{\langle \hat{S}_i^z \hat{S}_j^z \rangle_{\Psi_0}}. \tag{A.9}
$$

We make use of the fact that $\hat{S}_i^z = (\hat{n}_{i\uparrow} - \hat{n}_{i\downarrow})/2$ and rewrite the expression to obtain

$$
\begin{aligned}
4 \langle \hat{S}_i^z \hat{S}_j^z \rangle = {} & \langle \hat{n}_{i\uparrow}(1-\hat{n}_{i\downarrow})\hat{n}_{j\uparrow}(1-\hat{n}_{j\downarrow}) \rangle + \langle \hat{n}_{i\downarrow}(1-\hat{n}_{i\uparrow})\hat{n}_{j\downarrow}(1-\hat{n}_{j\uparrow}) \rangle \\
& - \langle \hat{n}_{i\uparrow}(1-\hat{n}_{i\downarrow})\hat{n}_{j\downarrow}(1-\hat{n}_{j\uparrow}) \rangle - \langle \hat{n}_{i\downarrow}(1-\hat{n}_{i\uparrow})\hat{n}_{j\uparrow}(1-\hat{n}_{j\downarrow}) \rangle .
\end{aligned} \tag{A.10}
$$

For illustrative purposes we find the Gutzwiller renormalization factor for the first term

$$
\begin{aligned}
g_{\mathrm{s}}^{z} &= \frac{n_{i\uparrow} n_{j\uparrow}}{n_{i\uparrow}^0 (1-n_{i\downarrow}^0) n_{j\uparrow}^0 (1-n_{j\downarrow}^0)} \\
&\approx \frac{1}{(1-n_i/2)(1-n_j/2)} = \frac{4}{(1+\delta_i)(1+\delta_j)}.
\end{aligned} \tag{A.11}
$$

The factors associated with the four terms in (A.10) are identical. The common Gutzwiller factor for the spin-spin term therefore takes the following form

$$
g_{\mathrm{s}}^{ij} = \frac{n_i n_j}{n_i^0 (1-n_i^0/2) n_j^0 (1-n_j^0/2)} = \frac{4}{(1+\delta_i)(1+\delta_j)}. \tag{A.12}
$$

Bibliography

[1] M. H. Anderson, J. R. Ensher, M. R. Matthews, C. E. Wieman & E. A. Cornell: *Observation of Bose-Einstein Condensation in a Dilute Atomic Vapor*, Science **269**, 198 (1995).

[2] K. B. Davis, M. O. Mewes, M. R. Andrews, N. J. van Druten, D. S. Durfee, D. M. Kurn & W. Ketterle: *Bose-Einstein Condensation in a Gas of Sodium Atoms*, Phys. Rev. Lett. **75**, 3969 (1995).

[3] W. C. Stwalley: *Stability of Spin-Aligned Hydrogen at Low Temperatures and High Magnetic Fields: New Field-Dependent Scattering Resonances and Predissociations*, Phys. Rev. Lett. **37**, 1628 (1976).

[4] E. Tiesinga, B. J. Verhaar & H. T. C. Stoof: *Threshold and resonance phenomena in ultracold ground-state collisions*, Phys. Rev. A **47**, 4114 (1993).

[5] S. Inouye, M. R. Andrews, J. Stenger, H.-J. Miesner, D. M. Stamper-Kurn & W. Ketterle: *Observation of Feshbach resonances in a Bose-Einstein condensate*, Nature **392**, 151 (1998).

[6] P. Courteille, R. S. Freeland, D. J. Heinzen, F. A. van Abeelen & B. J. Verhaar: *Observation of a Feshbach Resonance in Cold Atom Scattering*, Phys. Rev. Lett. **81**, 69 (1998).

[7] M. Greiner, O. Mandel, T. Esslinger, T. W. Hänsch & I. Bloch: *Quantum phase transition from a superfluid to a Mott insulator in a gas of ultracold atoms*, Nature **415**, 39 (2002).

[8] I. Bloch: *Ultracold quantum gases in optical lattices*, Nature Physics **1**, 23 (2005).

[9] B. DeMarco & D. S. Jin: *Onset of Fermi Degeneracy in a Trapped Atomic Gas*, Science **285**, 1703 (1999).

[10] G. Roati, F. Riboli, G. Modugno & M. Inguscio: *Fermi-Bose Quantum Degenerate* ^{40}K-^{87}Rb *Mixture with Attractive Interaction*, Phys. Rev. Lett. **89**, 150403 (2002).

[11] A. G. Truscott, K. E. Strecker, W. I. McAlexander, G. B. Partridge & R. G. Hulet: *Observation of Fermi Pressure in a Gas of Trapped Atoms*, Science **291**, 2570 (2001).

[12] F. Schreck, L. Khaykovich, K. L. Corwin, G. Ferrari, T. Bourdel, J. Cubizolles & C. Salomon: *Quasipure Bose-Einstein Condensate Immersed in a Fermi Sea*, Phys. Rev. Lett. **87**, 080403 (2001).

[13] S. R. Granade, M. E. Gehm, K. M. O'Hara & J. E. Thomas: *All-Optical Production of a Degenerate Fermi Gas*, Phys. Rev. Lett. **88**, 120405 (2002).

[14] Z. Hadzibabic, C. A. Stan, K. Dieckmann, S. Gupta, M. W. Zwierlein, A. Görlitz & W. Ketterle: *Two-Species Mixture of Quantum Degenerate Bose and Fermi Gases*, Phys. Rev. Lett. **88**, 160401 (2002).

[15] S. Jochim, M. Bartenstein, A. Altmeyer, G. Hendl, S. Riedl, C. Chin, J. Hecker Denschlag & R. Grimm: *Bose-Einstein Condensation of Molecules*, Science **302**, 2101 (2003).

[16] Z. Hadzibabic, P. Krüger, M. Cheneau, B. Battelier & J. Dalibard: *Berezinskii-Kosterlitz-Thouless crossover in a trapped atomic gas*, Nature **441**, 1118 (2006).

[17] M. W. Zwierlein, J. R. Abo-Shaeer, A. Schirtotzek, C. H. Schunck & W. Ketterle: *Vortices and superfluidity in a strongly interacting Fermi gas*, Nature **435**, 1047 (2005).

[18] J. Chin, D. Miller, Y. Liu, C. Stan, W. Setiawan, C. Sanner, K. Xu & W. Ketterle: *Evidence for superfluidity of ultracold fermions in an optical lattice*, Nature **443**, 961 (2006).

[19] C. Sanner, E. J. Su, A. Keshet, W. Huang, J. Gillen, R. Gommers & W. Ketterle: *Speckle Imaging of Spin Fluctuations in a Strongly Interacting Fermi Gas*, Phys. Rev. Lett. **106**, 010402 (2011).

[20] P. W. Anderson: *The Resonating Valence Bond State in La2CuO4 and Superconductivity*, Science **235**, 1196 (1987).

[21] P. A. Lee, N. Nagaosa & X.-G. Wen: *Doping a Mott insulator: Physics of high-temperature superconductivity*, Rev. Mod. Phys. **78**, 17 (2006).

[22] M. Ogata & H. Fukuyama: *The t-J model for the oxide high- T c superconductors*, Reports on Progress in Physics **71**, 036501 (2008).

[23] T. M. Rice & K. L. Hur: *Superconductivity close to the Mott state: From condensed-matter systems to superfluidity in optical lattices*, Annals of Physics **324**, 1452 (2009).

[24] Q. Beaufils, R. Chicireanu, T. Zanon, B. Laburthe-Tolra, E. Maréchal, L. Vernac, J.-C. Keller & O. Gorceix: *All-optical production of chromium Bose-Einstein condensates*, Phys. Rev. A **77**, 061601 (2008).

[25] T. Koch, T. Lahaye, J. Metz, B. Frölich, A. Griesmaier & T. Pfau: *Stabilization of a purely dipolar quantum gas against collapse*, Nature Physics **4**, 218 (2008).

[26] M. Lu, N. Q. Burdick, S. H. Youn & B. L. Lev: *Strongly Dipolar Bose-Einstein Condensate of Dysprosium*, Phys. Rev. Lett. **107**, 190401 (2011).

[27] K.-K. Ni, S. Ospelkaus, M. H. G. de Miranda, A. Peer, B. Neyenhuis, J. J. Zirbel, S. Kotochigova, P. S. Julienne, D. S. Jin & J. Ye: *A High Phase-Space-Density Gas of Polar Molecules*, Science **322**, 231 (2008).

[28] K.-K. Ni, S. Ospelkaus, D. Wang, G. Quemener, B. Neyenhuis, H. G. de Miranda, J. L. Bohn, J. Ye & D. S. Jin: *Dipolar collisions of polar molecules in the quantum regime*, Nature **464**, 1324 (2010).

[29] M.-S. Heo, T. T. Wang, C. A. Christensen, T. M. Rvachov, D. A. Cotta, J.-H. Choi, Y.-R. Lee & W. Ketterle: *Formation of Ultracold Fermionic NaLi Feshbach Molecules*, ArXiv e-prints (2012), 1205.5304.

[30] C.-H. Wu, J. W. Park, P. Ahmadi, S. Will & M. W. Zwierlein: *Ultracold Fermionic Feshbach Molecules of* $^{23}Na^{40}K$, ArXiv e-prints (2012), 1206.5023.

[31] C. J. Pethick & H. Smith: *Bose-Einstein Condensation in Dilute Gases*, Cambridge University Press (2004).

[32] J. M. Kosterlitz & D. J. Thouless: *Long range order and metastability in two dimensional solids and superfluids. (Application of dislocation theory)*, Journal of Physics C: Solid State Physics **5**, L124 (1972).

[33] J. M. Kosterlitz & D. J. Thouless: *Ordering, metastability and phase transitions in two-dimensional systems*, Journal of Physics C: Solid State Physics **6**, 1181 (1973).

[34] B. V. L.: *Destruction of Long-range Order in One-dimensional and Two-dimensional Systems Possessing a Continuous Symmetry Group. II. Quantum Systems.*, Sov. Phys. JETP **34**, 610 (1972).

[35] D. Gennes: *Superconductivity of Metals and Alloys*, W. A. Benjamin, Inc. (1966).

[36] J. Analytis, S. Blundell & A. Ardavan: *Landau Levels, Molecular Orbitals, and the Hofstadter Butterfly in Finite Systems*, Am. J. Phys. **72**, 613 (2004).

[37] S. Giorgini, L. P. Pitaevskii & S. Stringari: *Theory of ultracold atomic Fermi gases*, Rev. Mod. Phys. **80**, 1215 (2008).

[38] F. C. Zhang, C. Gros, T. M. Rice & H. Shiba: *A renormalised Hamiltonian approach to a resonant valence bond wavefunction*, Superconductor Science and Technology **1**, 36 (1988).

[39] M. C. Gutzwiller: *Correlation of Electrons in a Narrow s Band*, Phys. Rev. **137**, A1726 (1965).

[40] J. Bardeen, L. N. Cooper & J. R. Schrieffer: *Theory of Superconductivity*, Phys. Rev. **108**, 1175 (1957).

[41] J. Bardeen, L. N. Cooper & J. R. Schrieffer: *Microscopic Theory of Superconductivity*, Phys. Rev. **106**, 162 (1957).

[42] L. N. Cooper: *Bound Electron Pairs in a Degenerate Fermi Gas*, Phys. Rev. **104**, 1189 (1956).

[43] M. Greiner & S. Fölling: *Condensed-matter physics: Optical lattices*, Nature **453**, 736 (2008).

[44] P. M. Chaikin & T. C. Lubensky: *Principles of Condensed Matter Physics*, Cambridge University Press (1995).

[45] N. Nagaosa: *Quantum field theory in condensed matter physics*, Springer, Berlin (1999).

[46] A. Fetter & J. Walecka: *Quantum Theory of Many-Particle Systems*, Dover Publications (2003).

[47] M. Inguscio: *COURSE CLXIV: Ultra-cold Fermi Gases*, IOS PRESS, SOCIETÀ ITALIANA DI FISICA, Gazelle Books Services Ltd., IOS Press, Inc. (2007).

[48] Y. Chen, Z. Wang, F. Zhang & C. Ting: *Exploring Exotic Superfluidity of Polarized Ultracold Fermions in Optical Lattices*, Phys. Rev. B **79**, 054512 (2009).

[49] D.-H. Kim & P. Törmä: *Fulde-Ferrell-Larkin-Ovchinnikov state in the dimensional crossover between one- and three-dimensional lattices*, Phys. Rev. B **85**, 180508 (2012).

[50] M. Zwierlein, J. Abo-Shaeer, A. Schirotzek, C. Schunck & W. Ketterle: *Vortices and Superfluidity in a Strongly Interacting Fermi Gas*, Nature **435**, 1047 (2005).

[51] R. A. Williams, J. D. Pillet, S. Al-Assam, B. Fletcher, M. Shotter & C. J. Foot: *Dynamic optical lattices: two-dimensional rotating and accordion lattices for ultracold atoms*, Opt. Express **16**, 16977 (2008).

[52] S. Tung, V. Schweikhard & E. A. Cornell: *Observation of Vortex Pinning in Bose-Einstein Condensates*, Phys. Rev. Lett. **97**, 240402 (2006).

[53] E. Lundh: *Rotating States for Trapped Bosons in an Optical Lattice*, Europhys. Let. **84**, 10007 (2008).

[54] C. Wu, H. Chen, J. Hu & S. Zhang: *Vortex Configurations of Bosons in an Optical Lattice*, Phys. Rev. A **69**, 043609 (2004).

[55] N. Nygaard, G. M. Bruun, C. W. Clark & D. L. Feder: *Microscopic Structure of a Vortex Line in a Dilute Superfluid Fermi Gas*, Phys. Rev. Lett. **90**, 210402 (2003).

[56] M. E. Fisher, M. N. Barber & D. Jasnow: *Helicity Modulus, Superfluidity, and Scaling in Isotropic Systems*, Phys. Rev. A **8**, 1111 (1973).

[57] E. H. Lieb, R. Seiringer & J. Yngvason: *Superfluidity in dilute trapped Bose gases*, Phys. Rev. B **66**, 134529 (2002).

[58] E. Taylor, A. Griffin, N. Fukushima & Y. Ohashi: *Pairing fluctuations and the superfluid density through the BCS-BEC crossover*, Phys. Rev. A **74**, 063626 (2006).

[59] P. M. Chaikin & T. C. Lubensky: *Many-Particle Physics*, Kluwer Academics (2010).

[60] T. Paananen: *Superfluid Density of the Ultra-Cold Fermi Gas in Optical Lattices*, J. Phys. B: At. Mol. Opt. Phys. **42**, 165304 (2009).

[61] A. A. Shams & H. Glyde: *Superfluidity and Bose-Einstein Condensation in Optical Lattices and Porous Media: A Path Integral Monte Carlo Study*, Phys. Rev. B **79**, 214508 (2009).

[62] A.-L. Gadsbølle, H. F. Song & K. Le Hur: *d-wave superfluid with gapless edges in a cold-atom trap*, Phys. Rev. A **85**, 051603 (2012).

[63] J. G. Bednorz & K. A. Müller: *Possible highT_c superconductivity in the Ba-La-Cu-O system*, Z. Phys. B **64**, 189 (1986).

[64] D. A. Wollman, D. J. Van Harlingen, W. C. Lee, D. M. Ginsberg & A. J. Leggett: *Experimental determination of the superconducting pairing state in YBCO from the phase coherence of YBCO-Pb dc SQUIDs*, Phys. Rev. Lett. **71**, 2134 (1993).

[65] C. C. Tsuei, J. R. Kirtley, C. C. Chi, L. S. Yu-Jahnes, A. Gupta, T. Shaw, J. Z. Sun & M. B. Ketchen: *Pairing Symmetry and Flux Quantization in a Tricrystal Superconducting Ring of* $YBa_2Cu_3O_{7-\delta}$, Phys. Rev. Lett. **73**, 593 (1994).

[66] S. Trotzky, L. Pollet, F. Gerbier, U. Schnorrberger, I. Bloch, N. V. Prokof'ev, B. Svistunov & M. Troyer: *Suppression of the critical temperature for superfluidity near the Mott transition*, Nature Physics **6**, 998 (2010).

[67] M. Köhl, H. Moritz, T. Stöferle, K. Günter & T. Esslinger: *Fermionic Atoms in a Three Dimensional Optical Lattice: Observing Fermi Surfaces, Dynamics, and Interactions*, Phys. Rev. Lett. **94**, 080403 (2005).

[68] J. T. Stewart, J. P. Gaebler & D. S. Jin: *Using photoemission spectroscopy to probe a strongly interacting Fermi gas*, Nature **454**, 744 (2008).

[69] J. Simon, W. S. Bakr, R. Ma, M. E. Tai, P. M. Preiss & M. Greiner: *Quantum simulation of antiferromagnetic spin chains in an optical lattice*, Nature **472**, 307 (2011).

[70] R. Jordens, N. Strohmaier, K. Gunter, H. Moritz & T. Esslinger: *A Mott insulator of fermionic atoms in an optical lattice*, Nature **455**, 204 (2008).

[71] U. Schneider, L. Hackermüller, S. Will, T. Best, I. Bloch, T. A. Costi, R. W. Helmes, D. Rasch & A. Rosch: *Metallic and Insulating Phases of Repulsively Interacting Fermions in a 3D Optical Lattice*, Science **322**, 1520 (2008).

[72] R. Jördens, L. Tarruell, D. Greif, T. Uehlinger, N. Strohmaier, H. Moritz, T. Esslinger, L. De Leo, C. Kollath, A. Georges, V. Scarola, L. Pollet, E. Burovski, E. Kozik & M. Troyer: *Quantitative Determination of Temperature in the Approach to Magnetic Order of Ultracold Fermions in an Optical Lattice*, Phys. Rev. Lett. **104**, 180401 (2010).

[73] W. Hofstetter, J. I. Cirac, P. Zoller, E. Demler & M. D. Lukin: *High-Temperature Superfluidity of Fermionic Atoms in Optical Lattices*, Phys. Rev. Lett. **89**, 220407 (2002).

[74] B. M. Andersen & G. M. Bruun: *Magnetic and superfluid phases of confined fermions in two-dimensional optical lattices*, Phys. Rev. A **76**, 041602 (2007).

[75] P. W. Anderson, P. A. Lee, M. Randeria, T. M. Rice, N. Trivedi & F. C. Zhang: *The physics behind high-temperature superconducting cuprates: the 'plain vanilla' version of RVB*, Journal of Physics: Condensed Matter **16**, R755 (2004).

[76] K. Le Hur, C.-H. Chung & I. Paul: *Designing heterostructures with higher-temperature superconductivity*, Phys. Rev. B **84**, 024526 (2011).

[77] A. Paramekanti, M. Randeria & N. Trivedi: *Projected Wave Functions and High Temperature Superconductivity*, Phys. Rev. Lett. **87**, 217002 (2001).

[78] T. N. De Silva & E. J. Mueller: *Profiles of near-resonant population-imbalanced trapped Fermi gases*, Phys. Rev. A **73**, 051602 (2006).

[79] T. Kitagawa, A. Aspect, M. Greiner & E. Demler: *Phase-Sensitive Measurements of Order Parameters for Ultracold Atoms through Two-Particle Interferometry*, Phys. Rev. Lett. **106**, 115302 (2011).

[80] N. R. Cooper & Z. Hadzibabic: *Measuring the Superfluid Fraction of an Ultracold Atomic Gas*, Phys. Rev. Lett. **104**, 030401 (2010).

[81] A.-L. Gadsbølle & G. M. Bruun: *Harmonically trapped dipolar fermions in a two-dimensional square lattice*, Phys. Rev. A **85**, 021604 (2012).

[82] J. W. Park, C.-H. Wu, I. Santiago, T. G. Tiecke, S. Will, P. Ahmadi & M. W. Zwierlein: *Quantum degenerate Bose-Fermi mixture of chemically different atomic species with widely tunable interactions*, Phys. Rev. A **85**, 051602 (2012).

[83] J. G. Danzl, M. J. Mark, E. Haller, M. Gustavsson, R. Hart, J. Aldegunde, J. M. Hutson & H.-C. Nägerl: *An ultracold high-density sample of rovibronic ground-state molecules in an optical lattice*, Nature Physics **6**, 265 (2010).

[84] J. C. Cremon, G. M. Bruun & S. M. Reimann: *Tunable Wigner States with Dipolar Atoms and Molecules*, Phys. Rev. Lett. **105**, 255301 (2010).

[85] M. Maik, P. Buonsante, A. Vezzani & J. Zakrzewski: *Dipolar bosons on an optical lattice ring*, Phys. Rev. A **84**, 053615 (2011).

[86] A. G. Volosniev, D. V. Fedorov, A. S. Jensen & N. T. Zinner: *Model Independence in Two Dimensions and Polarized Cold Dipolar Molecules*, Phys. Rev. Lett. **106**, 250401 (2011).

[87] A. G. Volosniev, D. V. Fedorov, A. S. Jensen & N. T. Zinner: *Few-body bound-state stability of dipolar molecules in two dimensions*, Phys. Rev. A **85**, 023609 (2012).

[88] M. Baranov: *Theoretical progress in many-body physics with ultracold dipolar gases*, Physics Reports **464**, 71 (2008).

[89] T. Lahaye, C. Menotti, L. Santos, M. Lewenstein & T. Pfau: *The physics of dipolar bosonic quantum gases*, Reports on Progress in Physics **72**, 126401 (2009).

[90] T. Lahaye, C. Menotti, L. Santos, M. Lewenstein & T. Pfau: *The physics of dipolar bosonic quantum gases*, Reports on Progress in Physics **72**, 126401 (2009).

[91] K. Mikelsons & J. K. Freericks: *Density-wave patterns for fermionic dipolar molecules on a square optical lattice: Mean-field-theory analysis*, Phys. Rev. A **83**, 043609 (2011).

[92] C. Lin, E. Zhao & W. V. Liu: *Liquid crystal phases of ultracold dipolar fermions on a lattice*, Phys. Rev. B **81**, 045115 (2010).

[93] L. He & W. Hofstetter: *Supersolid phase of cold fermionic polar molecules in two-dimensional optical lattices*, Phys. Rev. A **83**, 053629 (2011).

[94] S. G. Bhongale, L. Mathey, S.-W. Tsai, C. W. Clark & E. Zhao: *Bond Order Solid of Two-Dimensional Dipolar Fermions*, Phys. Rev. Lett. **108**, 145301 (2012).

[95] I. Danshita & C. A. R. Sá de Melo: *Stability of Superfluid and Supersolid Phases of Dipolar Bosons in Optical Lattices*, Phys. Rev. Lett. **103**, 225301 (2009).

[96] I. Martin, G. Ortiz, A. V. Balatsky & A. R. Bishop: *competing quantum orderings in cuptare superconductors: a minimal model*, International Journal of Modern Physics B **14**, 3567 (2000).

[97] M. Ichioka, M. Takigawa & K. Machida: *Vortex Structure in Superconducting Stripe States*, Journal of the Physical Society of Japan **70**, 33 (2001).

[98] Y. Chen, Z. D. Wang, J.-X. Zhu & C. S. Ting: *Vortex Charges in High-Temperature Superconductors*, Phys. Rev. Lett. **89**, 217001 (2002).

[99] B. M. Andersen, P. J. Hirschfeld, A. P. Kampf & M. Schmid: *Disorder-Induced Static Antiferromagnetism in Cuprate Superconductors*, Phys. Rev. Lett. **99**, 147002 (2007).

[100] E. Müller-Hartmann: *Correlated fermions on a lattice in high dimensions*, Z. Phys. B **74**, 507 (1989), 10.1007/BF01311397.

[101] G. M. Bruun & E. Taylor: *Quantum Phases of a Two-Dimensional Dipolar Fermi Gas*, Phys. Rev. Lett. **101**, 245301 (2008).

[102] M. A. Baranov, L. Dobrek & M. Lewenstein: *Superfluidity of Trapped Dipolar Fermi Gases*, Phys. Rev. Lett. **92**, 250403 (2004).

[103] I. Bloch, J. Dalibard & W. Zwerger: *Many-body physics with ultracold gases*, Rev. Mod. Phys. **80**, 885 (2008).

[104] A. J. Leggett: *Can a Solid Be "Superfluid"?*, Phys. Rev. Lett. **25**, 1543 (1970).

[105] G. V. Chester: *Speculations on Bose-Einstein Condensation and Quantum Crystals*, Phys. Rev. A **2**, 256 (1970).

[106] M. H. W. Chan: *Supersolidity*, Science **319**, 1207 (2008).

[107] E. Kim & M. H. W. Chan: *Probable observation of a supersolid helium phase*, Nature **427**, 225 (2004).

[108] B. Capogrosso-Sansone, C. Trefzger, M. Lewenstein, P. Zoller & G. Pupillo: *Quantum Phases of Cold Polar Molecules in 2D Optical Lattices*, Phys. Rev. Lett. **104**, 125301 (2010).

[109] I. Danshita & C. A. R. Sá de Melo: *Stability of Superfluid and Supersolid Phases of Dipolar Bosons in Optical Lattices*, Phys. Rev. Lett. **103**, 225301 (2009).

[110] K. Pilch, A. D. Lange, A. Prantner, G. Kerner, F. Ferlaino, H.-C. Nägerl & R. Grimm: *Observation of interspecies Feshbach resonances in an ultracold Rb-Cs mixture*, Phys. Rev. A **79**, 042718 (2009).

[111] S. Kotochigova & E. Tiesinga: *Ab initio relativistic calculation of the RbCs molecule.*, J Chem Phys **123**, 174304 (2005).

[112] J. Deiglmayr, M. Repp, A. Grochola, O. Dulieu, R. Wester & M. Weidemüller: *Dipolar effects and collisions in an ultracold gas of LiCs molecules*, Journal of Physics: Conference Series **264**, 012014 (2011).

[113] J. F. Sherson, C. Weitenberg, M. Endres, M. Cheneau, I. Bloch & S. Kuhr: *Single-atom-resolved fluorescence imaging of an atomic Mott insulator*, Nature **467**, 68 (2010).

[114] W. S. Bakr, J. I. Gillen, A. Peng, S. Folling & M. Greiner: *A quantum gas microscope for detecting single atoms in a Hubbard-regime optical lattice*, Nature **462**, 74 (2009).

[115] E. Altman, E. Demler & M. D. Lukin: *Probing many-body states of ultracold atoms via noise correlations*, Phys. Rev. A **70**, 013603 (2004).

[116] A.-L. Gadsbolle & G. M. Bruun: *Dipolar fermions in a two-dimensional lattice at non-zero temperature*, ArXiv e-prints (2012), 1206.4974.

[117] K. Sun, C. Wu & S. Das Sarma: *Spontaneous inhomogeneous phases in ultracold dipolar Fermi gases*, Phys. Rev. B **82**, 075105 (2010).

[118] Y. Yamaguchi, T. Sogo, T. Ito & T. Miyakawa: *Density-wave instability in a two-dimensional dipolar Fermi gas*, Phys. Rev. A **82**, 013643 (2010).

[119] L. M. Sieberer & M. A. Baranov: *Collective modes, stability, and superfluid transition of a quasi-two-dimensional dipolar Fermi gas*, Phys. Rev. A **84**, 063633 (2011).

[120] M. M. Parish & F. M. Marchetti: *Density Instabilities in a Two-Dimensional Dipolar Fermi Gas*, Phys. Rev. Lett. **108**, 145304 (2012).

[121] J. K. Block, N. T. Zinner & G. M. Bruun: *Density wave instabilities of tilted fermionic dipoles in a multilayer geometry*, ArXiv e-prints (2012), 1204.1822.

[122] E. M. Lifshitz & L. P. Pitaevskii: *Statistical Physics*, Reed Publishing, Oxford (1998).

[123] K. Miyake: *Fermi Liquid Theory of Dilute Submonolayer ^{3}He on Thin ^{4}He II Film*, Progress of Theoretical Physics **69**, 1794 (1983).

[124] L.-M. Duan, E. Demler & M. D. Lukin: *Controlling Spin Exchange Interactions of Ultracold Atoms in Optical Lattices*, Phys. Rev. Lett. **91**, 090402 (2003).

[125] A. W. Sandvik: *Critical Temperature and the Transition from Quantum to Classical Order Parameter Fluctuations in the Three-Dimensional Heisenberg Antiferromagnet*, Phys. Rev. Lett. **80**, 5196 (1998).

[126] G. M. Bruun, O. F. Syljuåsen, K. G. L. Pedersen, B. M. Andersen, E. Demler & A. S. Sørensen: *Antiferromagnetic noise correlations in optical lattices*, Phys. Rev. A **80**, 033622 (2009).

[127] A. Paramekanti, N. Trivedi & M. Randeria: *Upper bounds on the superfluid stiffness of disordered systems*, Phys. Rev. B **57**, 11639 (1998).

[128] B. Liu & L. Yin: *Topological $p_{x}+ip_{y}$ Superfluid Phase of a Dipolar Fermi Gas in a 2D Optical Lattice*, ArXiv e-prints (2012), 1202.4924.

[129] B. Edegger, V. N. Muthukumar & C. Gros: *Gutzwiller-RVB theory of high-temperature superconductivity: Results from renormalized mean-field theory and variational Monte Carlo calculations*, Advances in Physics **56**, 927 (2007).